



universität
wien

DISSERTATION

Title der Dissertation

Artificial Receptors for Membrane Glycoproteins – Comparing Systems Derived from Nature with Imprinted Polymers

Verfasser

Thipvaree Wangchareansak

Angestrebter akademischer Grad

Doktor der Naturwissenschaften (Dr. rer.nat.)

Wien, 2011

Studienkennzahl It. Studienblatt: A791 419

Dissertationsgebiet It. Studienblatt: Chemie

Betreuer: Ao. Univ.-Prof. Mag. Dr. Peter Lieberzeit

ACKNOWLEDGEMENTS

This work would not have been possible to success without the help and support of many people. I would like to grateful thanks:

My supervisor: **Ao. Univ. Prof. Mag. Dr. Peter Lieberzeit**, who was especially involved in this project and helped with solution of many problems. He was always supportive and taught me many things. Moreover, my supervisor in Thailand: **Assist. Prof. Chak Sangma**, who inspired this work and also was never failing source of answer and supporting. Also, **O. Univ.-Prof. Mag Dr. Franz Dickert** who was providing the laboratory resources and always provided solutions of problems. **Prof. Frank M Unger** and **O. Univ.-Prof. Mag Dr. Helmut Viernstein** who were supporting me in the synthesis laboratory including the synthesis ideas and answer of many problem. Also, my friend in Thailand, especially, **Ms. Supatta Midpanon** at the Department of Chemistry, University of Vienna who taught me in the synthesis technique and **Dr. Teerachart Leepasert**, who was teaching me in NMR technique and as well as the synthesis training and resources of equipment and suggestion.

Furthermore, all of my colleagues at the Department of Analytical Chemistry, University of Vienna, for making a convivial place to work and also giving helpful suggestions. Moreover, my Thai friends in Vienna who have been a constant source of encouragement during my study in Vienna.

Deepest thanks are to my family for the support and encourage me during my study. This work would not have been possible without them.

Finally, the work would not succeeded without the funding support including Royal Golden Jubilee Ph.D. program (RGJ) and Faculty of Science, Kasetsart University, Thailand which are the main support and also Asia Uninet and Österreichischer Austauschdienst (OeAD) for funding during my studies at the University of Vienna.

Abbreviations

AAM	Acrylamide
Ac ₂ O	Acetic anhydride
AcOH	Acetic acid
ADVN	2,2'-azobis(2,4-dimethylvaleronitrile)
AIBN	2,2'-azobis(isobutyronitrile)
BET isotherm	Brunauer-Emmett-Teller isotherm
BMA	Butylmethacrylate
BOP	Benzotriazol-1-yloxytris(dimethylamino)-phosphonium hexafluorophosphate
br	Broad
BSA	Bovine serum albumin
BVD circuit	Butterworth Van Dyke circuit
Con A	Concanavalin A
d	Doublet
dd	Double doublet
DHEBA	<i>N,N'</i> -(1,2-Dihydroxyethylene) bisacrylamide
DMF	Dimethylformamide
DMSO	Dimethyl sulfoxide
DVB	Divinyl benzene
EGDMA	Ethylene glycol dimethacrylate
Et ₂ O	Diethyl ether
EtOAc	Ethyl acetate
FET	Field effect transistor
GlcNAc	N-acetyl-D-glucosamine

HOBt	N-Hydroxybenzotriazole
IP	Isoelectric point
m	multiplet
MAA	Methacrylic acid
MBAM	N,N'-methylene bisacrylamide
MeOH	Methanol
MIP	Molecularly imprinted polymer
MMA	Methylmethacrylate
NeuNAc	N-acetyl-D-neuraminic acid
NIP	Non-imprinted polymer
NMR	Nuclear magnetic resonance
PBS	Phosphate-buffered saline
PCR	Polymerase chain reaction
PDMS	Polydimethylsiloxane.
PMMA	Poly(methyl methacrylate)
<i>p</i> NP-GlcNAc	<i>p</i> -nitro- <i>N</i> -acetylglucosamine
QCM	Quartz crystal microbalance
s	Singlet
SBA	Soybean agglutinin
SDS	Sodium dodecyl sulfate
SDS gel	Polyacrylamide gel electrophoresis
SPR	Surface plasmon resonance
STM	Scanning tunneling microscope
t	Triplet
THF	Tetrahydrofuran
TLC	Thin layer chromatography
TMDMA	Tetramethylene dimethacrylate

Table of Contents

Acknowledgements	3
Abbreviations	4
1. Introduction	9
1.1 Lectins and Carbohydrate – Lectin interaction	9
1.2 Wheat germ agglutinin lectin	11
1.3 Biomimetic receptors	14
1.3.1 Molecularly imprinted polymers	14
1.3.2 Carbohydrate self-assembly monolayer	23
1.4 Mass sensitive sensing	24
1.5 Scanning tunneling microscopy	28
1.6 Aim of this thesis	30
2. Experimental part	31
2.1 Instruments	31
2.1.1 Apparatus	32
2.2 Synthesis of the glycosidic receptor analogue	36
2.2.1 synthesis of 1,2,3,4,6-Penta-O-Acetyl-D-Glucopyranose	38
2.2.2 Synthesis of 3,4,6-tri-acetyl-glucal	38
2.2.3 Synthesis of 3,4,6-Tri-O-acetyl-2-azido- α -nitro-D-Glucopyranose	42
2.2.4 Synthesis of 2-azido-3,4,6-tri-O-acetyl-2-deoxy- α -Glucopyranose chloride	42
2.2.5 Synthesis of 4-Nitrophenyl 2-azido-3,4,6-tri-O-acetyl-2-deoxy- α -D-Glucopyranose	44
2.2.6 Synthesis of 4-Nitrophenyl 2-Acetamido-2-deoxy- β -D-Glucopyranose	45

2.2.7	Synthesis of 4-Nitrophenyl 2-Acetamido-2-deoxy- α -D-mannopyranoside	45
2.2.8	Synthesis of p-Aminophenyl-2-Acetamido-2-deoxy- β -D-glucopyranoside (p-aminophenyl-GlcNAc)	46
2.2.9	Cysteine- p-aminophenyl-GlcNAc	49
2.3	Immobilization of the artificial receptor analogue on QCM surfaces	49
2.4	Molecularly imprinted polymer (MIP) preparation	50
2.4.1	General polymer synthesis	51
2.4.2	Stamp preparation	51
2.4.3	Preparation of MIP-coated QCM	51
2.4.4	QCM measurement	52
2.4.5	Scanning tunneling microscopy (STM) analysis	53
3.	GlcNAc receptor analogue as recognition element	55
3.1	Synthesis of Receptor analogue	55
3.2	Immobilization of Receptor Analogue on QCM	56
3.2.1	Artificial receptor analogue preparations	56
3.2.2	Optimization of artificial receptor immobilization	57
3.2.3	STM analysis of artificial receptor on gold electrode	59
3.3	QCM recognition and analysis	61
3.4	Adsorption isotherm for WGA-GlcNAc binding	65
4.	Molecularly imprinted polymers	73
4.1	Protein imprinting	73
4.1.1	Polymer optimization	74
4.1.2	STM analysis of WGA stamp and the imprinted surface	76
4.1.3	Sensor characteristic of Butylmethacrylate co-polymer system	80
4.1.4	Sensor characteristic of Methylmethacrylate co-polymer system	85
4.2	Non-Sauerbrey behavior	93
4.3	Brunauer-Emmett-Teller (<i>BET</i>) analysis	96
4.3.1	Interaction Isotherm – Binding properties	97

5. Comparison of sensors: receptor analogue vs. MIP	102
Conclusion	106
Outlook	106
Abstract	107
Zusammenfassung	109
References	111
Curriculum vitae	118

Chapter 1

Introduction

1.1 Lectins and Carbohydrate–Lectin interactions

Lectins are a class of protein that can agglutinate the erythrocytes and other types of cells and, furthermore, can interact with oligosaccharides. They can be found in viruses, animals, bacteria and also in plants, where they were actually discovered for the first time. A large class of proteins that interact with carbohydrate by non-covalent interaction, the lectins are defined as the third class of carbohydrate-specific protein. They bind to mono- and oligosaccharides reversibly with high specificity, but they are devoid of catalytic activity compared to an enzyme and are not part of immune response, such as antibodies. The first pure lectin which was isolated by Summer¹ in 1919 from jack beans is Concanavalin A (Con A), whose crystallographic structure is show in Figure 1.

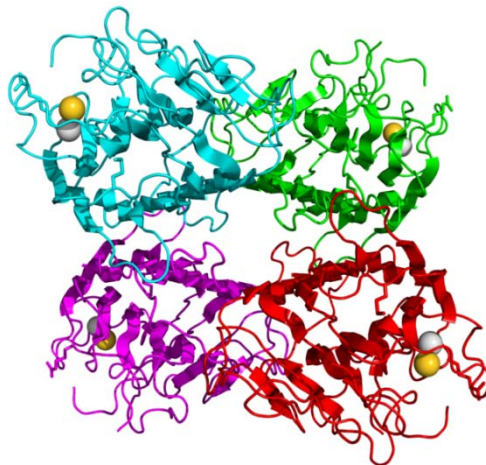


Figure 1 Crystallographic structure of a tetramer of jack bean concanavalin A (the single peptide strands are colored cyan, green, red and magenta, respectively). Calcium (gold) and manganese cations (grey) are depicted as spheres ².

Lectins from different sources such as in animal and in plant serve many different biological functions. Lectin from animal can bind soluble extracellular and intercellular glycoproteins. For example, some lectins are found on the surface of mammalian liver cells that specifically recognize galactose residues while another lectin is a receptor that recognizes hydrolytic enzymes containing mannose-6-phosphate, and target these proteins for delivery to the lysosomes. Concerning lectins from plant, their function is still uncertain. However, several member of this group such as wheat germ agglutinin (WGA), concavalin A (con A) and Soybean agglutinin (SBA) have been found to bind to a specific carbohydrate. Figure 2 shows the amino acid residues of plant lectin that interact with oligosaccharide.

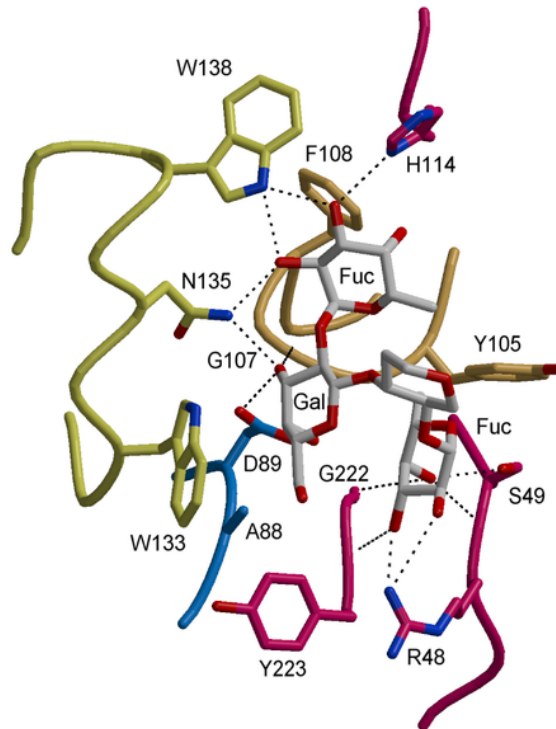


Figure 2 An oligosaccharide (shown in grey) bound in the binding site of a plant lectin (*Griffonia simplicifolia* isolectin IV in complex with the Lewis b blood group determinant). Only a part of the oligosaccharide (central, in gray) is shown for clarity.

[<http://en.wikipedia.org/wiki/Lectin>]

However, lectins play an important role in biotechnology and biosensors, because the interactions of carbohydrate-protein are crucial in several biological processes such as cell-cell recognition, characterization and purification of sugar-containing molecules and cellular structures. Normally, each lectin molecule contains typically two or more carbohydrate-binding sites. Therefore, they can have multiple carbohydrate interactions on the cell surface, which finally results in the cross-linking of the cells and their subsequent precipitation. Based on their specific glycosidic binding partner, lectins are classified into five groups, namely those preferably interacting with mannose, galactose/*N*-acetylgalactosamine, *N*-acetylglucosamine, fucose and *N*-acetylneuraminic acid, respectively³. Usually, the affinity of the lectins for monosaccharides is weak with association constants in the millimolar range; however it is highly selective.

1.2 Wheat germ agglutinin lectins

Wheat germ agglutinin (WGA) is plant lectin belonging to the legume family. This class of lectin protein is capable of agglutinating erythrocytes and other types of cells, which was discovered by Aub et al⁴ in 1971 in wheat germ lipase. They found that this enzyme contains an agglutinin that specifically interacts with malignant cells. Afterwards Burger et al succeeded in isolating WGA from lipase^{5, 6}, which was further purified by Ozanne and Sambrook⁷. In 1972, Nagata and Burger⁸ obtained highly purified WGA in crystalline form. Its estimated molar mass was 23.5 kDa determined by sedimentation equilibrium and SDS gel electrophoresis. However, recent structures of WGA resulting from x-ray crystallography suggest a homodimer form with 36 kD in molecular weight and with a twofold symmetry axis. Normally, it has three major isoforms, namely WGA1, WGA2 and WGA3, which are composed of subunits with almost identical amino acid sequences. The polypeptide chain form contains 171 amino acids with four hevein domains A, B, C and D, respectively. Each of them is 43 amino acid residues long and contains four disulfide bridges as shown in Figure 3. The cysteins forming the bridges are spaced three to six residues apart from one another and occur at homologous positions in the four domains. Therefore, there are 16 S-S bridges per sub unit of the lectin leading to the highly stable molecule.

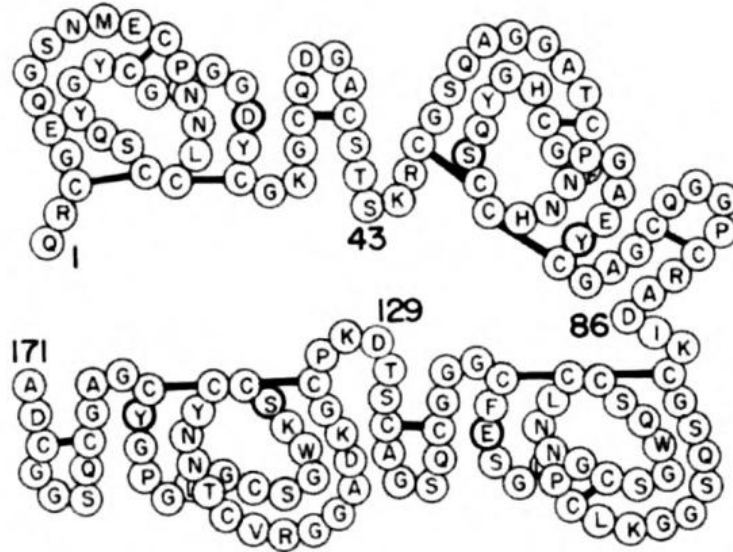


Figure 3 Diagrammatic represent of the covalent structure of WGA isolectin 2. The residues believed to interact with specific ligand are denoted by bold circles⁹

In WGA dimer, the subunits associate in a head to tail fashion, resulting in subdomain pairs. Another uncommon feature of WGA is the presence of multiple carbohydrate binding sites. WGA has two sugar binding sites per protomer for different sugar types. The primary binding site can be occupied by GlcNAc or terminal of N-acetyl-D-neuraminic acid (NeuNAc) while the secondary binding site can recognize only GlcNAc. Figure 4 shows the secondary binding with five binding sites towards GlcNAc, four of which are unique sites due to the twofold symmetry of WGA dimer. Generally, a binding site for GlcNAc or β -(1,4)-linked GlcNAc oligomer is formed by each hevein domain. The interaction occurs, because the polar residues of one chain undergo interactions with the adjacent domain of another chain, which provides the hydrogen bonding network leading to binding WGA and GlcNAc as shown in Figure 4. Therefore, WGA interacts with GlcNAc and NeuNAc but the strongest ligands are β -(1,4)-linked GlcNAc oligomers. Furthermore, studies^{10, 11} on such homogeneous GlcNAc oligomers have shown that the binding affinities are increased when going from one to three GlcNAc units.

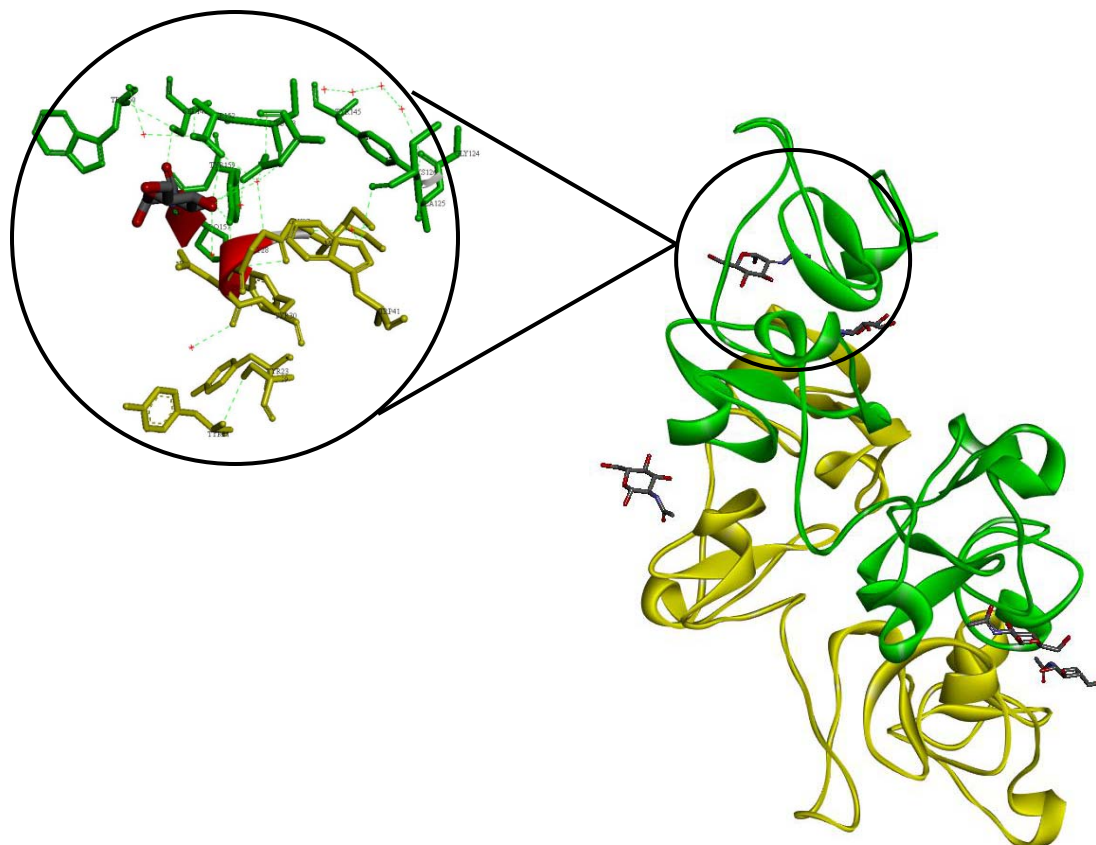


Figure 4 Crystallographic structure of a dimer of wheat germ agglutinin (Agglutinin isolectin 1), WGA (the chain A and are colored green and yellow, respectively) with multiple NAcGlc binding sites (Adapted from PDB: 2UVO¹²) and the binding site of WGA to GlcNAc at Chain F, residue number 1177 (adapted from reference¹²)

In this research, the analyte protein, therefore, is wheat germ agglutinin lectin (WGA) with two subunits of one distinct peptide entity. It measures approximately 14 nm × 9 nm × 4.5 nm. This diameter was obtained by modeling a published lectin structure¹² (2UVO from protein data bank, PDB) with the tools provided by the Protein Data Bank Europe (<http://www.ebi.ac.uk/pdbe/>). The isoelectric point (IP) is 8.3 thus they are charged in solutions at neutral pH.

1.3 Biomimetic receptors

In recent years, the importance of receptor design and recognition principles has substantially increased in science and technology, because chemistry is increasingly interested in biological systems, of which recognition is an essential key feature. Such strategies therefore require highly selective recognition materials to target specific analytes. The most straightforward approach would be to utilize biological compounds for this purpose. However, these systems are usually complex and sensitive to environmental parameters, such as temperature, pH and media composition. Hence, designing mimics of natural systems to recognize biological species to overcome these limitations has become a highly important issue. Generally speaking, it is necessary to implement “natural” functionality into an artificial material. Such man-made receptors for a wide range of compounds including biomolecules that mimic a bioreceptor are often termed biomimetic receptors. A range of different methods have been developed over the years for designing them. These include e.g. molecular imprinting, self-assembled monolayer (SAM), genetically engineered molecules and also fabricating artificial membranes. The molecular imprinting technique also utilized within this work relies on the specific interaction between the polymer system and template (or analyte molecule). In contrast to self-assembling techniques, which allow for the synthesis or modification of a wide variety of substrates with e.g. DNA, RNA, aptamer, protein and oligosaccharides, genetical engineering modifies a biological molecule on the DNA level and thus is more a single molecule approach. Generally speaking, MIP and SAM have been developed to mimic the natural receptor of biological cells and have been used for the construction of biosensors based on a range of transducers, such as quartz crystal microbalance (QCM)^{13, 14}, surface plasmon resonance (SPR)¹⁵⁻¹⁷, field effect transistor (FET)¹⁸ and electrochemistry^{19, 20}.

1.3.1 Molecularly imprinted polymers

The essential key of biomolecule recognition is the ability to bind to a specific substrate. Interaction partners have complementary functionalities along which they can form

non-covalent, intermolecular interaction networks. One of the very interesting techniques to achieve this in a rather straightforward way is realized by molecular imprinting into polymers.

Molecularly imprinted polymers (MIP)²¹⁻²⁸ aim to mimic a bioreceptor by their bulk or on their surface. The general idea behind them is the assumption that functional groups of the respective monomer molecules interact with a template thus leading to an intermolecular network. The respective interactions are hydrogen bonding, electrostatic, apolar and any other non-covalent interaction such as ionic, Van der Waals and π - π interaction. Therefore, if the functional groups are complementary to the template, the functional molecules arrange themselves around it in a clearly defined way. This arrangement is stabilized by the backbone of the developing polymer that is highly cross-linker. Otherwise, of course, the pre-arrangement of the monomers would be immediately lost for thermal reasons when removing the template for thermal reasons.

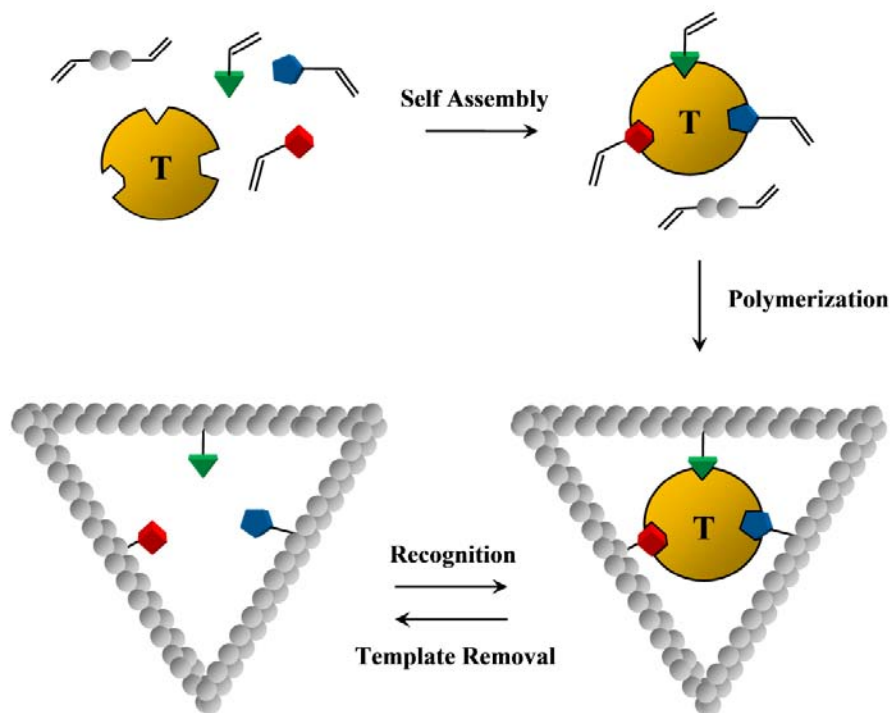


Figure 5 Schematic illustration of molecular imprinting

In principle, the molecular imprinting process consists of the following three steps as summarized in Figure 5: The first is pre-forming of the interaction network. In this step, all interactions, such as covalent conjugates or non-covalent adducts between a functional monomer and template molecule, form in solution. The second step is polymerization, which stabilizes the monomer-template conjugates and preserves their structural features within the polymer. Hence, the conformations of those monomer-template conjugates formed in step 1 are “frozen” within the three-dimensional network of the polymer. Finally, the template is removed from the polymer within the third step leaving behind adapted recognition cavities that are adapted to the template both in dimensions and functionality. Under appropriate conditions, these cavities therefore satisfactorily bind this molecule (or its analog) efficiently and selectively.

1.3.1.1 Strategies of molecular imprinting

The type of interaction between functional monomer and template molecule results in fundamentally different approaches, namely covalent or non-covalent molecular imprinting. Typical examples of those two strategies are presented in Figure 6 and Figure 7 by the imprinting of mannopyranoside and theophylline, respectively. Both have their inherent advantages and disadvantages, so choosing the appropriate method depend on various factors including template, polymer and their interaction.

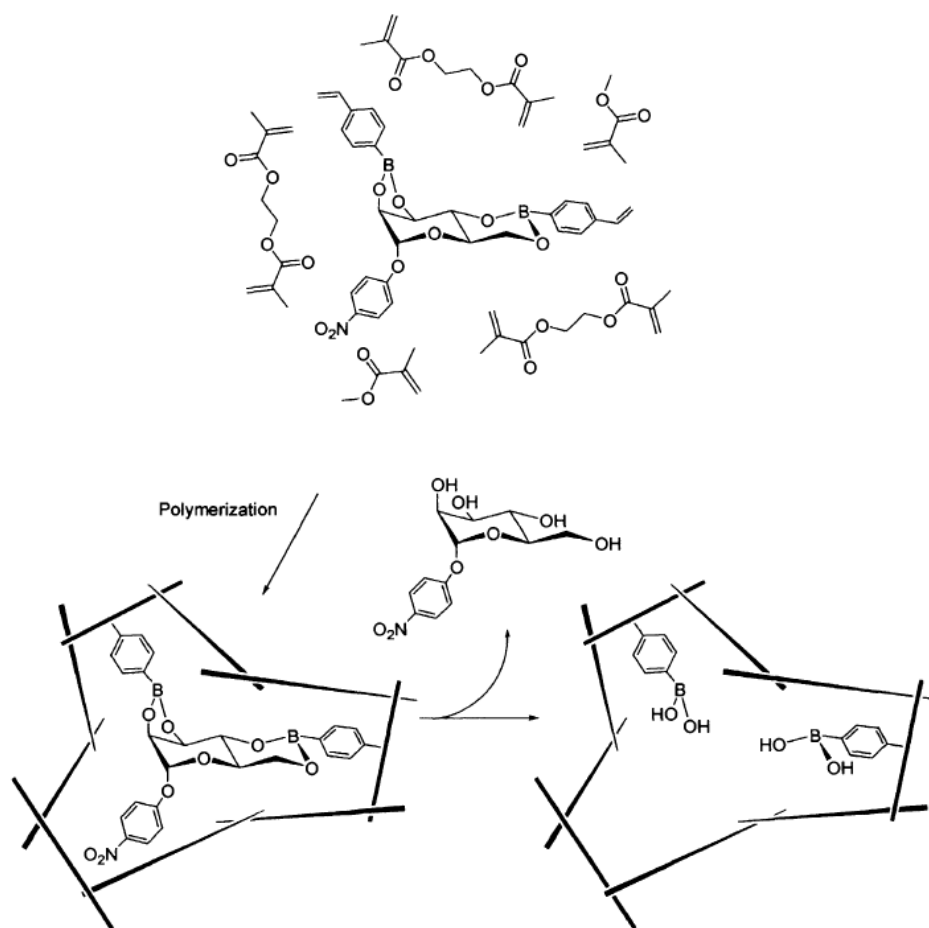


Figure 6 Covalent imprinting of mannopyranoside using its 4-vinylphenylboronic acid ester as a functional monomer²⁹

Covalent imprinting²⁹

As its name implies, covalent imprinting relies on the covalent bond between functional monomer and the template (see also Figure 6). The essential key for success in covalent imprinting is the choice of the respective covalent linkage. They have to be sufficiently stable to be conserved during polymerization, but also reversible in character, which in a certain sense contradicts one other. Furthermore, they should be easily removable or cleavable from the polymer under mild conditions without damaging the recognition site

generated. Also, the formation and dissociation of covalent linkage should be fast during the rebinding step of the guest target. Generally speaking, the number of covalent bonds which fulfill both of these thermodynamic and dynamic requirements is comparably small. At present the available linkages include boronic acid esters, acetals, ketals, Schiff bases, disulfide bonds, coordination bonds, among others. General experimental procedures for imprinting are essentially the same for all cases.

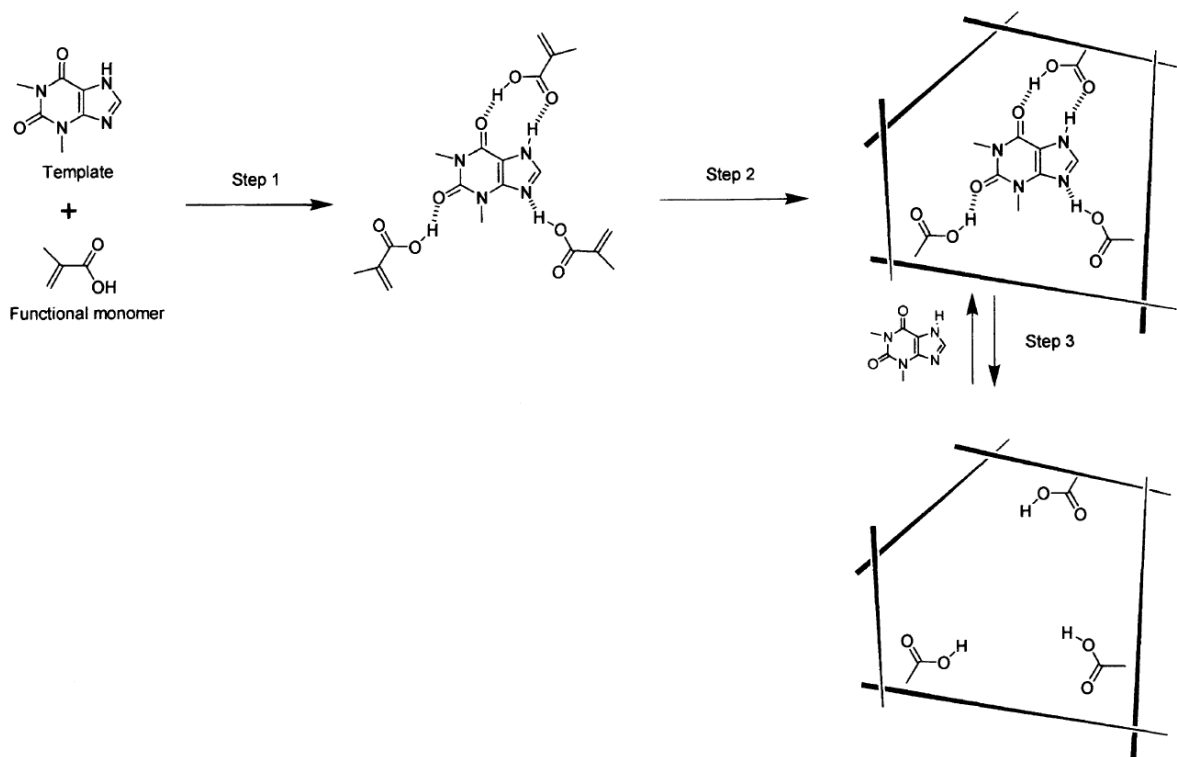


Figure 7 Non-covalent imprinting by theophylline (a drug): **Step1:** Pre-organization of functional monomers through non-covalent interactions. **Step2:** Polymerization of pre-organized functional monomers. **Step 3:** Removal of the template²⁹

Non-covalent imprinting²⁹

Non-covalent imprinting is usually experimentally more straightforward than covalent imprinting. It relies on non-covalent interactions, for example, hydrogen bonding or electrostatic forces between functional monomer and template molecule. This adduct formed in situ is then “frozen” in the final polymer. Furthermore, the template is easily removed after polymerization by simple extraction or evaporation. A wide range of analytically important analytes, such as biological species or substrates, pharmaceuticals, herbicides and environmental contaminants e.g. possess polar groups, for example, hydroxyl, carboxyl, amino, and amide for the required non-covalent interactions. Due to its simplicity and versatility, this type of imprinting is widely applied. In principle, hydrogen bonding is a very advantageous interaction for precise molecular recognition, since it substantially depends on distance and direction of monomer and template molecules. However, the nature of non-covalent interactions in this case also is determined by the pK values of both components (monomer and template). For example, when both acid and base are very strong, a proton can be transferred from acid to base leading to forming of an electrostatic interaction. The disadvantage of this interaction is that it is less directed, which makes it more unfavorable for precise molecular recognition. Therefore, good-quality non-covalent imprinting requires thoroughly controlling those interactions via the respective experimental conditions.

Summarizing, each imprinting technique has its specific advantages and drawbacks as described in Table 1. Hence, the most suitable technique for any given application has to be found by evaluating those against one another.

Table 1 Specific properties of covalent and non-covalent imprinting²⁹

	Covalent	Non-covalent
Synthesis of monomer-template conjugate	Necessary	Unnecessary
Polymerization condition	Nonrestricted	Restricted
Removal of template after polymerization	Sometimes Tedious	Straightforward
Guest-binding and guest-release	Slow	Fast
Structure of guest-binding site	Clearly defined	Less clear

1.3.1.2 Factors influencing the quality of MIP

To achieve a high imprinting efficiency, a range of different factors has to be considered, such as necessary reagent, reaction conditions and the possibility to achieve high-efficiency imprinting. A wide range of compound are needed in molecular imprinting, including functional monomer (bound to template in the case of covalent imprinting), crosslinker reagent, initiator, solvent for polymerization and solvent for cleaving or remove the template from polymer. All components have an influence in terms of sensitivity and selectivity of the final MIP material.

Functional monomer

All kinds of polymerization, for example, free radical, anionic, cationic and polycondensation can be utilized for molecular imprinting. A fundamentally important factor is the interaction between monomer and template during imprinting. As already mentioned, in covalent imprinting, the templates are chemically bound to the functional monomer. Therefore, the most popular monomers in that case include ester and amides of acrylic acid or methacrylic acid, respectively, because they can easily form covalent bonds with a template. In the case of non-covalent imprinting, due to a variety of non-covalent interactions, a wide range of functional monomers can be applied and designed depending on the type of interaction with template. For example, in protein imprinting, amine and carboxylic monomers can be applied for forming hydrogen bonds while, in the case of non-polar or π - π -interaction, e.g. styrene plays an important role.

Crosslinking agent

The cross linker is one of the main factors in determining the selectivity of molecular imprints. Wulff at al.³⁰ studied the influence of the degree and type of crosslinking on the suitability of MIP to separate enantiomers by chromatographic techniques.

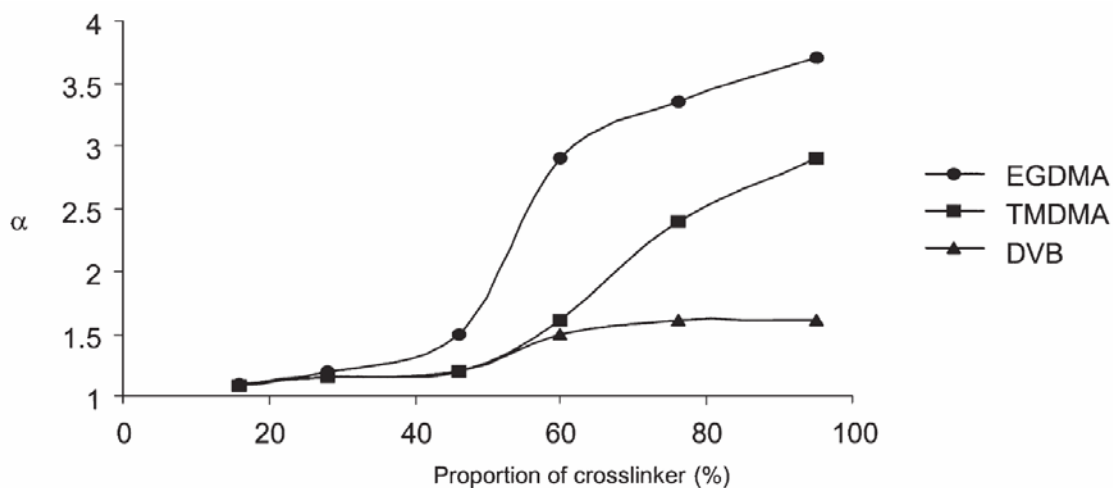


Figure 8 Influence of the proportion of crosslinker on the recognition specificity of MIPs. The crosslinkers represented is ethylene glycol dimethacrylate (EGDMA), tetramethylene dimethacrylate (TMDMA) and divinyl benzene (DVB)^{30, 31}

The result can be seen in Figure 8, where the selectivity in binding is represented by the separation factor α . The different types of crosslinker (e.g. ethylene glycol dimethacrylate (EGDMA), tetramethylene dimethacrylate (TMDMA) and divinyl benzene (DVB)) have an effect on a specific recognition. A higher degree of cross linking usually leads to higher selectivity. Also, shorter, but not too rigid crosslinkers (EGDMA rather than DVB) lead to improved selectivity, as can be seen in the selectivity order, where EGDMA exceeds both TMDMA and DVB, because it has a more flexible structure. Furthermore, Figure 8 also clearly indicates that a high degree of crosslinker enhances selective recognition: as can be seen, the ratio of crosslinker should in this case be over 70 mol%. While a high degree of crosslinker enhances the mechanical stability of MIP, it also reduces deformation of the imprinted sites because the polymeric network is more rigid. In a MIP based on non-covalent interactions, up to 10% of the sites formed are active and used for analytical purposes because the high proportion of crosslinker brings about a decrease in capacity. However, the crosslinker should be able to interact in the same way as functionalized monomer, therefore its degree has to be optimized individually in each molecular imprinting experiment.

Solvent

The main role of the solvent is obviously to dissolve reagents for polymerization, but it also provides the porous structure to the MIP and thus promotes guest binding. During the polymerization step, solvent molecules are incorporated inside the polymer and are removed in the course of post-treatment. During this process, the space originally having been occupied by them leaves behind pores in the polymer. Thus, polymers prepared without solvent are usually too firm and dense hence hardly binding guests. Another important role of the solvent is to disperse the heat of reaction generated during polymerization. Otherwise, the temperature of reaction mixtures would be locally elevated and undesired reactions could occur. Furthermore, it supports the random mobility of monomers and templates, so formation of an interaction network is supported. This is especially important for efficient non-covalent imprinting. The choice of the solvent depends on the kind of imprinting. In covalent imprinting, a variety of solvents can be used as long as they can dissolve all components. In non-covalent imprinting, the type of solvent is more critical as it has to promote the formation of the non-covalent adduct between functional monomer and template. Therefore, the interaction between solvent and the dissolved compounds should be slightly less advantageous than the ones leading to the interaction network.

Polymerization procedures

There are two main types of polymerization in MIP: addition polymerization and condensation polymerization. Addition polymerization, generally, usually requires a single type of monomer functionality by opening double bonds to form the polymer, while condensation polymerization is based on different functional groups in monomers. Comparing both processes, condensation polymerization often is slower than the addition polymerization. In addition polymerization, moreover, the condition of reaction can alter the properties of the polymer. During the polymerization process, the radical reaction can be initialized by thermal decomposition or UV light decomposing a suitable radical starter. However, the decomposition procedure should not change the structure of the template

molecule. Thus, if for instance the template is thermally unstable, polymerization should be carried out under UV light. In any case, it is important to remove molecular oxygen from polymerization mixtures, since it traps the radical and retards (or even stops) the polymerization. In order to do so, degassing with nitrogen or argon, as well as freeze-and-thaw cycles under reduced pressure, are effective. Typical initiators are 2,2'-azobis(isobutyronitrile) (AIBN) and 2,2'-azobis(2,4-dimethylvaleronitrile) (ADVN).

Template molecule extraction stage

The final step of molecular imprinting is template molecule extraction. To achieve high efficiency in imprinting, the template interacting with the forming polymer during polymerization has to be removed to leave behind cavities in the polymer. It is estimated that about 90% of the template species are removed during this step. The remaining molecules are trapped in a highly cross linked zone, which is often found with macromolecular structures. In principle, the extraction step uses an appropriate solvent or simple evaporation. Normally, the process leaves behind a three-dimensional material in which the cavity shapes and functional group locations are complementary to the respective guest molecule.

1.3.2 Carbohydrate self-assembled monolayer

Self-assembling monolayers (SAM) is a technique generating dense arrangements of molecules leading to structures suitable for modeling e.g. cell surfaces. SAMs are created by the chemisorptions of molecule on substrate surface via covalent interaction, for example, chemisorbing of thiols (R-SH) onto gold surface resulting in forming of Au-SR bond. The advantage of this technique is that a small amount of compound is needed for fabricating. Furthermore, they are e.g. suitable for proof of concept experiments with carbohydrate-binding proteins. The first developments of this technique were to immobilize organics on glass or metal surfaces. More recently, this technique has been developed further to immobilize biomolecules or their receptors on surfaces for studying biological processes. As carbohydrate molecules are found in several organism and often interact with a range of

biomolecules, carbohydrates immobilized on the solid surface, therefore, can be advantageous in SAM technology as a recognizing the protein-carbohydrate interaction: it in this case acts similarly to a glycan on a cell surface and thus allows functional studies.

1.4 Mass sensitive sensing

Measuring small changes in mass has become a popular type of transduction in sensing. All such transducers are based on the piezoelectric effect. The word “piezoelectric” comes from Greek and means “electricity by pressure” (*Piezo* means pressure). It was discovered by Pierre and Jacques Curie in 1880³²: the name was proposed by Hankel³³ one year later. They observed that positive and negative charges appeared on crystal surfaces when compressing the crystal in different directions.

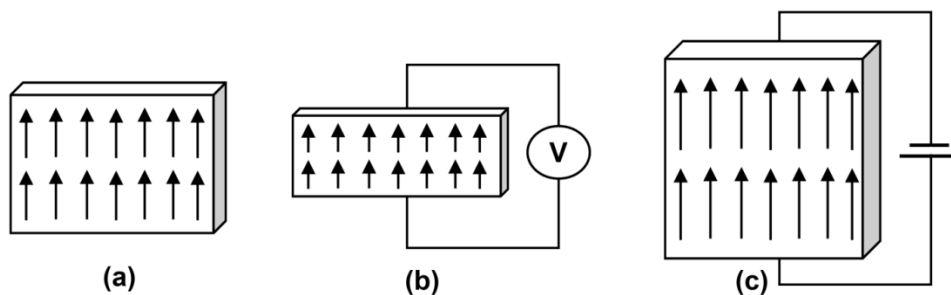


Figure 9 (a) A piezoelectric material. (b) A voltage response can be measured as a result of a compression or expansion. (c) An applied voltage expands or compresses a piezoelectric material (adapted from reference³⁴).

On the other hand, a piezoelectric substrate is mechanically deformed when an electric field is applied as described in Figure 9 (the so-called inverse piezo effect). Generally speaking, this effect only occurs in crystals that have no center or symmetry along at least one of their crystallographic axes.

One of the sensors based on the piezoelectric effect is the quartz crystal microbalance (QCM). Quartz has hexagonal crystallography with no symmetry along the y axis. Both the

magnitude of the piezoelectric coefficient and extent of its temperature sensitivity depend on the orientation of the substrate with respect to the crystallographic main axis. The most popular orientation for sensing purposes is the so-called AT-cut at an angle of $35^{\circ} 10''$ with respect to the yz-plane, see in Figure 10. This can be operated at the ambient temperature ($25\text{-}45^{\circ}\text{C}$) encountered in sensing.

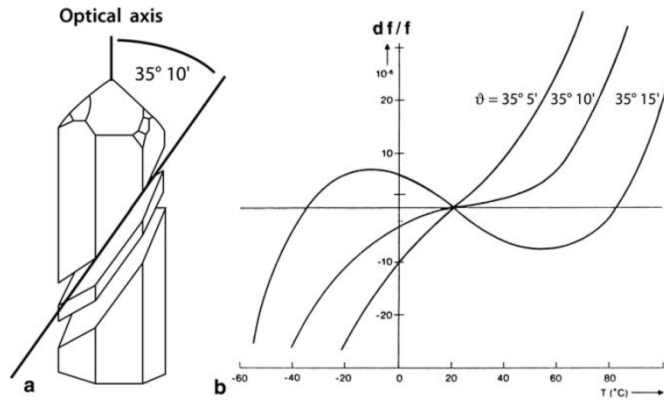


Figure 10 (a) Orientation of the AT-cut of the quartz crystal; (b) Dependence of relative frequency of quartz crystal microbalance (QCM) on temperature³⁵

QCM generally comprise of thin quartz wafer with 0.25-1.0 inch in diameter. Two metal electrodes are deposited on the two faces, which are used to establish an electric field across the crystal. When applying an alternating field, under certain conditions the electrical energy is retransformed into a mechanical shear oscillation basically without loss. The respective frequency depends on a combination of thickness of the quartz wafer, the metal electrode and the material deposited on the quartz crystal microbalance surface. However, mass changes on the QCM surface result in additional frequency changes that can be described and quantified by the Sauerbrey equation. Figure 11 shows the relationship between wavelengths of the shear wave in quartz wafer with 2 metal electrodes before and after mass loading when the shear-mode vibration of quartz crystal of mass and thickness t , at resonance, the wavelength λ is

$$\lambda = 2t/n \quad (1)$$

Where $n = 1$ designates the frequency F and $n > 1$ its higher harmonics.

According the relationship between wavelength and frequency: $v = f\lambda$, the equation (1) can be rewrite in term of frequency:

$$f = v/2t \quad (2)$$

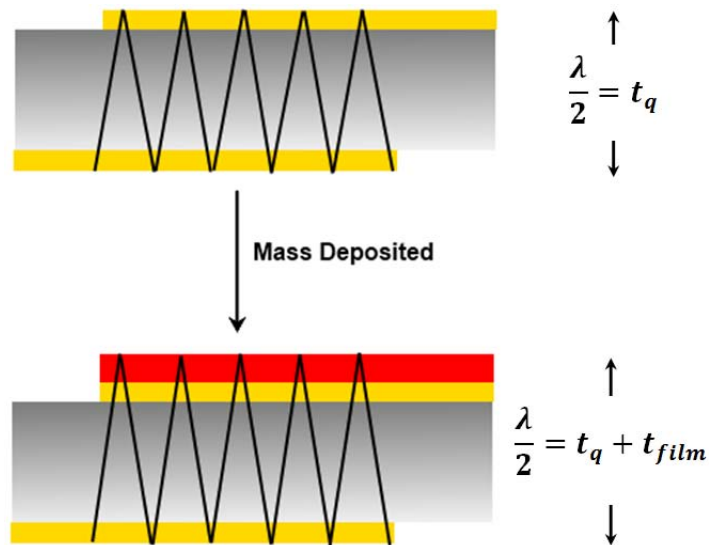


Figure 11 Shear mode vibrations in QCM. Incremental increase λ is due to increased thickness (adapted from reference³⁵)

The frequency change caused by a small additional thickness on quartz layer (dt), as seen in Figure 11, therefore the small frequency change can be obtained by

$$df = -\frac{v}{2t^2} dt \quad (3)$$

Due to the relative of thickness and mass loading, the ratio of fundamental frequency and frequency change can be wrote in term of mass change in equation

$$\frac{\Delta f}{f} = \frac{\Delta M}{M} \quad (4)$$

This, therefore, leads to the relationship between frequency change and additional mass which so-call the Sauerbrey equation

$$\Delta f = -\frac{2f_0^2}{A\sqrt{\rho_q\mu_q}} \Delta m \quad (5)$$

Where f_0 is the resonant frequency of the quartz resonant, Δm is the mass change, A is the piezoelectrically active crystal area (Area covered by the electrodes), μ_o is the shear modulus of quartz AT-cut crystal ($\mu_q = 2.947 \times 10^{11} \text{ g/cm.s}^2$) and ρ_q is the density of quartz ($\rho_q = 2.648 \text{ g/cm}^3$).

In the case of QCM operating in conducting liquids, the two electrodes cannot be exposed to the electrolyte together, because this would lead to electrical field lines outside the substrate leading to substantial frequency effects. Therefore, only one side electrode of QCM is usually exposed to the liquid. To minimize the abovementioned effects of solution conductivity, the electrodes on opposite faces usually are different in size. The larger electrode of each pair is usually switched to ground in the oscillator circuit and exposed to the analyte solution.



Figure 12 The different size of metal electrodes on QCM for operation in liquid

Parameters affecting the performance of QCM in liquids include excessive mass loading at the sensitive layer, the change in mechanical properties of QCM due to exposition to liquids, but also conductivity and viscosity of the respective liquid. The detailed electronic properties to understand such as system can be derived by the modeling as equivalent electrical circuits. For a QCM, the equivalent circuit is given by the so-called Butterworth

Van Dyke (BVD) circuit depicted in Figure 13. It relies on the behavior of resonators mimicking resonating QCM. The physical properties of QCM are represented by four electrical elements. There is a single element of capacitor on the bottom branch which is parallel to the series of resistor, capacitor and conductance.

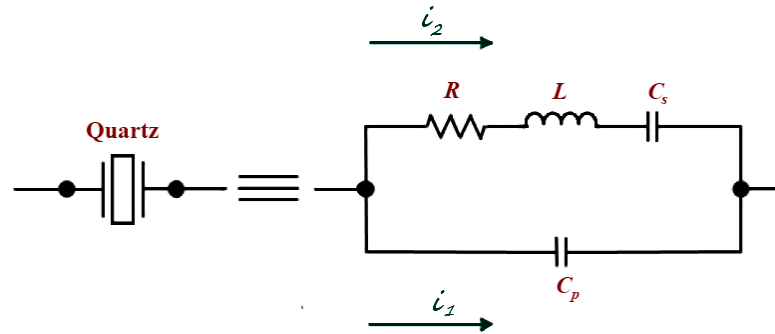


Figure 13 Butterworth–van Dyke (BVD) equivalent circuit³⁵

In Figure 13, the bottom branch is the so-called static branch, which is the dielectric capacitance representing the quartz capacitance and the external connection capacitance. The top side of BVD circuit is called motional branch consisting of the series of resistor, inductor and capacitor which represent the resonance of the quartz and its mass load. This part is disturbed by the external mass loading, because the energy of oscillator is stored in the capacitor, c_s ; the resistor, R , refer to the energy loss and addition of mass on the QCM, for example, by films or liquids is represented by inductance, L .

1.5 Scanning tunneling microscopy

Scanning tunneling microscopy (STM) is a surface analysis technique that operates by scanning a probe over a surface. It was invented by Heinrich Rohrer and Gerd Binnig of IBM's Zurich Research Laboratory in 1982. This technique is based on tunneling phenomena which occur between a conducting sharp tip and the sample when voltage is applied. Then, the tip is scanned above a conductive sample, which leads to the flow of electrons across the

gap between probe and surface resulting in a measurable current, as seen in Figure 14. For imaging, one makes use of the fact that the tunneling current exponentially depends on the distance between tip and surface.

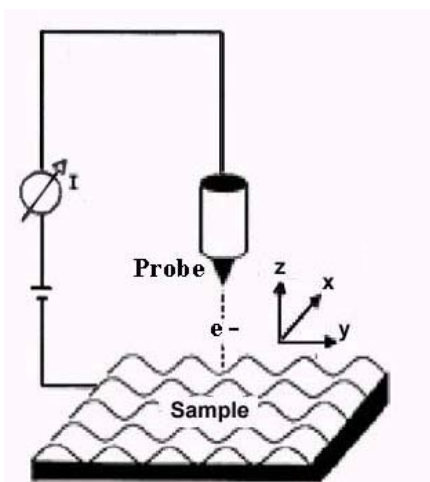


Figure 14 Tunneling of electrons from an etched STM probe (i.e. tungsten wire) to a conductive surface [<http://invsee.asu.edu/nmodules/spmmod/senses.html>]

There are two different experimental methods in STM, namely constant current imaging and constant height imaging. In the first technique, constant current is maintained during scanning. When the probe is moved at each (x,y) data point, its vertical position is corrected until it reaches the preselected setpoint current, the vertical position of the probe at each (x,y) data point will be stored by computer to generate the topographic image of the sample surface. On the other hand, the constant height measurement is performed by fixing the probe-sample distance. The image is generated by a variation of tunneling current forms. This approach is faster in generating an image, but it only allows to works on flat samples.

The main advantage of this microscopy is its ability to perform high-resolution imaging of surfaces over a relatively large range in both horizontal and vertical directions. Furthermore, it can be performed in vacuum, air and liquid environments making it very convenient measuring a wide range of samples without the necessity of tedious sample pretreatment. However, the limitation of STM is that it can generate only images of conducting surfaces, which inherently excludes most ceramic and polymeric materials. This

problem can be solved by applying a conducting coating, such as gold, on that surface. Due to these properties, the STM is used in many applications to obtain topography of surface at high resolution, either for atomic imaging such as Si, Gold and SiC, or for general surface roughness determination. Moreover, STM can be used for imaging studies of biological molecules due to its high resolution property.

1.6 Aim of this thesis

WGA binds to residues that are present on a range of biological membranes, especially to sialic acid and *N*-acetylglucosaminyl (GlcNAc) sugar residues. It is a highly suitable model for elucidating the binding reactions on the way to better understand receptor-substrate interactions e.g. during infection processes. This work aims at directly comparing the binding properties of a receptor analogue being closely related to the natural system and a fully artificial sensitive material according to their WGA binding properties. In principle, this can lead to strategies replacing the natural system entirely by an artificial one. Hence, this work on the one hand describes the development of a synthetic strategy for a receptor analogue, namely GlcNAc, immobilization experiments of this artificial receptor analogue on QCM, and the respective sensor characteristic. Additionally, a parallel approach focuses on the development of MIP for WGA and sensor characterization to establish a fully artificial system suitable for recognition. This then allows comparing the two techniques to gain insight into the binding characteristics. Finally, a sensor system for Wheat germ agglutinin will be reported as a potential sensor model for future pathogen detection and can be used as model for investigating carbohydrate – protein and sensor design.

Chapter 2

Experimental part

2.1 Instruments

The work station for protein analysis consists of four main parts, namely the measuring cell for QCM installed, oscillator circuit, frequency counter and computer including software as shown in Figure 15. The functions of the individual devices will be discussed in a bit more detail in the following chapters.

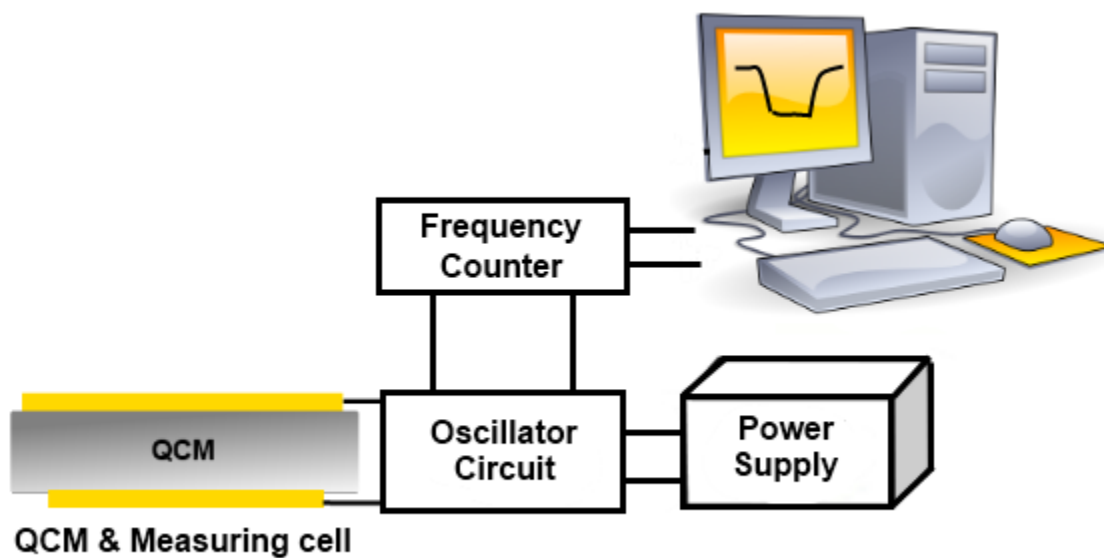


Figure 15 Quartz crystal microbalance (QCM) measuring station in laboratory

2.1.1 Apparatus

Quartz and electrode design

For the work presented in this thesis, 10 MHz AT-cut Quartz crystal with 13.8 mm diameter and 168 μm thickness was applied. The bare quartz crystal is shown in Figure 16a and Figure 16b shows quartz crystal with dual electrode structures deposited.

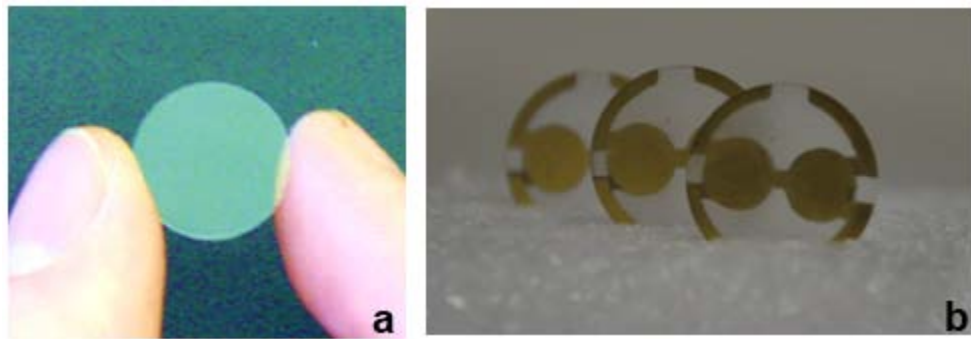


Figure 16 Bare quartz crystal and quartz crystal with dual gold electrode

Such an electrode design allows for compensation of external effects, for example, temperature drift or conductivity of the sample solutions. As protein measurements have to be done in liquid phase by exposing the QCM to different protein solutions, those parameters have to be taken into account. Furthermore, it turned out necessary to use different electrode diameters (5 mm towards the sample, 4 mm on the air side) (Figure 17). This prevents excessive leakage of electrical field lines into the aqueous phase.

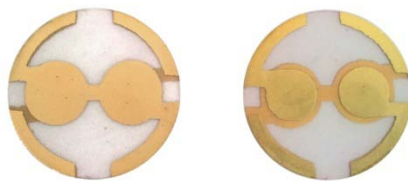


Figure 17 Gold dual electrode structure on both sides **a)** electrode in the liquid phase **b)** electrode in air phase

Measuring cell

The respective QCM are installed in a custom-made measuring cell optimized for protein analysis as can be seen in Figure 18.

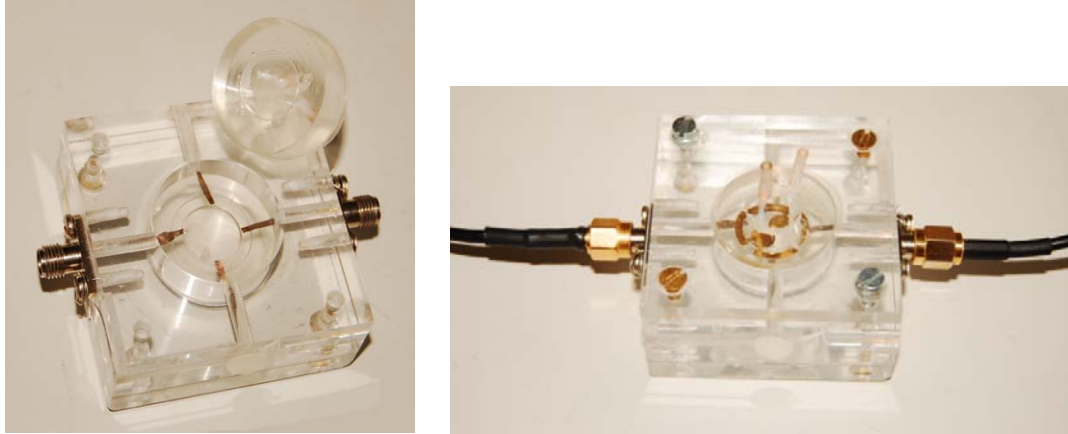


Figure 18 Measuring cell from silicone mold and quartz crystals microbalance installed

The cell holder is rectangular, manufactured from PMMA and supports a PDMS cell sandwich; on the lower side the QCM is exposed to air, while the upper side has the sample inlet and outlet, as seen Figure 19.

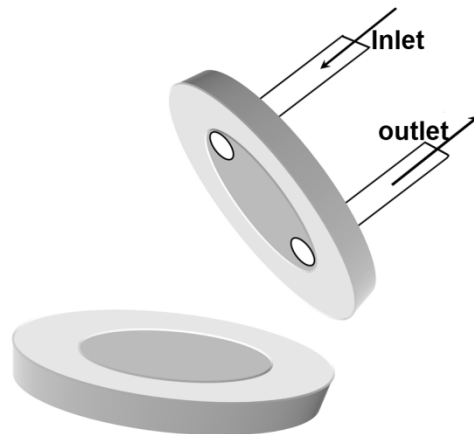


Figure 19 PDMS cell for protein analysis

This sandwich structure fulfils three tasks: first, it provides the sample cell itself containing the sample inlet and outlet, respectively; second, it ensures direct electrical contact between the tin-plated copper wires functioning as electrodes due to its elasticity and third, it thermally insulates the sample area. The electrode contacts are lead out via SMA ports, of which one wire (the phase) connects to one face of the QCM and the other (mass side) to the other one facing the sample chamber. The setup allows measuring in both flow and stopped flow mode.

Oscillator circuit

The QCM measurement operates as the frequency-determining element in an oscillator circuit. This oscillator circuit was designed in the group for measurements in liquid phase. Figure 20 shows the 2 channel oscillator circuit for dual electrode QCM. Each channel consists of 3 electronic modules including the actual oscillator based on an operational amplifier, phase correction and an amplification circuit increasing the signal by a factor of ten. The electronics are operated with 12 V DC, signal inputs from the measuring cell are SMA sockets, the signal output to the frequency counter is realized by BNC connection.

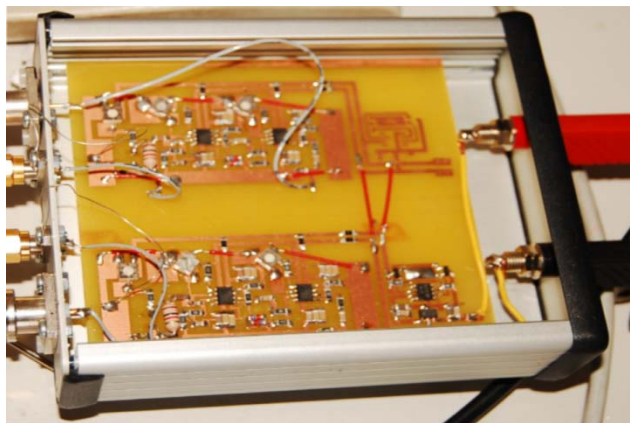


Figure 20 Oscillator circuit for 2 channels

Network analyzer

QCM have to be characterized prior to use in the oscillator setup with respect to their resonance frequency and damping, which are both determined by a network analyzer (Figure 21). Basically, a network analyzer exposes the device to be tested to a frequency band and measures either transmission of these frequencies through the device or their reflection, respectively. This is a passive method that has proven invaluable for determining e.g. layer heights. Additionally, the qualities of quartz crystals can be identified by damping value and electronic quality factor. The good quality should have low damping and sharp resonance peak as shown in Figure 21.

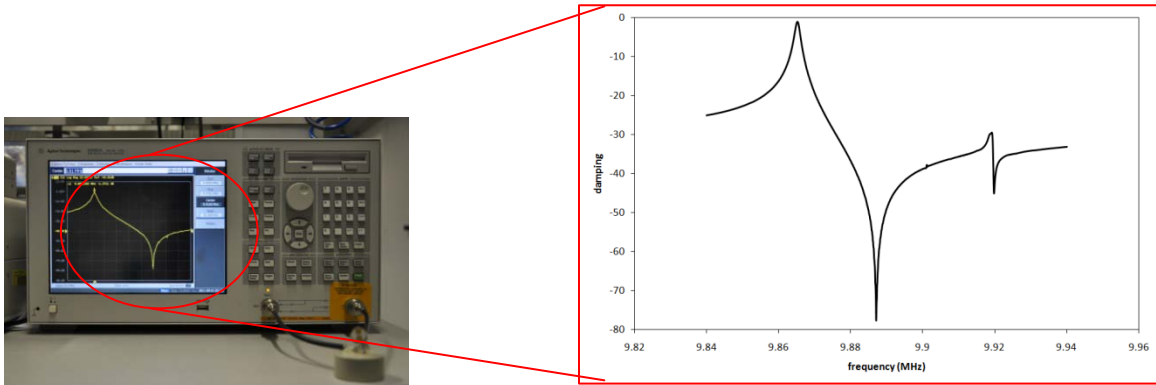


Figure 21 Network analyzer with quartz crystal microbalance damping spectrum

Screen printing technique

The electrodes are deposited on the quartz substrate by screen printing. Figure 22 illustrates the method for preparing the electrode on quartz crystal and the pattern of dual electrode on homemade sieve. Sieves are patterned by gluing a 20 micron mesh on a frame followed by coating it with Azocol poly-plus S positive photoresist and leaving it to harden for 2 hours in darkness at 25°C. Afterwards, it is exposed to UV for 30 seconds via a mask containing the electrode pattern. This hardens the exposed areas and thus clogs the pores of

the sieve. The unexposed parts in the shape of the future electrode pattern can be removed by brilliant gold paste and burning at 400C for 5 hours to remove organic residues.

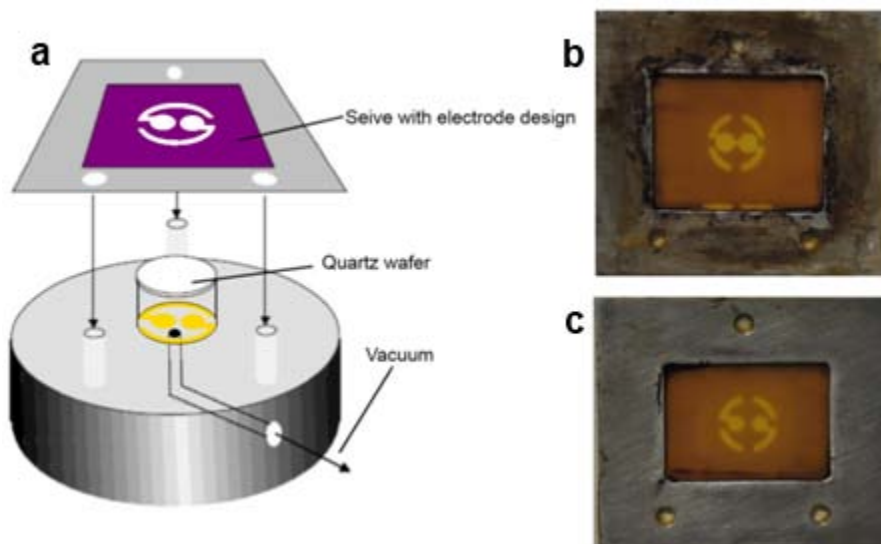


Figure 22 The production of dual electrode by screen printing technique (a) and sieves for screen printing (b,c)

2.2 Synthesis of the Glycosidic Receptor analogue

Within the present work, the receptor for WGA lectin has been *N*-acetyl- β -*D*-glucosamine (*GlcNAc*) which is specific to WGA as there is high binding constant¹⁰ (in the order of magnitude of around 10^2). For this purpose, receptor analogue was synthesized from glucose introducing also a linker group for immobilizing it on gold surface of QCM. For this purpose, *p*-nitrophenol link with cysteine molecule has been used, because those molecules are hydrophilic and therefore preserve the natural properties of *GlcNAc*. The synthesis pathway is given in Figure 23.

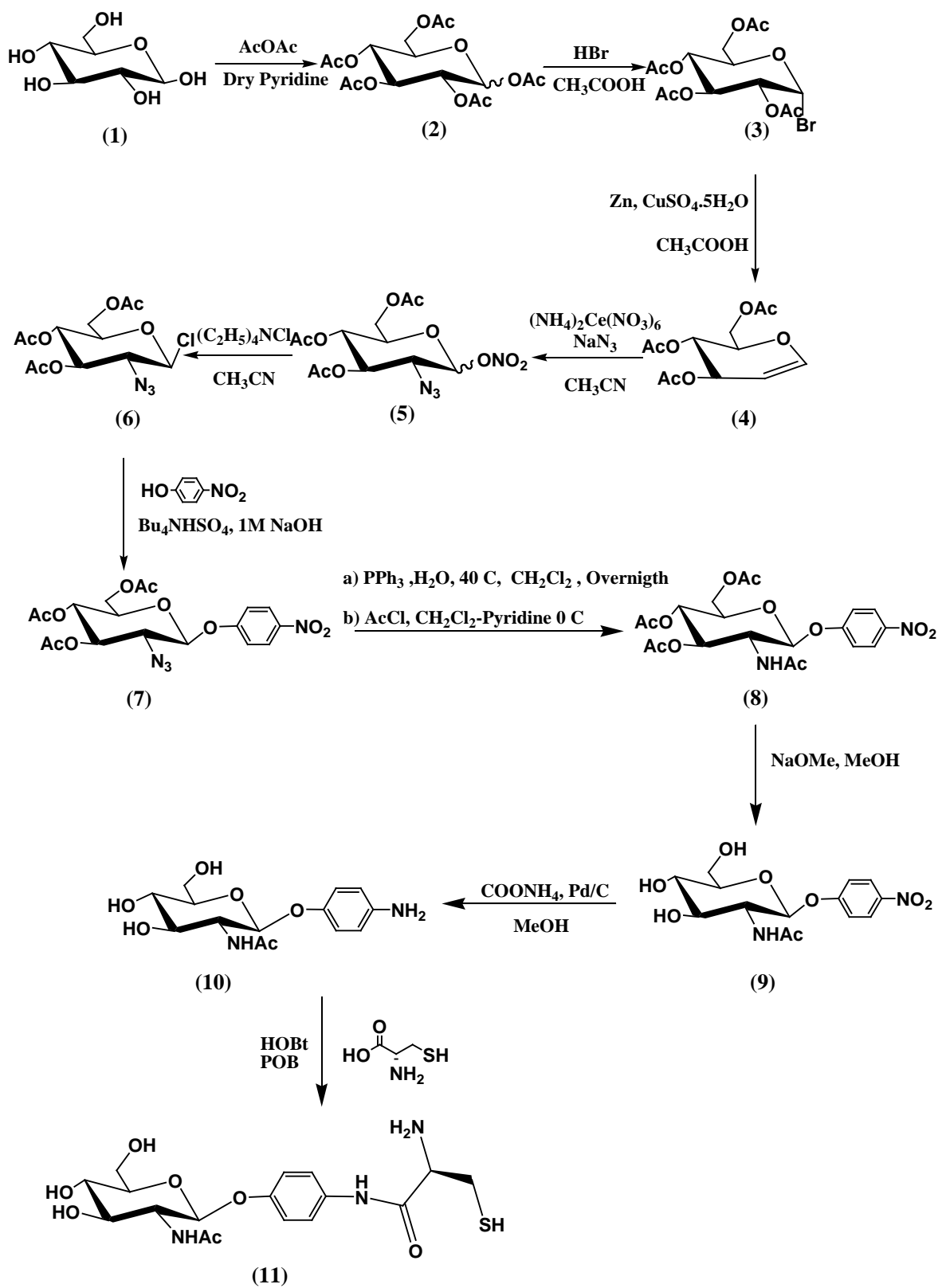
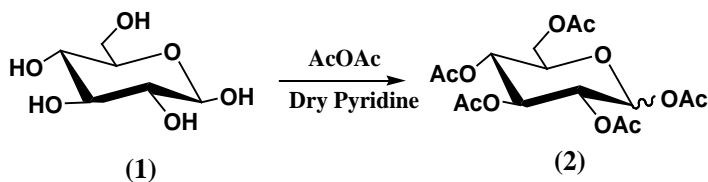


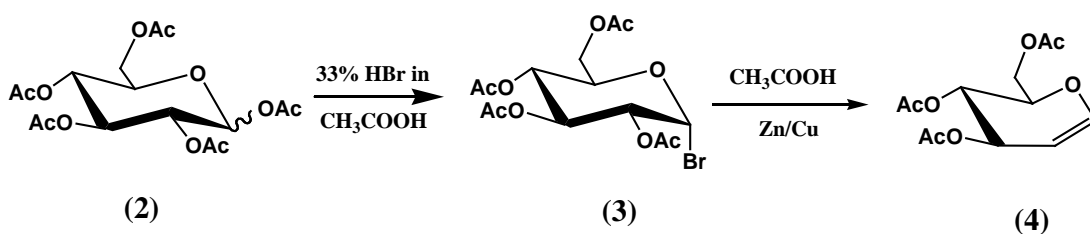
Figure 23 Synthesis pathway of *p*-nitro-*N*-acetyl-*D*-glucosamine.

2.2.1 Synthesis of 1,2,3,4,6-Penta-*O*-Acetyl-*D*-Glucopyranose



D-glucose (1 g, 0.1667 moles) was dissolved in dry pyridine (10 ml) following by adding 10 ml of acetic anhydride. The reaction mixture was stirred at 0 °C for 24 hours. The completed reaction was confirmed by thin layer chromatography (TLC) in ethyl acetate-hexane (1:1) system. To develop the product spot, anisaldehyde was applied to TLC following by heating at 100 °C for 5-10 minutes. Afterwards, reaction mixture was diluted with CH₂Cl₂ (20 ml) and washed 2 times with H₂O (20 ml) and 2 times with an aqueous solution of 1% NaHCO₃ (20 mL). The product remained dissolved in the organic phase, which was dried with anhydrous MgSO₄. The final product was obtained by evaporating the solvent under reduced pressure leaving behind a white solid (95% yield).

2.2.1 Synthesis of 3,4,6-tri-acetyl-glucal³⁶



Penta-acetyl-glucal (0.9 mg, 2.2 mmol) was dissolved in dry CH₂Cl₂ (20 ml). Then 33% HBr (5 ml) in acetic acid was added dropwise to the mixture and then stirred overnight at 0 °C. Completion of the reaction was confirmed by TLC in ethyl acetate-hexane (1:1) system. Afterward, the mixture was poured into a pulverized suspension of CuSO₄·5 H₂O (0.18 g, 0.7 mmol) and Zn (7.3 g, 112 mmol) in H₂O (10 mL) and AcOH (15 mL). The

resulting mixture was stirred vigorously at room temperature for 1.5 h. Finally, the reaction mixture was filtered and washed with CH_2Cl_2 (100 mL) and H_2O (100 mL), respectively. The organic layer of the filtrate was washed successively with saturated NaHCO_3 (100 mL) and brine (100 mL). Furthermore, the product solution was dried with MgSO_4 anhydrate and concentrated under reduced pressure to give a crude oil. This product can be recrystallized by diethyl ether and petroleum ether to afford glucal (1.12 g, 72%). The full characterization of glucal is in reference³⁷. Again, the ^1H NMR and ^{13}C NMR spectrum of 3,4,6-tri-acetyl-glucal is shown in Figure 24 and Figure 25, respectively.

^1H NMR (200 MHz, CDCl_3): $\delta(\text{ppm}) = 2.01\text{-}2.04$ (m, 9H), 4.14-4.27 (m, 2H), 4.33-4.74 (m, 1H), 4.79-4.85 (m, 1H), 5.17-5.23(m, 1H), 5.30-5.34 (m, 1H), 6.46 (d, $J = 6.06$ Hz, 1H).

^{13}C NMR (50 MHz, CDCl_3): $\delta(\text{ppm}) = 20.6$ (CH_3), 20.7 (CH_3), 20.9 (CH_3), 61.3 (C-6, CH_2), 67.1 (C-4, CH_3), 67.3 (C-3, CH_3), 73.8 (C-5, CH_3), 98.9 (C-2, CH_3), 145.5 (C-1, CH_3), 169.5 (CH_3CO), 170.4 (CH_3CO), 170.6 (CH_3CO).

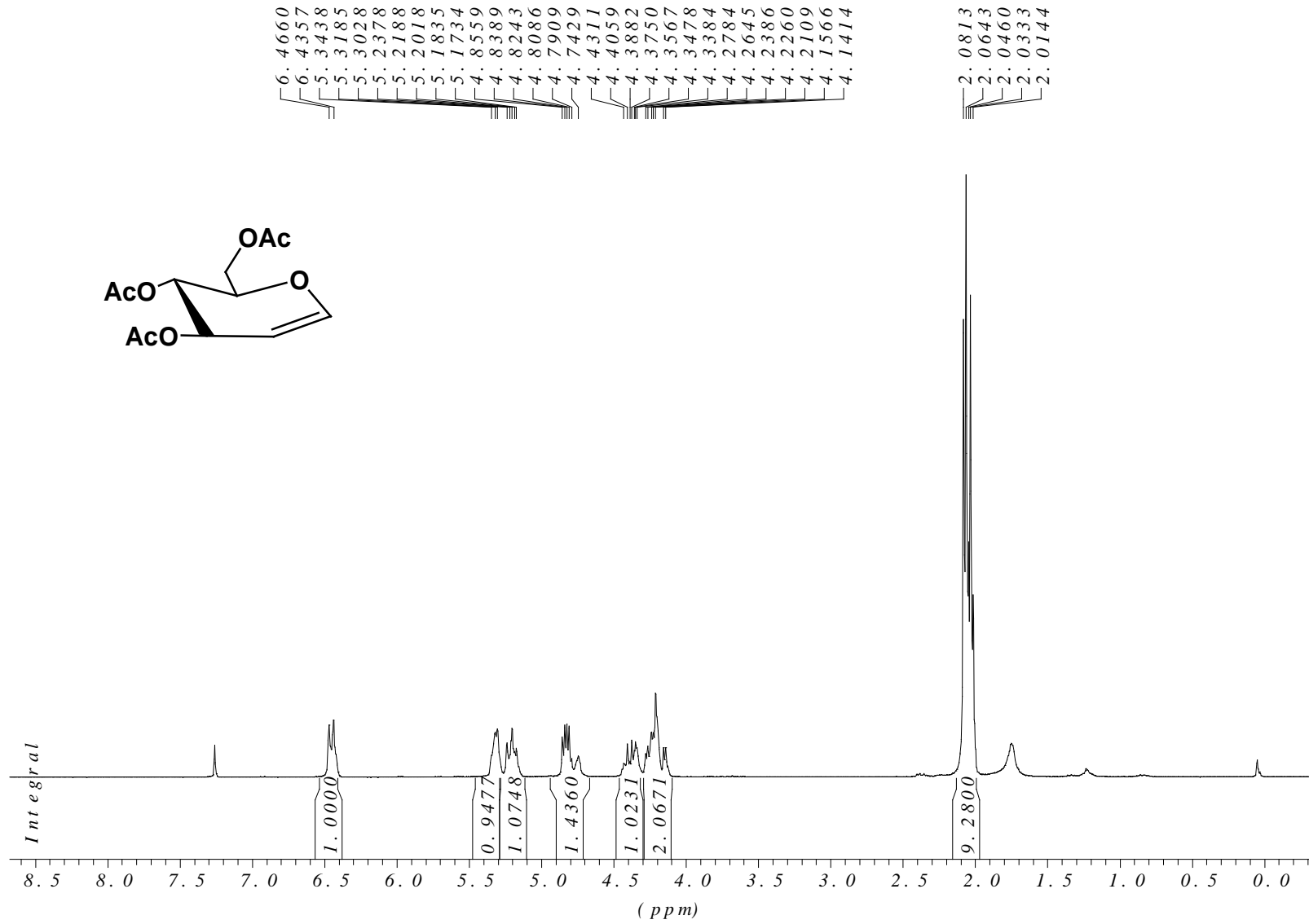


Figure 24 ¹H NMR spectrum of 3,4,6-tri-acetyl-glucal

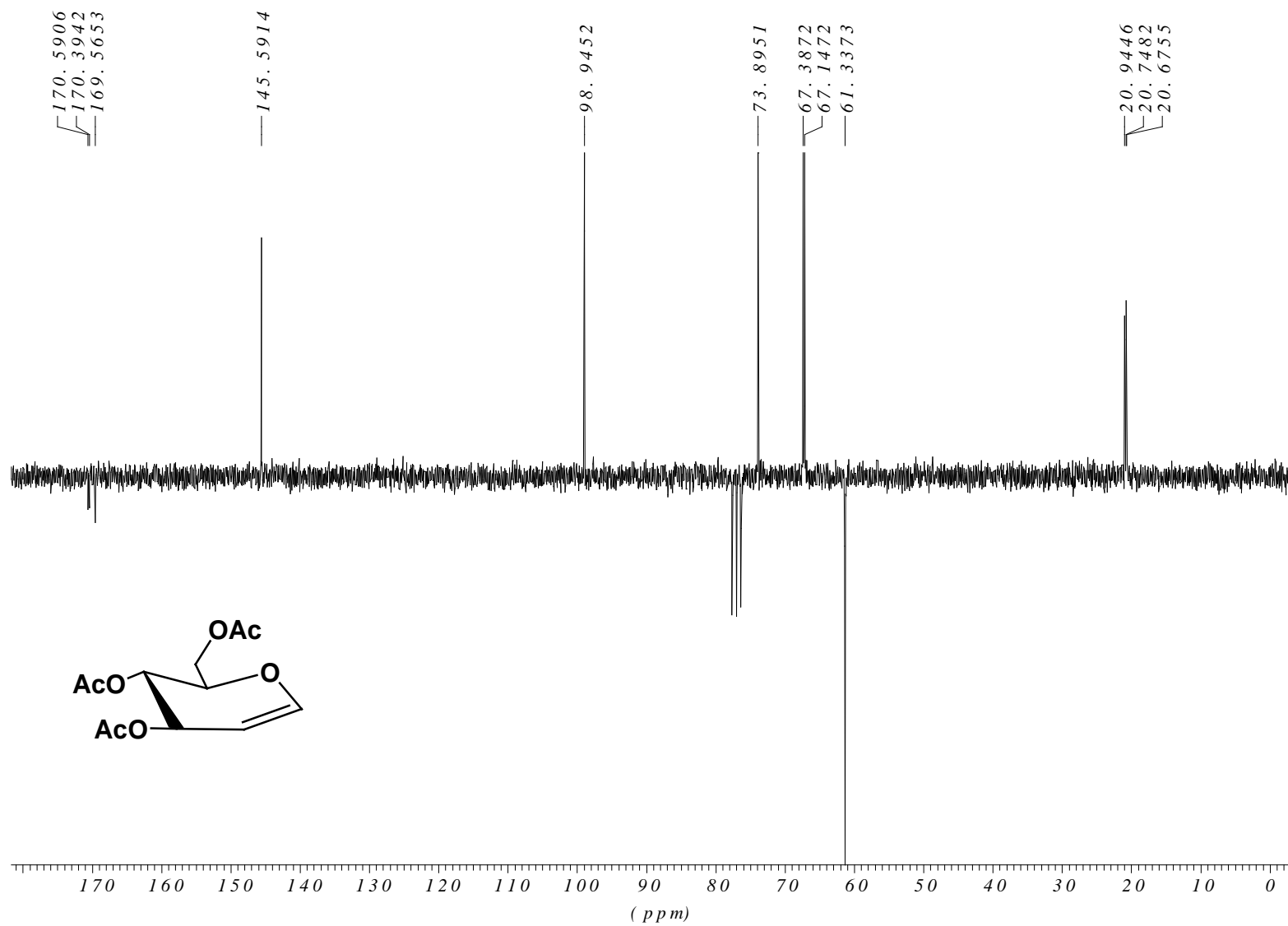
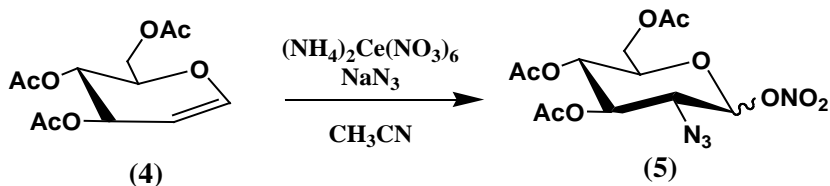


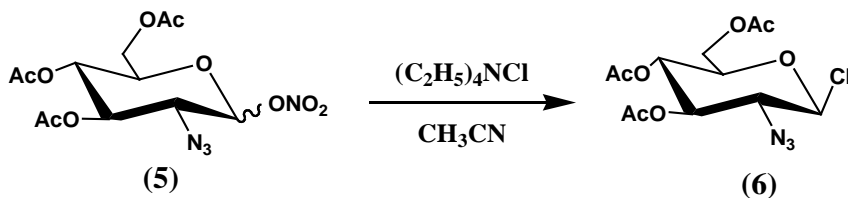
Figure 25 ^{13}C NMR spectrum of 3,4,6-tri-acetyl-glucal

2.2.3 Synthesis of 3,4,6-Tri-O-acetyl-2-azido- α -nitro-D-Glucopyranose³⁸



The Azide glucal was synthesized by following the Lemieux and Radcliffe procedure. Briefly, gltal-(OAc)₃ (1 g, 3.67 mmol, 1.0 equiv), ceric ammonium nitrate (6.03 g, 11.01 mmol, 3 equiv), and NaN_3 (0.36 g, 5.50 mmol, 1.50 equiv) were dissolved in 25 mL of CH_3CN and allowed to react at $-15\text{ }^\circ\text{C}$ in the presence of 2.0 g of 4 Å molecular sieves for 3 h. After 3 h the glycal had been consumed (TLC, $R_f = 0.67$). Afterwards, the reaction mixture was diluted with 25 mL of cold Et_2O and 25 mL of cold H_2O . The product was filtered through Celite and washed 3x20 mL of Et_2O . The organic layer was separated and dried over anhydrous Mg_2SO_4 . The product was purified by Column chromatography with 2:1, EtOAc /hexane. Concentration yielded 0.82 g of yellowish oil.

2.2.4 Synthesis of 2-azido-3,4,6-tri-O-acetyl-2-deoxy- α -Glucopyranose chloride³⁹



The syrupy azidonitration product (0.377 g) was dissolved in acetonitrile (12 mL) which contained tetraethylammonium chloride (0.754 g). After 5 h, the solution was diluted with CH_2Cl_2 (25 mL) and treatment with water (2 x 10mL).

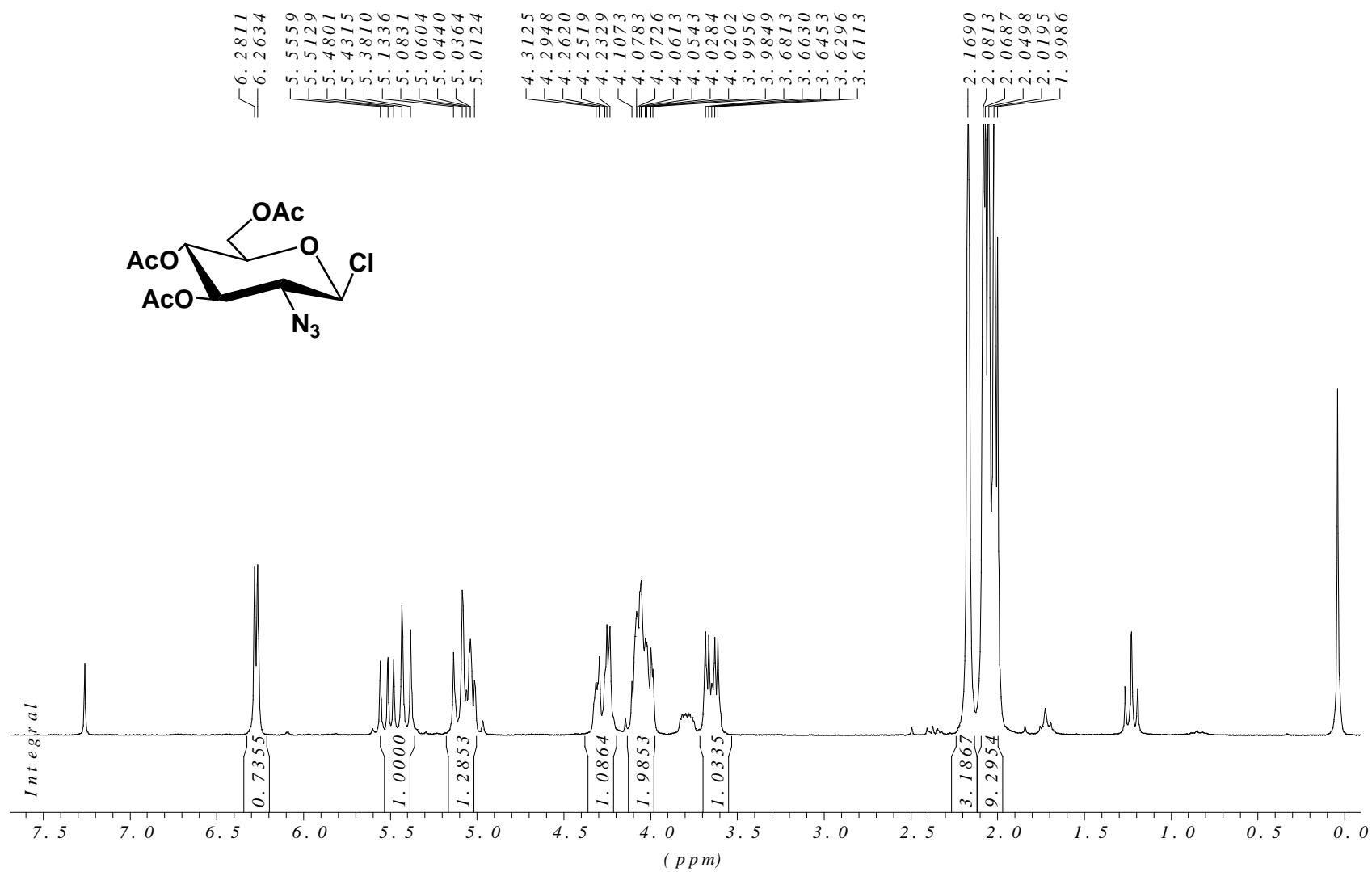


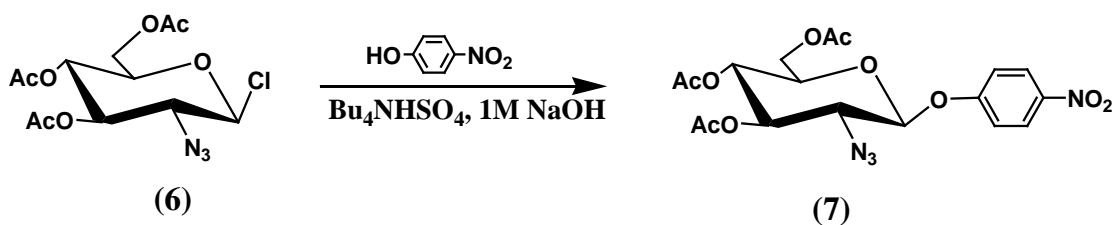
Figure 26 The ^1H NMR spectrum of 2-azido-3,4,6-tri-*O*-acetyl-2-deoxy- α -Glucopyranose chloride

Solvent removal yielded a syrup (0.325 g), which was recrystallized from diethyl ether-pentane finally resulting in the α -D-chloride (0.260 g, 74%). The full characterization can be found in reference⁴⁰. Again, the ¹H NMR spectrum of 2-azido-3,4,6-tri-O-acetyl-2-deoxy- α -Glucopyranose chloride is shown in Figure 26.

$R_f = 0.40$ (TLC developing solution: EtOAc/Hexane = 1/2).

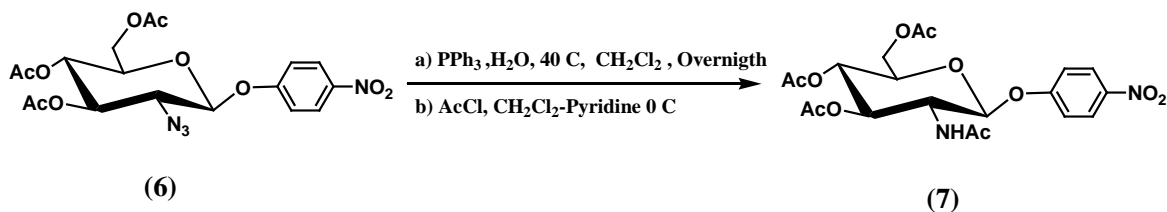
¹H NMR (200 MHz, CDCl₃) δ (ppm) = 2.01-2.08 (m, 9H), 3.64 (dd, J=3.66, 3.66 Hz, 2H), 3.98-4.10 (m, 2H), 4.23-4.31 (m, 1H), 5.01-5.13 (m, 1H), 5.38-5.55 (m, 1H), 6.28 (d, J=3.5 Hz, 1H).

2.2.5 Synthesis of 4-Nitrophenyl 2-azido-3,4,6-tri-O-acetyl-2-deoxy- α -D-Glucopyranose⁴¹



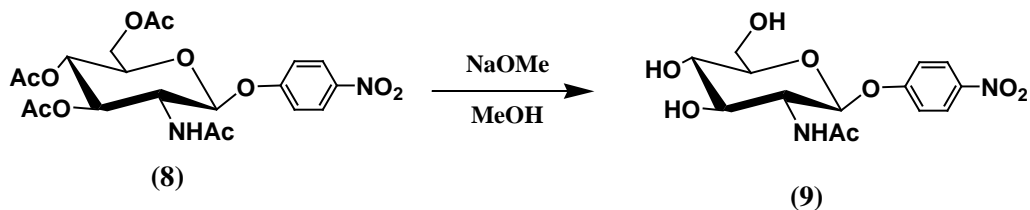
A solution of 2-acetamido-3,4,6-tri-O-acetyl-2-deoxy- β -glucopyranosyl chloride (1 g, 2.86 mmol, 1 equiv), tetrabutylammonium hydrogen sulfate (0.97 g, 9.6 mmol, 1 equiv), and *p*-nitrophenol (1.94 g, 5.72 mmol, 2 equiv) in a mixture of CH₂Cl₂ (15 mL) and 1 M NaOH (15 mL) was stirred vigorously for 1.5 h. The mixture was extracted with CH₂Cl₂ (4 X 50 mL), and washed with 1 M NaOH (4 X 50 mL), water (until the yellow color vanished) and saturated aqueous NaCl (100 mL). The organic phase was dried (Na₂SO₄) and evaporated under reduced pressure to give *p*-nitrophenyl-2-acetamido-3,4,6-tri-O-acetyl-2-deoxy- β -glucopyranoside (0.95 g, 74%), which was crystallized from MeOH-EtOAc.

2.2.6 Synthesis of 4-Nitrophenyl 2-Acetamido-2-deoxy- β -D-Glucopyranose⁴²



Triphenylphosphine (165 mg, 0.63 mmol) was added at a room temperature to a stirred solution of compound 6 (190 mg, 0.42 mmol) in CH_2Cl_2 (10 ml) and the reaction mixture was kept at 40°C . After 4 h water (10 ml) was added and the stirring was continued overnight. The organic phase was separated, concentrated, and co-evaporated twice with toluene. The residue was dissolved in CH_2Cl_2 -pyridine (1:1, 10 ml) and acetyl chloride (45 μl , 0.63 mmol) was added at 0°C . After 1 h the mixture was concentrated and co-evaporated *p*-Nitrophenyl-2-acetamido-2-deoxy-*D*-mannopyranosides twice with toluene. The residue obtained after evaporation was chromatographed (CH_2Cl_2 -EtOAc, 2:3) to afford compound 7 (167 mg, 57%), in form of yellowish solid.

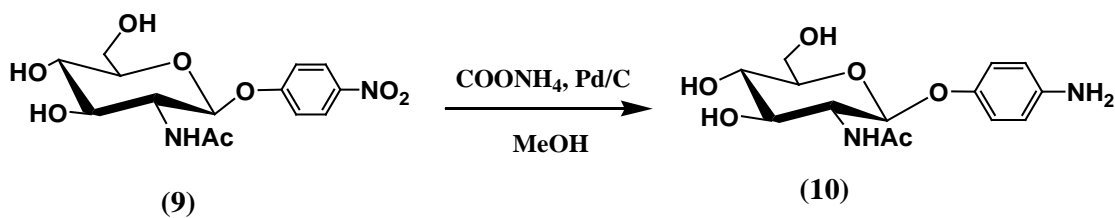
2.2.7 Synthesis of 4-Nitrophenyl 2-Acetamido-2-deoxy- α -D-mannopyranoside⁴²



Compound 8 (50 mg, 0.11 mmol) was dissolved in methanol (5 ml), sodium methoxide (2 M in methanol) was added, and the mixture was stirred for 2 h until the

complete conversion of Compound 9 (TLC; CH₂Cl₂-EtOAc, 1:4). The reaction mixture was neutralized with Dowex 50W-X2 (hydrogen form), filtered and concentrated to give 14 (35 mg, 94%) as a white solid.

2.2.8 Synthesis of *p*-Aminophenyl-2-Acetamido-2-deoxy- β -D-glucopyranoside (*p*-aminophenyl-GlcNAc)



p-aminophenyl-*N*-acetylglucosamine was prepared from *p*-nitro-*N*-acetylglucosamine (*p*NP-GlcNAc) 50 mg (0.146 mmol) of *p*NP-GlcNAc was dissolved in 10 ml of MeOH containing 10% Pd/C (10.6 mg, 0.0146 mmol) as a catalyst as well as ammonium formate (147 mg, 2.336 mmol). The reaction mixture was stirred and gently warmed for 2 hr. The reaction was confirmed by TLC in methanol and dichloromethane with 3:1 ratio. Then, the mixture was cooled down to room temperature. The product was then filtered through a pad of Celite and concentrated under reduced pressure. The crude residue was purified by flash column chromatography on silica gel (10% MeOH) to give the desired product as white solid (42 mg, 92.2%). The full characteristic of *p*-Aminophenyl-2-Acetamido-2-deoxy- β -D-glucopyranoside is shown in Figure 27 and Figure 28.

¹H NMR (200 MHz, DMSO-d₆): δ (ppm) = 1.95 (s, 3 H), 3.51-3.86 (m, 5H), (br, s, 2H), 4.84 (d, J=8.34 Hz, 2H), 5.08 (br, s, 2H), 6.61 (d, J=8.7 Hz, 2H), 6.82 (d, J=8.7 Hz, 2H), 7.91 (d, J= 8.8 Hz, 1H).

¹³C (50 MHz, DMSO-d₆): δ (ppm) = 21.2 (CH₃), 53.8 (CH₃), 59.1 (CH₂, C-6), 68.6 (CH₃), 72.3 (CH₃), 75.1 (CH₃), 99.1 (CH₃), 112.8 (CH₃), 116.0 (CH₃), 141.6 (CH₃), 147.4 (CH₃), 167.5 (CH₃).

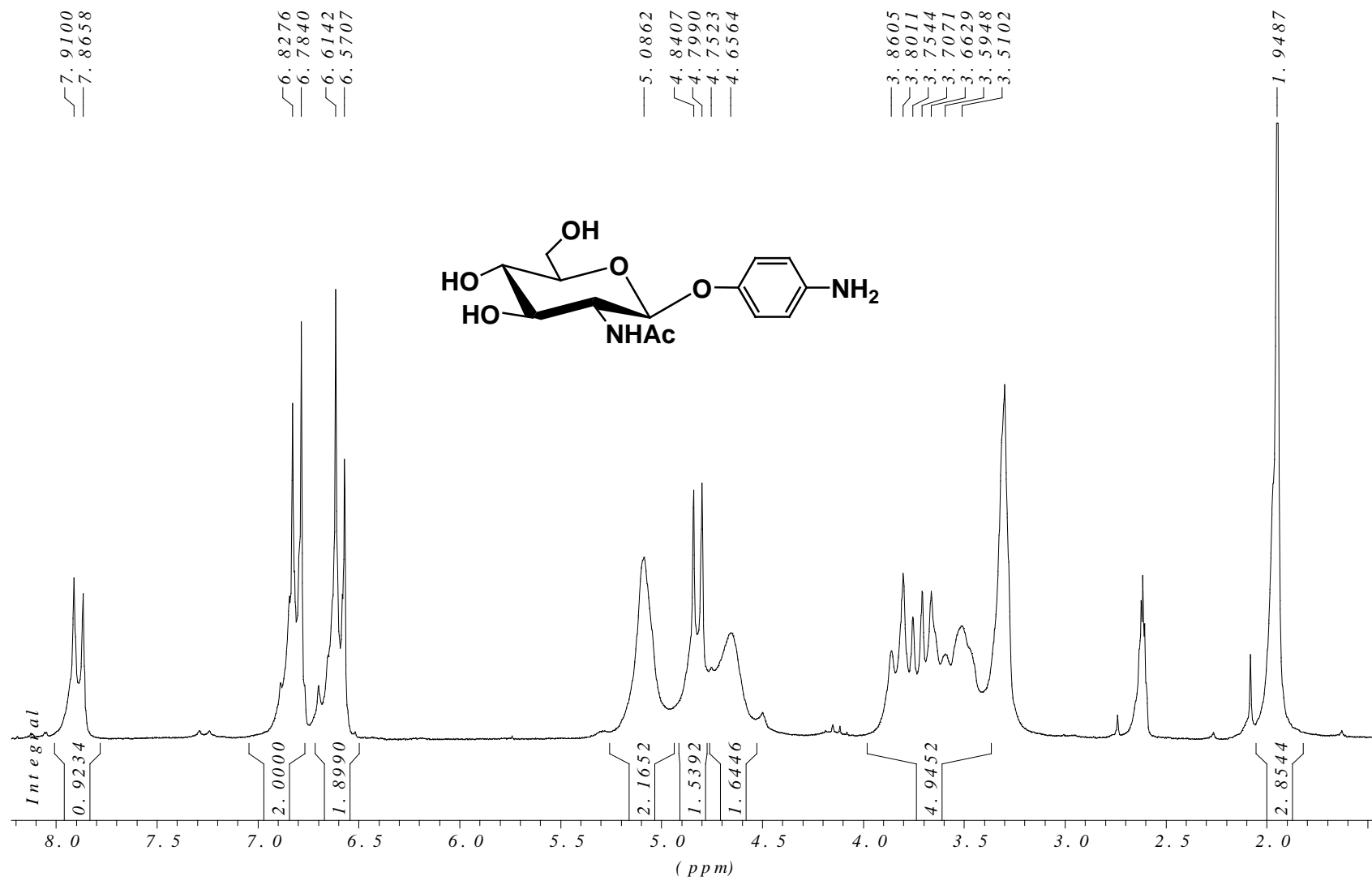


Figure 27 The ^1H NMR spectrum of *p*-Aminophenyl-2-Acetamido-2-deoxy- β -D-glucopyranoside

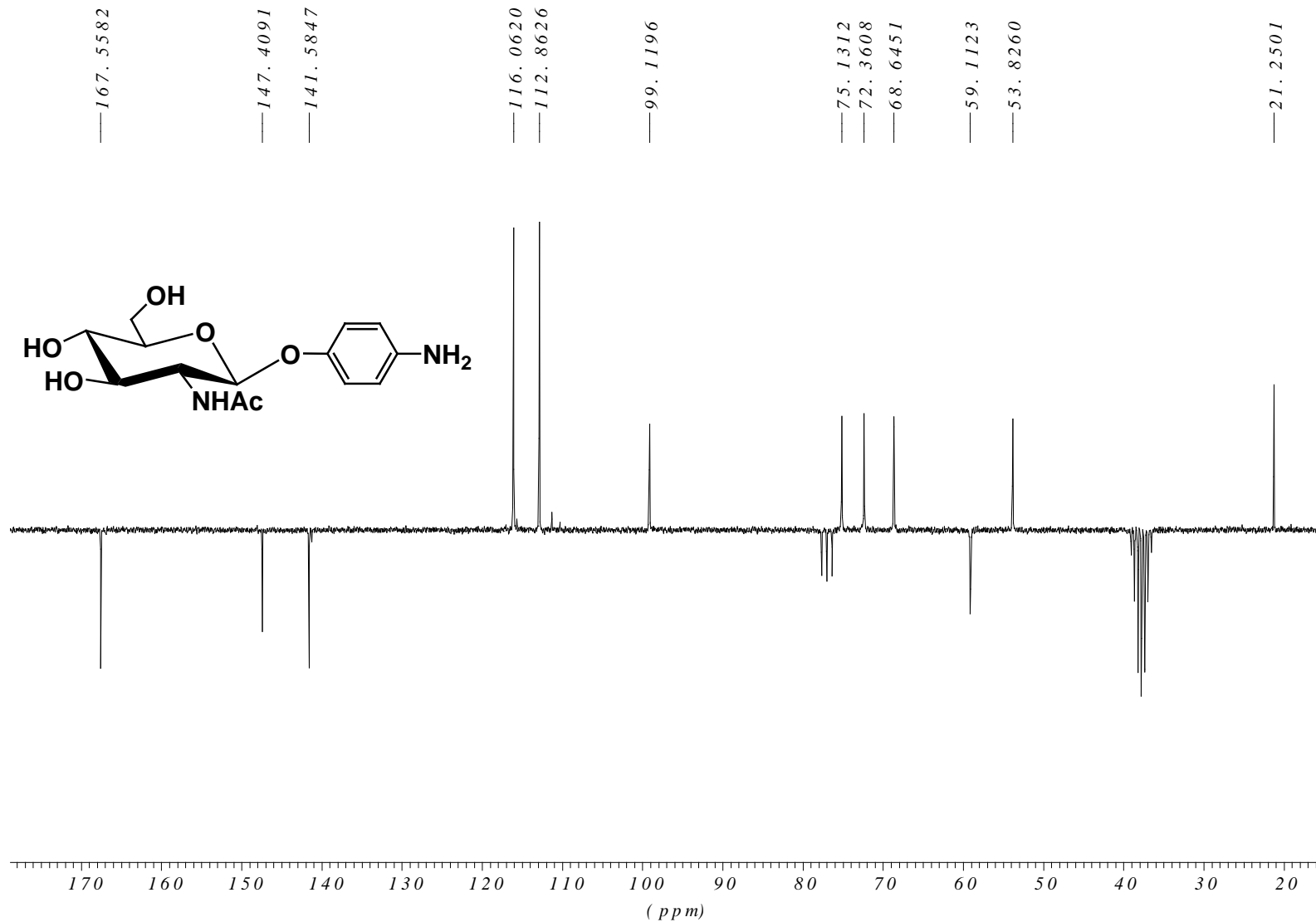
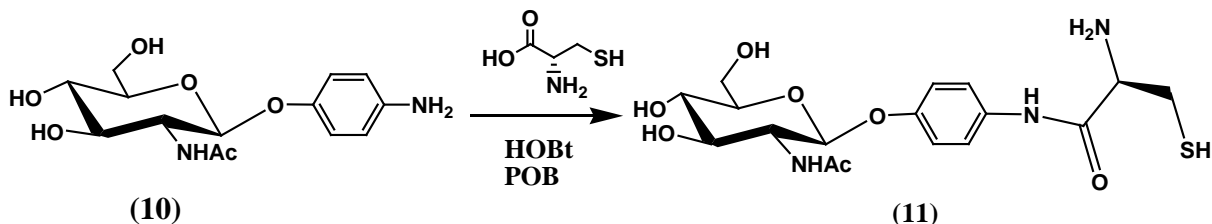


Figure 28 The ^{13}C NMR spectrum of *p*-Aminophenyl-2-Acetamido-2-deoxy- β -D-glucopyranoside

2.2.9 Cysteine- *p*-aminophenyl-GlcNAc



p-aminophenyl-GlcNAc (30 mg, 0.088 mmol) was dissolved in Dimethyl sulfoxide (DMSO) (5 mL); then cysteine (32 mg, 0.264 mmol), HOBt (24 mg, 0.176 mmol) and BOP (195 mg, 0.44 mmol) were added. This reaction mixture was stirred at room temperature for 1 hr or until TLC showed that the reaction was complete. The crude product was used without purification.

2.3 Immobilization of the artificial receptor analogue on QCM surfaces

Cysteine-*p*-aminophenyl-GlcNAc (0.01 mM) was directly immobilized by dropping 5 μ l onto the future working electrode. Afterward, the gold electrode was left at room temperature for 2 hours followed by washing out the excess molecules on the surface by rinsing 3 times with ethanol. For the purpose of using cysteine molecules acting as spacer, cysteine-*p*-aminophenyl-GlcNAc (0.01 mM) was mixed with 10 mM of cysteine following by directly immobilized the mixture on gold electrode. 5 μ l of this mixture was dropped on gold electrodes and left for 2 hours at room temperature. In parallel, reference electrodes were modified by 5 μ l of cysteine 10 mM for 2 hours at room temperature. Sketches of both modified electrodes are shown in Figure 29. Afterwards, both electrodes were rinsed with water and ethanol to remove excess residues and dried under N_2 gas for 30 minutes.

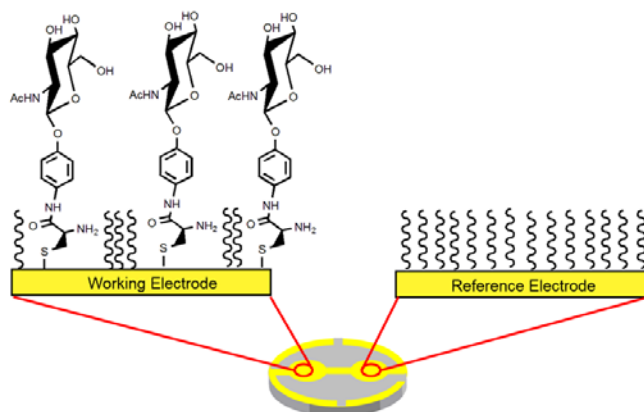


Figure 29 Working electrode modified with cysteine-*p*-aminophenyl-GlcNAc and reference electrode with modified cysteine, respectively

2.4 Molecularly imprinted polymer (MIP) preparation

The affinity of polymer recognition depends on the interaction between functional groups of monomer and cross linker. As the H-bond is the major interaction in biomolecules, it was considered having the highest priority in finding suitable monomers followed by sites addressing hydrophobic and hydrophilic interaction, respectively. Hence, the starting point was to select acrylamide and methacrylic acid as monomers, because they contain the amide and the carboxylic group, respectively, which can form H-bonds with the amino groups of the protein surface. As the most frequent amino acids of WGA are glycine and cysteine, an extra monomer is needed to support hydrophobic interactions. For this purpose, the first choices were butyl methacrylate and methyl methacrylate. Finally, the monomer ratio was optimized. As the cross linker, *N,N'*-(1,2-dihydroxyethylene) bisacrylamide was applied, as its properties turned out to be suitable for protein detection and this copolymer system.

2.4.1 General polymer synthesis

For synthesizing the copolymer, we mixed monomers; acrylamide, methacrylic acid and butylmethacrylate or methylmethacrylate and *N,N'*-(1,2-dihydroxyethylene) bisacrylamide as the cross-linker. Those components were dissolved together with 1 mg of 2,2'-azobis(isobutyronitrile) as the initiator in 300 μ l of dimethyl sulfoxide. This was then followed by prepolymerization at 70 °C for 1 h until the gel point was approached. Afterward, this prepolymer could be immediately used. The detailed monomer ratios are discussed in the result section beginning in chapter 4 on polymer optimization.

2.4.2 Stamp preparation

The template stamps were prepared by immobilizing WGA on a glass substrate by sedimentation from phosphate-buffered saline (PBS; pH 7.4): 5 μ l of WGA solution (0.5 mg/ml) was drop-coated onto 5 \times 5 mm² glass plates. To avoid buffer recrystallization, the coated substrate was kept at 4°C for 30 min followed by spinning off the stamp at 3000 rpm to remove an excess solution. Finally, these stamps could directly be used for molecular imprinting.

2.4.3 Preparation of MIP-coated QCM

The stamping procedure is illustrated in Figure 30 following by spin-coated the prepolymer onto both QCM electrodes. 5 μ l of the mixture is dropped onto the respective electrode and then spun off at 3000 rpm for 10 seconds to obtain thin layer in the range of 250-350 nm thickness. Immediately after this, the stamp was pressed onto the polymer and left to polymerize overnight under UV light at 254 nm. To remove the template, the QCM was finally stirred in water at room temperature for 2 h. Finally, this resulted in rigid, hardly swellable polymers that can readily be applied as sensor coatings for the QCM.

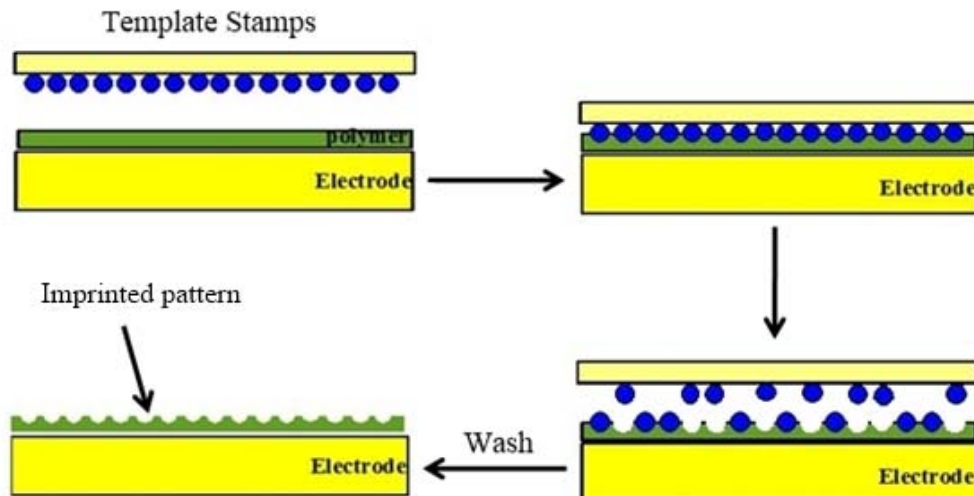


Figure 30 Procedure for protein molecularly imprinted polymer on quartz crystal microbalance by using surface imprinting technique.

2.4.4 QCM measurements

All QCM measurements were performed on 10 MHz AT-cut QCM in a custom-made measuring cell of 75 μl volume cast from poly(dimethylsiloxane) at room temperature in stop-flow mode. The QCM connected to an oscillator circuit and it connected to frequency counter (Agilent 53131A) then read out by custom-made Labview routine via a GPIB USB interface. During a typical measurement, the QCM was mounted in the cell followed by filling with PBS (10 mM, pH 7.4) and measuring the resonance frequency until stable signal had been reached. Then, the PBS was removed by flushing of analyte into the measuring cell two time followed by injecting the fresh analyte and restarting the measurement. After again reaching the constant value of frequency, the analyte was removed followed by flushing once with a washing solution (10% sodium dodecyl sulfate and 10% acetic acid or 3M of NaCl and 0.5M of NaOH) and three times PBS (10 mM, pH 7.4). Finally, we filled the measuring chamber with PBS (10 mM, pH 7.4) and started recording the frequency.

2.4.5 Scanning tunnelling microscopy (STM) analysis

In order to verify the sensitive surface in both cases - artificial receptor and MIP - high-resolution images were recorded with a Veeco Nanoscope IVa operated in scanning tunneling microscope (STM) mode (Figure 31).

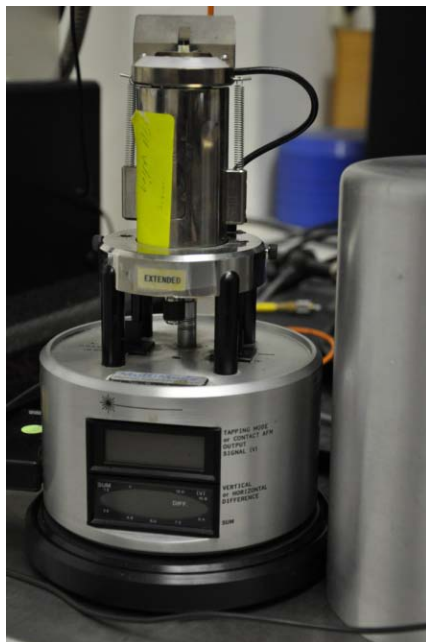


Figure 31 The scanning tunneling microscope

For visualizing the immobilized receptor analogue, STM measuring parameters were 500 mV voltage bias and a current set point of 50 pA. We started to record surfaces covered only with cysteine and comparing those with cysteine-receptor mixture films afterwards. In the next step, different concentrations of WGA were dropped onto the surface modified with artificial receptor analog for testing interaction. For this purpose, we used two concentrations, namely 10 $\mu\text{g/ml}$ and 80 $\mu\text{g/ml}$ respectively.

STM for molecularly imprinted polymer

Prior to obtaining the images, we needed a conducting surface for STM measurement. This, we generated by sputtering both MIP and their nonimprinted counterparts with approximately 40 nm of gold. The sample-pretreatment procedure is summarized in Figure 32.

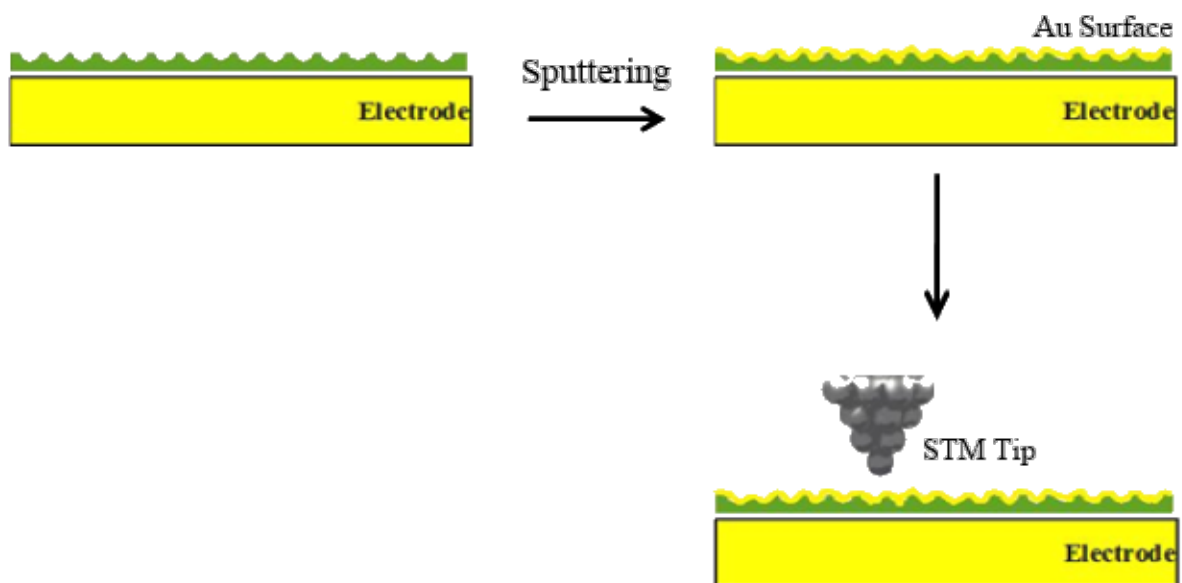


Figure 32 Procedure for generating protein imprint image by STM.

For this purpose, we placed both MIP and NIP polymer in a Cressington 208HR Turbo Sputter, which is a magnetron based system allowing for process pressures of 0.02 mbar. Afterwards, gold is homogeneously deposited on the polymer surface. During the process, planetary rotation of the sample head was turned on. Both the operation pressure and this motion lets one validly assume that surface structures are evenly coated and thus are correctly reproduced by the conducting film surface. The STM measuring parameters were a voltage bias of 500 mV and a current set point of 50 pA.

Chapter 3

GlcNAc receptor analogue as recognition element

As previously mentioned, the simplest model for a WGA receptor is given by GlcNAc, the “monomeric” N-acetyl glucosamine. Therefore, natural β -(1,4)-linked GlcNAc was mimicked by nitrophenol-(1,4)-GlcNAc, because it is synthetically rather simple to prepare and has similar polarity and linkage as the natural compound, which should guarantee high affinity recognition. To ensure covalent binding of this receptor system on the sensor surface, we furthermore reduced the nitro group of the nitrophenol to NH_2 and derivatized it with cysteine. This offers an SH functionality that is able to bind covalently to the gold surface.

3.1 Synthesis of Receptor analogue

In order to investigate carbohydrate-lectin interaction, various strategies have been developed^{15, 43-48}. Regioselectivity is a well-known problem in carbohydrate chemistry, as saccharides usually contain several hydroxyl groups which often differ substantially in reactivity. Therefore, strategies of protecting group, deprotecting group and selection of specific position in carbohydrate synthesis are crucial importance and have been developed⁴⁹⁻⁵⁴. In this study, the preparation of *N*-acetyl- β -D-glucosamine for WGA binding investigation on QCM by peptide coupling reagent has been developed.

The overall synthesis pathway is already mentioned in the experimental chapter 2, see Figure 23. Our synthesis route started from a basic monosaccharide as glucose **1** which is commercially easily available. Per-acetylation was started to protect the hydroxyl groups then followed by transformation into glucosyl bromide **3**. Afterwards, glucosyl bromide was

subsequently treated with zinc in acetic acid, which yielded acetylated D-glucal **4** that can in turn be transformed to azidenitration by the procedure proposed Lemieux and Radcliffe^{39, 55}. This step yields a mixture of two gluco-epimers which can be separated by column chromatography. The α -chloride **6** was readily obtained in crystalline shape by replacement of the nitrate group of compound **5** using an appropriate soluble halide salt which already reported by Lemieux and Hayami⁵⁵. Finally, p-nitrophenol was added by phase transfer reaction to yields compound **7** followed by converting azide group to acetate group using triphenylphosphine. Subsequent peracetylation following by O-deacetylation finally resulted in compound **9**.

3.2 Immobilization of Receptor Analogue on QCM

3.2.1 Artificial receptor analogue preparations

The *N*-Acetylglucosamine (GlcNAc) moiety was modified in 2 steps, namely reduction and amidation. In the first step, the nitro group of *p*NP-GlcNAc was reduced to an amino group (~90% yield) by ammonium formate in the presence of 10% Pd/C as a catalyst. In the second step, the amino group of glycoside was coupled with the carboxylic group of cysteine in presence of benzotriazole-*l*-yl-oxy-tris-(dimethylamino)-phosphonium hexafluorophosphate (BOP) and *N*-Hydroxybenzotriazole (HOBt) as peptide coupling reagent. After the completion of the reaction, TLC shows two product spots. The reason for this is that a coupling reaction between the amino group of one cysteine molecule and the carboxylic group of another cysteine molecule may also occur as a side reaction. Therefore, excess amount of cysteine was used to overcome this problem. Then, the obtained crude product was used without purification for immobilizing an electrode, since the side product and unconsumed cysteine can serve as spacers needed to separate the receptors laterally one from another.

3.2.2 Optimization of artificial receptor immobilization

In principle, monolayer surfaces are needed for protein-receptor binding because the simple binding mechanism leads to a one-to-one adduct, which means that sensitivity has to be kept in mind. Theoretically, it therefore could be interesting to deposit a monolayer of artificial receptor on the gold surface of this reason. However, during immobilization the receptor density per surface area has to be suitable for WGA binding. In the ideal case, every two receptor molecules should be separated from one other in range of the protein dimensions. In this work, the analyte is WGA lectin, which its dimensions of $14 \text{ nm} \times 9.5 \text{ nm} \times 4 \text{ nm}$. This means that a gold electrode of 5 mm diameter should contain $\sim 10^{11}$ molecules of artificial receptor to achieve a dense monolayer of WGA and thus ensure optimal binding. However, a monolayer of the artificial receptor consists of approximately 5×10^{14} molecules, which is 1000 times more than needed for optimal binding. Furthermore, a dense monolayer of the receptor prevents optimal interaction between individual molecules and the binding pocket in WGA. Due to this sterical reason, spacers between each receptor are needed for separating them from one another. Choosing the spacer requires to carefully consider the rate of adsorption between spacer molecule and artificial receptor. Ideally, they should be the same. Due to this reason, cysteine is selected as spacer because it is the part of the receptor that forms covalent bond to the gold surface. Therefore, the mixture of cysteine and artificial receptors were immobilized on the working electrode while only cysteine was immobilized on the reference electrode. Such a coating on the reference electrode ensured that indeed only the effects caused by the receptor are measured on the QCM, because cystein in principle can also interact with WGA lectin via H-bond interaction via the amino group.

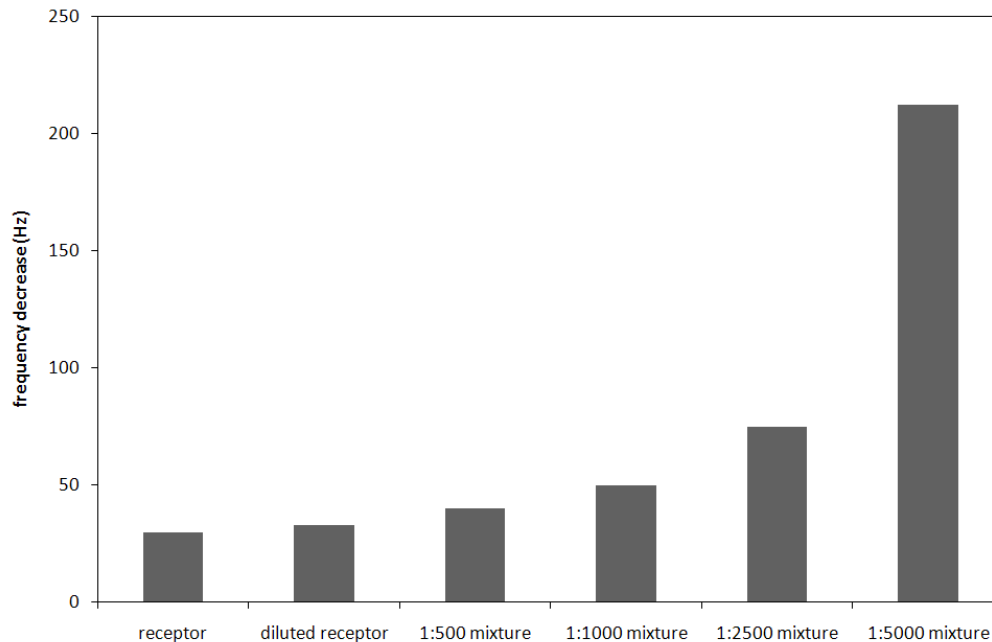


Figure 33 Sensor signal of GlcNAc obtained from different immobilization condition

Afterwards, modified QCM was installed into the measuring cell for recognizing WGA lectin. Figure 33 shows the outcome for a range of recognition materials when exposed to 160 $\mu\text{g/ml}$ WGA lectin. As can be seen in the first column, the frequency decreases only by 30 Hz (which is far lower than the response resulting from a WGA monolayer (216 Hz)), when only the receptor analogue is immobilized. This result clearly supports the idea that each receptor has to be separated from the others. Obviously, the density of receptor layer has an effect on sensor sensitivity. When the coating solution containing the receptor is further diluted with DMSO, QCM responses for WGA still remain similar, because again a monolayer of artificial receptor is deposited on the surface. The idea of a utilizing a spacer is strongly supported by the third column in Figure 33. Obviously, the frequency change is increased when cysteine was mixed to artificial receptor in ratio of 1+500 (receptor+cysteine). Furthermore, the sensitivity also increased when we increased the mixture ratio from 1+500 to 1+1000, 1+2500 and 1+5000, respectively. Frequency shifts were increased from ~ 30 Hz (without cysteine as a spacer) to ~ 210 Hz (1:5000 ratio of artificial receptor/cysteine). Due to the free space between every two receptor molecules,

there is sufficient WGA binding leading to enhanced sensitivity. Figure 34 shows a sketch of the expected effects.

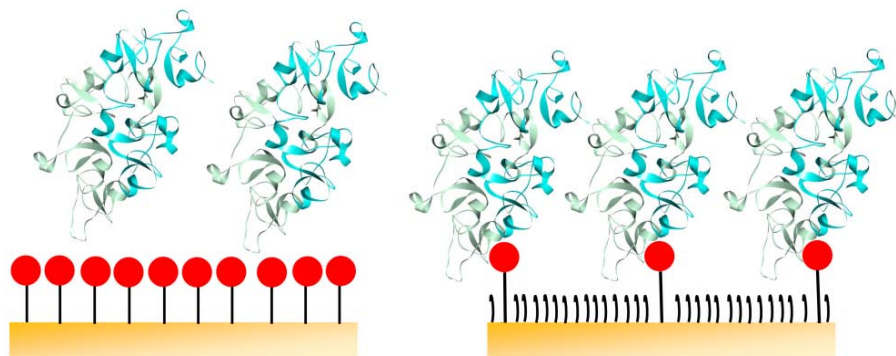


Figure 34 The binding of WGA on immobilized receptor on gold electrode

3.2.3 STM analysis of immobilized receptor

In a first step, we verified the surface immobilization steps of receptor by scanning tunneling microscopy (STM). STM is performed on 3 different surfaces including gold surface, gold surface modified with cysteine (i.e. the reference system in QCM measurements) and gold surface with mixture of cysteine and receptor. Figure 35 shows the outcome of this approach: it summarizes the STM images of the abovementioned three surfaces. As can be seen in Figure 35a, the unmodified gold surface is smooth showing a roughness of less than 0.7 nm. However, the gold surface with immobilized cysteine shows roughness with roughly 1 nm in height (Figure 35b) which corresponds to approximately the length of individual cysteine molecules. In contrast to this, the gold surface with immobilized GlcNAc-chain receptor as depicted in Figure 35c yields small granules with about 3 nm in height that correspond to the approximate size of GlcNAc-Chain receptor. Therefore, one can validly assume that immobilization has been successful.

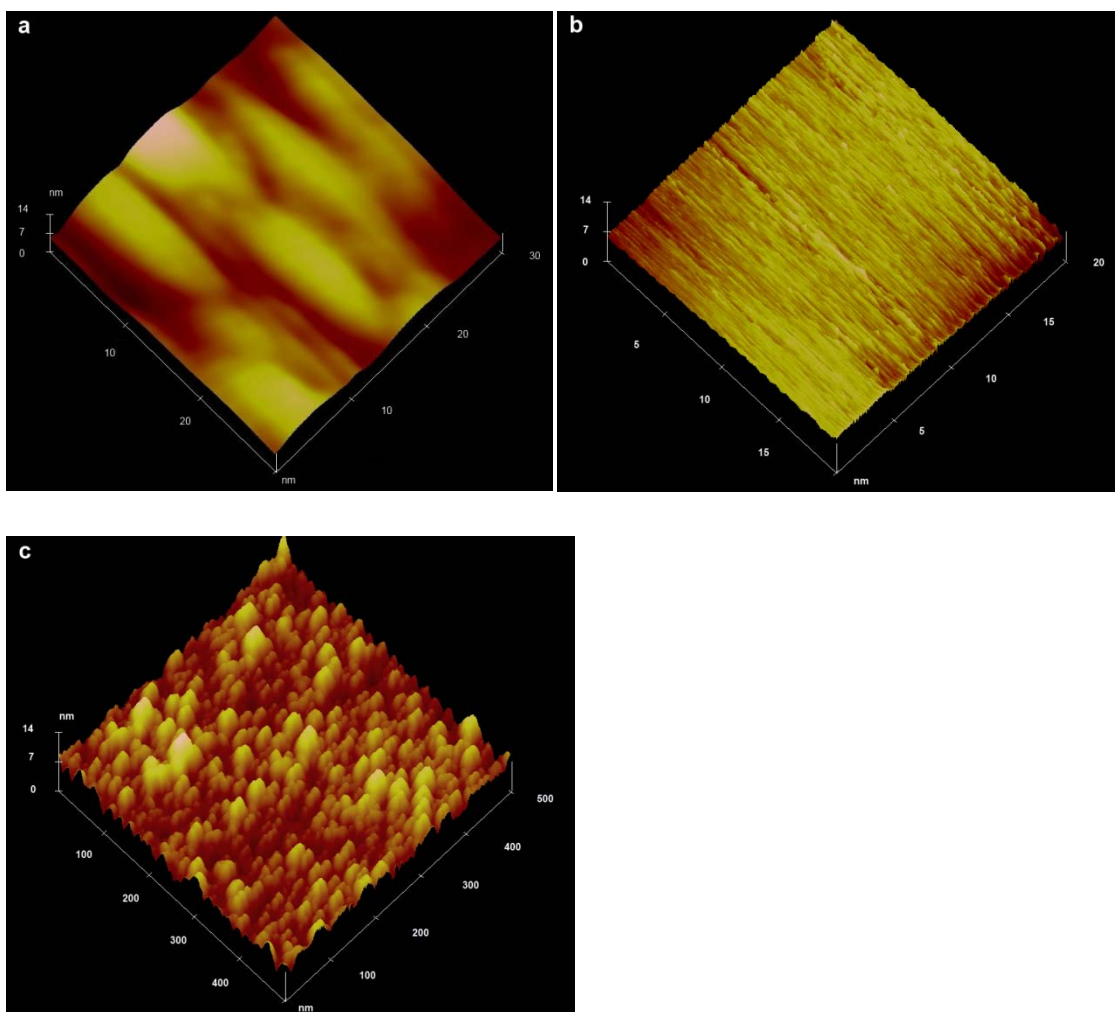


Figure 35 STM images of three different surfaces, namely, pure gold (a), gold surface with cysteine (b) and gold surface with GlcNAc-chain receptor (c), respectively, with voltage bias 500 mV and current setpoint at 67 pA

In the next step, we exposed the surfaces to solutions containing two different concentrations of WGA lectin (10 $\mu\text{g/ml}$ and 80 $\mu\text{g/ml}$, respectively) and again recorded STM images of the resulting surfaces after the excess WGA lectin was removed by rinsing with water, which is summarized in Figure 41 with 500 x 500 nm in size. Both images show structure with lateral dimensions somewhat larger than 50 nm and a height of 14 nm that agglomerate. These dimensions correspond quite well to the size of WGA lectin forming surface aggregates. Moreover, it is also evident that the amount of immobilized WGA lectin

depends on concentration: in Figure 36a (expose to the solution containing 10 $\mu\text{g/ml}$) the amount of bound molecules is much lower than for the higher concentration (80 $\mu\text{g/ml}$). In the second case, hardly any unoccupied sites can be seen and almost of the surface is covered by WGA lectin (as marked by dark circles in Figure 36b).

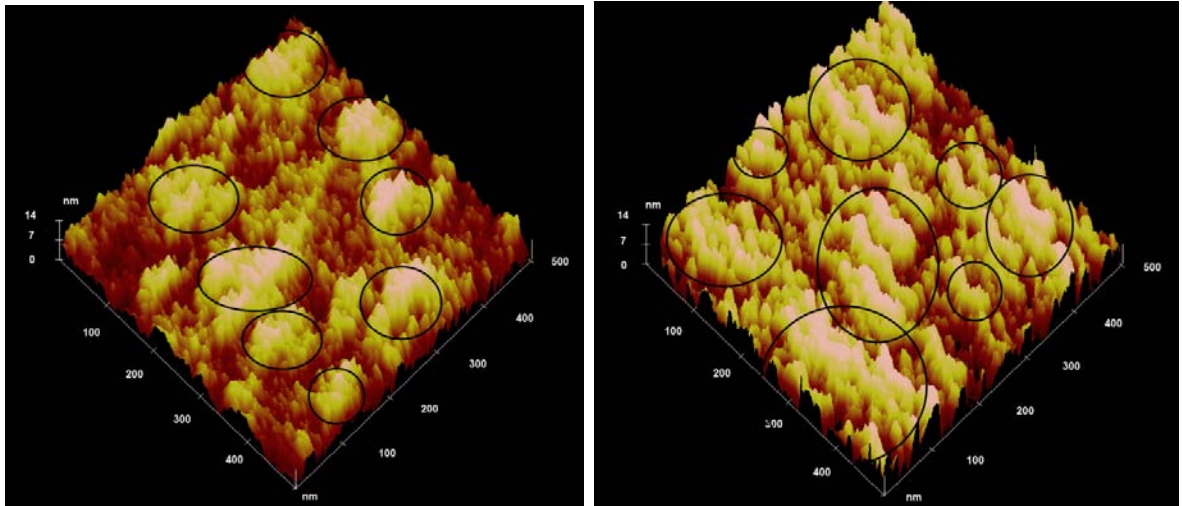


Figure 36 STM image of gold surface with artificial receptor and WGA lectin at 10 $\mu\text{g/ml}$ (left) and 80 $\mu\text{g/ml}$ (right). The aggregation of WGA lectin bound to the surface is indicated by dark circles

3.3 QCM recognition and analysis

Obviously, STM studies indicate the binding ability between GlcNAc-chain receptor and WGA lectin, which we therefore assessed by QCM. The outcome of this approach is depicted in Figure 37: after reaching constant frequency on the QCM, which lasted for about 15 minutes, we exposed the device to 160 $\mu\text{g/ml}$ of WGA.

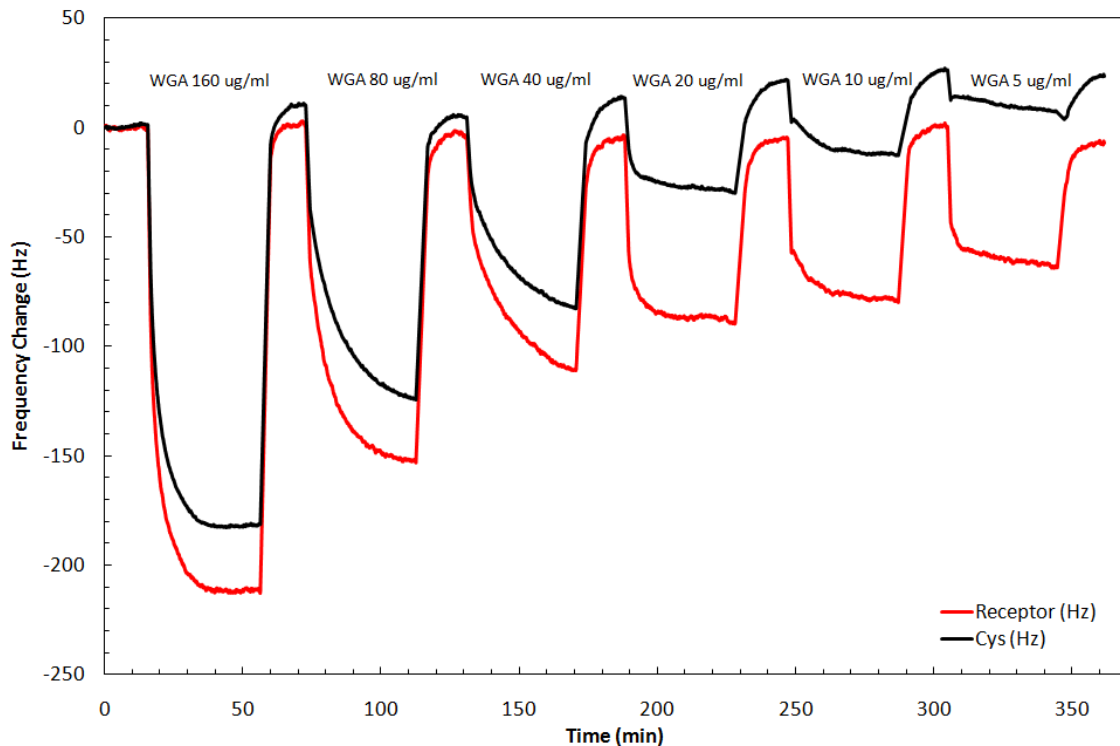


Figure 37 Quartz crystal microbalance (QCM) sensor responses of immobilized receptor and reference electrode towards different WGA concentrations at 25 °C

Immediately, the frequency decreased by 210 Hz on the electrode containing the immobilized GlcNAc-chain receptor, while the reference electrode yielded a response of -180 Hz. Therefore, the difference in frequency shift between both electrodes is only 30 Hz and in both cases WGA forms nearly a monolayer on the surface, which would correspond to -216 Hz. Apparently, the reason that the reference electrode responds very similarly to the measuring electrode is the cysteine coating: its amino groups can interact with WGA via hydrogen bonding at amide and carboxylic groups. In contrast to this, at low WGA solution concentration (5 µg/ml), the working electrode exhibits substantially larger frequency shifts than the reference electrode. Both signals indicate that the coverage of WGA on the surface is by far less than a monolayer. The difference in signal between both electrodes is increased from 30 Hz at 160 µg/ml to 50 Hz (compared to an overall frequency shift of 65 Hz on the measuring electrode). This means that the synthetic receptor indeed substantially increases the binding affinity of the surface towards WGA leading to larger responses on the QCM

already at lower solution concentrations. In contrast to this, at higher concentrations there is no thermodynamic gain by the selective recognition. Anyway, both response characteristics indicate mass uptake according to the Sauerbrey theory. Furthermore, the signal of both channels can be reverted by washing the electrodes with 0.5 M NaOH and 3 M NaCl (which leads to the dynamic response behavior of the QCM after the WGA has been removed). Finally, the frequency shifts also depend on WGA concentration, thus proving the suitability of the approach in the design of a selective sensor system.

To gain deeper insight into the binding properties, we calculated the number of adsorbed molecules and number WGA layers adsorbed on the sensor calculated from Sauerbrey equation (6).

$$\Delta f = -c\Delta m \quad (6)$$

Where c equal to 4.61 Hz/ng

According to the estimated WGA size, the maximum of WGA on electrode is 7.85×10^{11} molecules. Due to the frequency change on QCM and Sauerbrey equation, we calculated the number of WGA molecule and number of WGA layers. The results of calculation are shown in Table 2, which confirms that maximum a monolayer of WGA occurs on the receptor surfaces. However, the difference at low concentration of course reveals that immobilizing the receptor analogue indeed substantially increases the affinity of the electrode as compared to the pure cystein layer. Basically, the interaction is therefore still mainly governed by the specific interaction between GlcNAc and WGA lectin.

Table 2 Amount of WGA monolayers adsorbed by cystein and receptor, respectively

Stock concentration (ug/ml)	cystein	receptor
160	0.84	0.98
80	0.57	0.72
40	0.38	0.52
20	0.20	0.41
10	0.15	0.35
5	0.07	0.30

To test selectivity, BSA was applied as competing analyte, as it belongs to a class of compounds ubiquitously present in mammalian sera and has small affinity bind to GlcNAc-chain. Figure 38 gives the frequency response between GlcNAc-electrode and cysteine-electrode of 160 $\mu\text{g/ml}$ of BSA. For this purpose, we exposed dual channel QCM coated with GlcNAc and cysteine, respectively, to 160 $\mu\text{g/ml}$ of BSA in PBS (pH.7.4); immediately the frequency decreased in both channel following the mass amount uptake to electrode surface. The response amounted to 32 Hz with the GlcNAc-coated electrode and 5 Hz on the cysteine electrode. Compared to these shifts, WGA at 160 $\mu\text{g/ml}$ leads to much larger signals than BSA. This result verifies that the GlcNAc modified electrode is selective to the analyte protein. Generally, the frequency change of BSA occurs because of the formation of unspecific hydrogen bonds between the hydroxyl groups of GlcNAc and amide or carboxyl groups of amino acid.

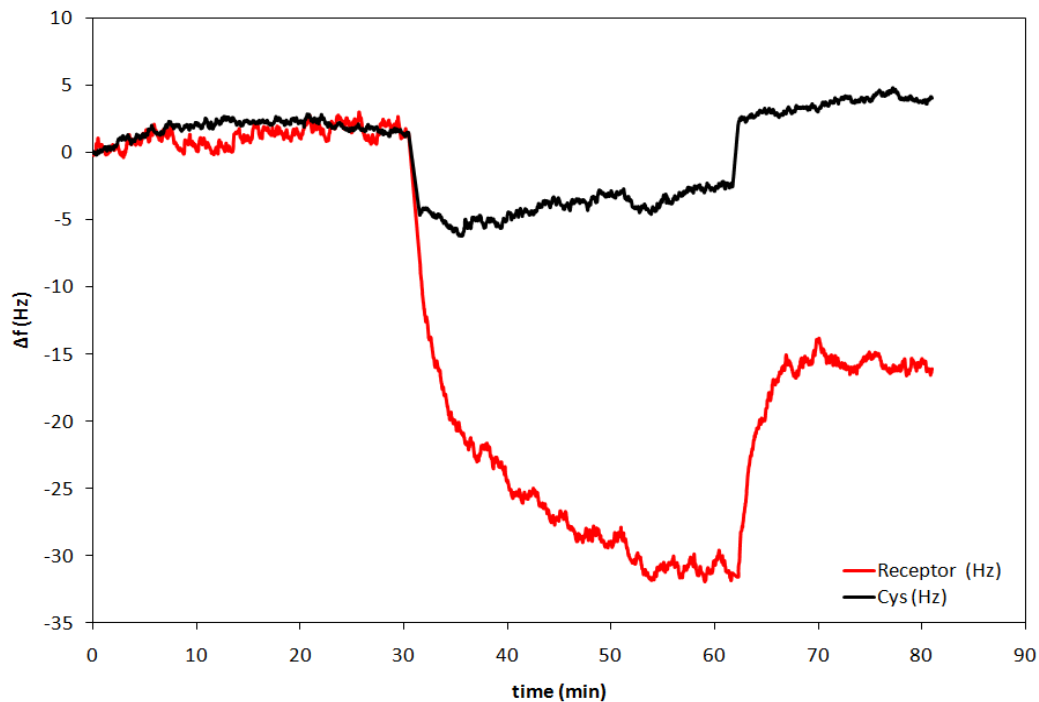


Figure 38 Sensor responses of immobilized receptor and reference electrode to 160 $\mu\text{g/l}$ BSA, respectively.

3.4 Adsorption isotherm for WGA-GlcNAc binding

The adsorption between WGA and the immobilized receptor can be described by the respective adsorption isotherm. For the carbohydrate-protein binding, the adsorption can be illustrated by Langmuir adsorption model, because at all sample concentrations the maximum sensor signal indicates adsorption of sub-monolayers.

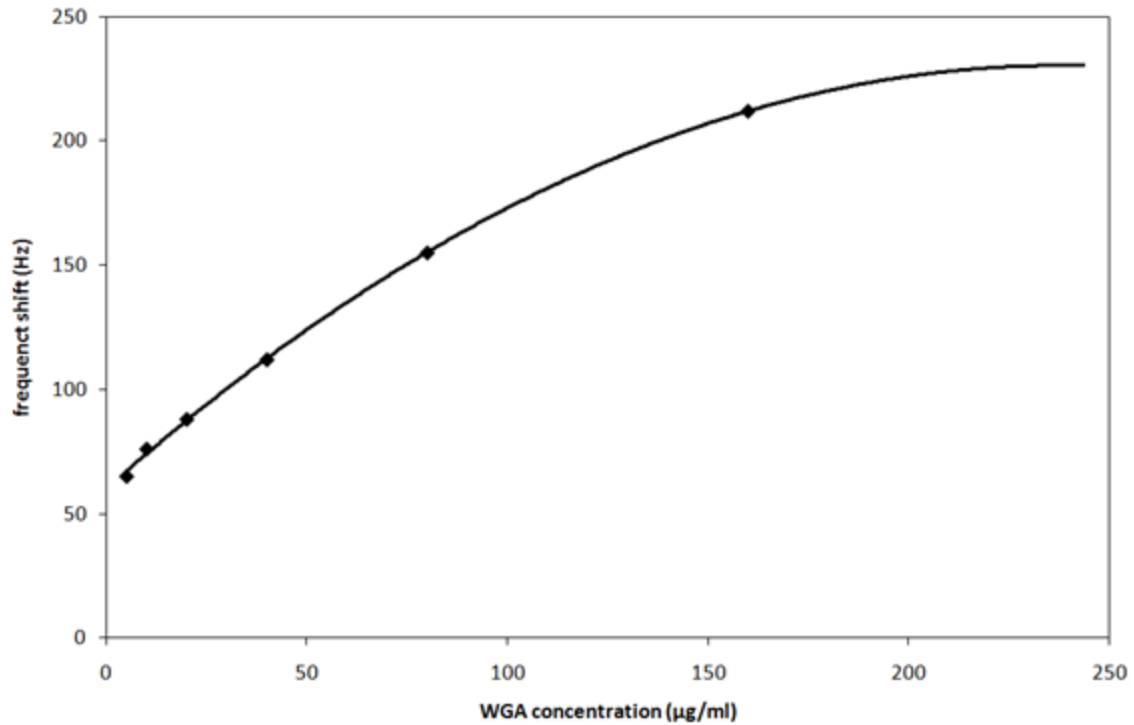


Figure 39 QCM sensor characteristic of WGA on the artificial receptor (GlcNAc) surface at 25 °C

The mathematical relation between frequency shift and WGA concentration (Figure 39) is similar to the Langmuir adsorption isotherm, which is also supported by the amount of “layers” adsorbed as calculated in Table 2. Therefore, the binding affinity can be calculated based on the association constant with Langmuir equation fitting. According the Langmuir equation:

$$\Gamma = \Gamma_{\max} \frac{Kc}{1+Kc} \quad (7)$$

Where K = Langmuir equilibrium constant or adsorption constant, c = concentration of WGA in solution, Γ = the amount adsorbed WGA at equilibrium, and Γ_{max} = the maximum amount adsorbed at saturated level.

In principle, the Langmuir equation can be fitted to data by linear regression. This can be achieved by rewriting equation (7) to:

$$\frac{c}{\Gamma} = \frac{c}{\Gamma_{max}} + \frac{1}{K\Gamma_{max}} \quad (8)$$

Base on equation (8), a plot of (c/Γ) versus (c) yields a linear whose slope is $1/\Gamma_{max}$ and whose intercept is $1/(K\Gamma_{max})$. Referring to the Sauerbrey equation, the Langmuir adsorption equation (8) can be rewritten in terms of frequency shift to

$$\frac{c}{\Delta f_{eq}} = \frac{c}{\Delta f_{max}} + \frac{1}{K_a \Delta f_{max}} \quad (9)$$

Where Δf_{eq} is the frequency shift at equilibrium of each concentration (Hz), Δf_{max} is the frequency shift at an finite concentration (Hz), c = concentration of WGA in solution (mol/l), and K_a is the association saturation constant (M^{-1}), which can be obtained by the ratio of slope to intercept according to the plot of $\frac{c}{\Delta f_{eq}}$ vs. c . After applying equation (9) one obtains the results depicted in Figure 40.

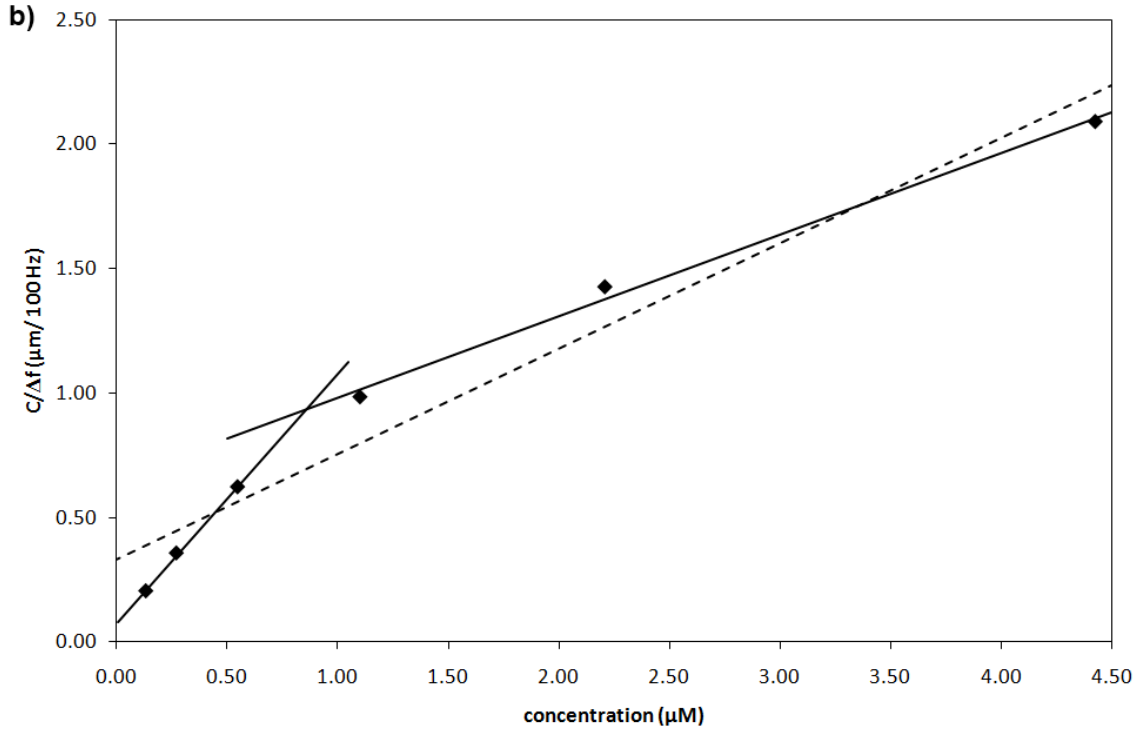


Figure 40 The corresponding linearized Langmuir plot by QCM

Consequently, the linear trend line was fit to the calculated data leading to the desired slope and intercept values. Finally, the outcome of first calculation (dashed line in Figure 40) are summarized in Table 3. The Gibbs energy was calculated from the standard Gibbs energy of adsorption formula.

$$\Delta_{ad}G_m^0 = -RT \ln K_a \quad (10)$$

Therefore, the binding constant of GlcNAc and WGA (K_a) can be derived as $1.28 \times 10^6 M^{-1}$ and the Gibbs energy of adsorption is -34.82 kJ.

Table 3 Calculated values for each parameter from Figure 38b and equation (9) and equation (10)

Parameter	Langmuir single range	Langmuir two ranges		Cysteine monolayer
		Low concentration	High concentration	
Slope	4.23×10^{-3}	1.00×10^{-2}	3.27×10^{-3}	3.90×10^{-3}
Intercep	3.34×10^{-9}	7.75×10^{-10}	6.55×10^{-9}	7.50×10^{-9}
$K_a (M^{-1})$	1.27×10^6	1.29×10^7	5.00×10^5	5.21×10^5
$\Delta_{ad}G_m^0$ (kJ)	-34.82	-40.55	-32.50	-32.60
R^2	0.95	0.99	0.99	0.98

According to the model and the actual data, however, no simple linear relation can be assumed. Therefore, in the second approximation, the data was split into two different concentration ranges, namely low (up to 20 $\mu\text{g/ml}$) and high (from 40 $\mu\text{g/ml}$). To these, the Langmuir model was applied separately. Table 3 also summarizes the binding constants and Gibbs Free Energies of each concentration range. At the low concentration, of the adsorbed amount of WGA is less than 50% of a monolayer, as seen in Table 2. The binding constant is $1.29 \times 10^7 M^{-1}$ and the Gibbs Energy is -40.55 kJ/mol. Due to the rather high binding constant, it can be assumed that the binding mechanism in this case is based on multivalent interactions, also because WGA has several binding sites for GlcNAc. Due to the maximum coverage of less than 50% of the theoretical binding sites, one can assume that one WGA molecule can binds to two GlcNAc, as depicted in Figure 41, hence leading to the high binding constant. In contrast to this, at higher concentration the calculated binding constant is $5.00 \times 10^5 M^{-1}$. This is 25 times lower than in the low concentration range. Also, the Gibbs Energy is less, namely -32.50 kJ/mol. This difference can be explained by geometrical constraints: due to the amount of adsorbed WGA molecules on the surface, only few binding sites are still available for binding to GlcNAc in a ratio of 1:2 (WGA:GlcNAc). However,

still some bivalent binding occurs, because the binding constant is higher than in the case of 1:1 (GlcNAc-GlcNAc = $4.5 \times 10^3 \text{ M}^{-1}$)¹⁰.

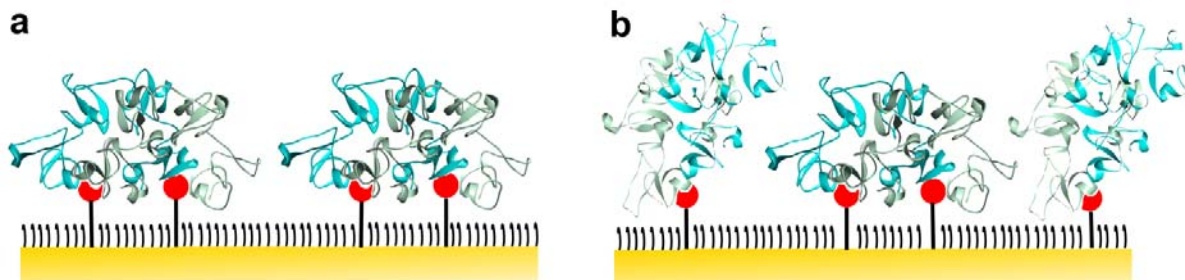


Figure 41 Schematic representation of WGA binding behavior on GlcNAc-chain **(a)** binding behavior of low concentration range and **(b)** high concentration range

As in any case the K_a is higher than that of monovalent GlcNAc-WGA interaction¹⁰, namely in the order of 10^3 M^{-1} , it confirms that GlcNAc residues interact with WGA by multivalent interactions in a cluster glycoside effect. Moreover, the value of K_a is in the same order order of magnitude as other multivalent carbohydrate-lectin interactions, for example between ConA and glucose^{56, 57}. Therefore, the results suggest successful multivalent binding of the sample. Furthermore, this strategy can be used to recognize and sense WGA lectin.

In contrast to this, the cysteine monolayer shows a saturation of the signal at 160 $\mu\text{g/ml}$, as can be seen in Figure 42. After applying the Langmuir adsorption model, the linear plot that was obtained from the data in Figure 42 and using equation (9), which is shown in Figure 43. The calculated binding constant is $5.21 \times 10^5 \text{ M}^{-1}$. This value is rather high and can be explained that WGA molecules have several positions that can in principle interact with cysteine. As the cysteine molecules are of course amino acids, they can interact with peptide and peptide group in each amino acid as shown in Figure 44 leading to a sensor characteristic and comparably high binding constant.

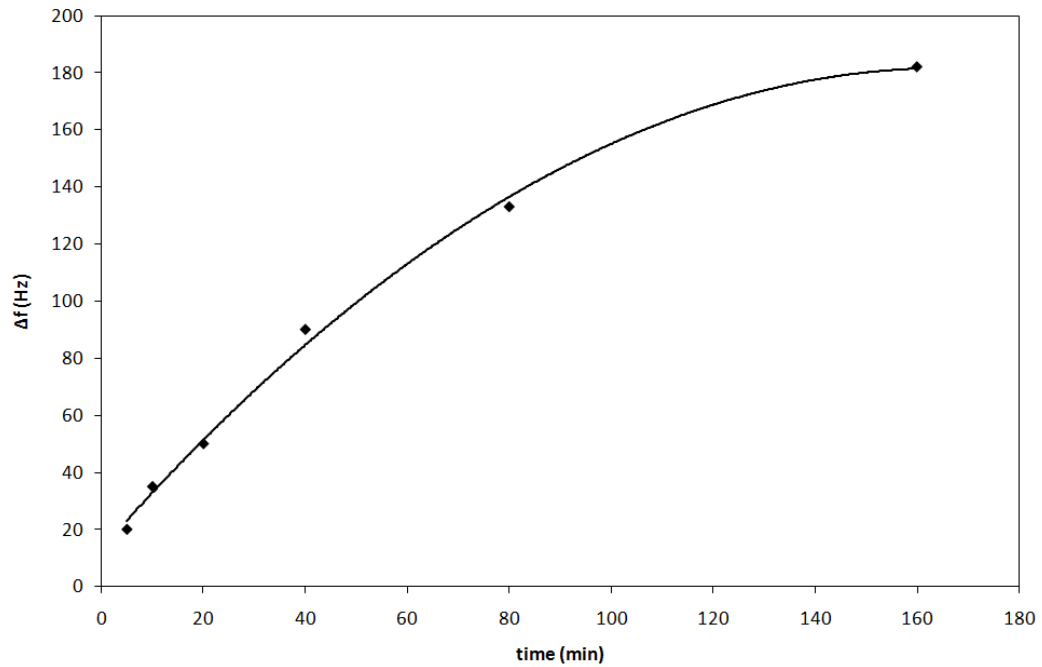


Figure 42 The frequency shifts varying with the concentrations of WGA on the cysteine monolayer at 25 °C

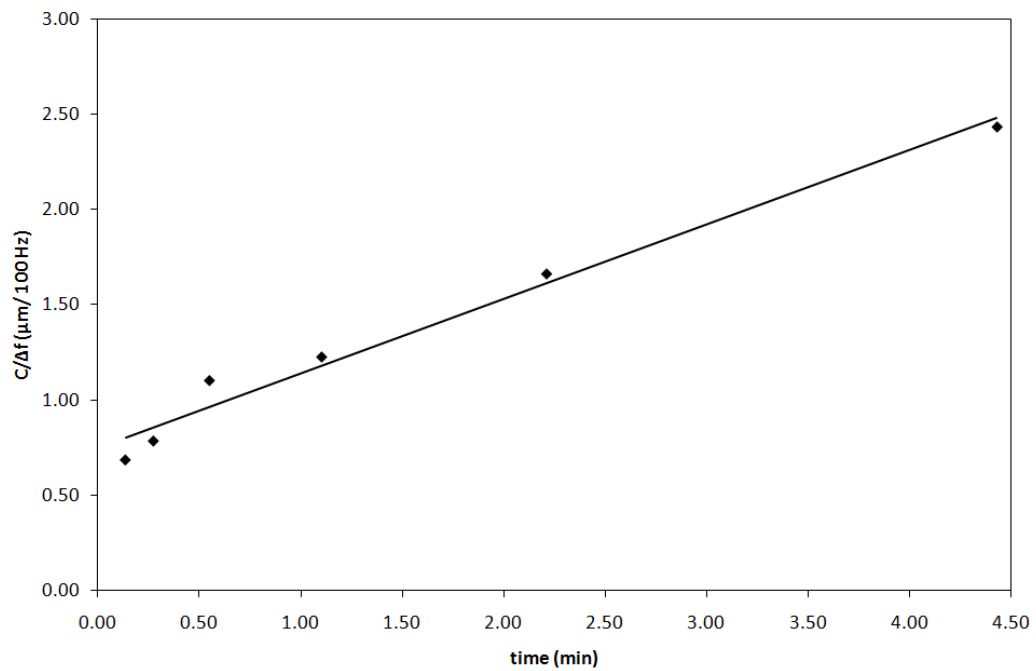


Figure 43 Langmuir plot corresponding to WGA concentration by QCM from Figure 42 and equation (9)

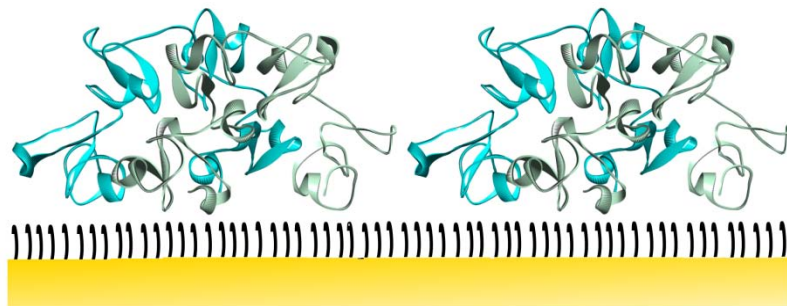


Figure 44 Schematic representation of WGA binding behavior on cysteine monolayer

When comparing the binding constants, that of WGA on cysteine monolayer is in the same range than for GlcNAc at high WGA concentration. The reason is that WGA can have multipoint interactions with cysteine while in the case of the GlcNAc multidentate bonds have to be broken and monodentate ones be formed for the monolayer to occur. However, at low WGA concentrations their binding constant of the receptor surface is about 25 times larger than for the cysteine monolayer. This result verifies that the immobilized GlcNAc receptor substantially increases binding sensitivity, however also leading to maximum adsorption of a monolayer of WGA on the surface.

Chapter 4

Molecularly imprinted polymers

4.1 Protein imprinting

Surface properties of proteins have large influence on the recognition site generated by molecular imprinting, because this technique targets the functionality of the respective template, for example, charge, hydrophobicity and H-bond interaction, to create an interaction network ideally suited to re-incorporate the latter. The actual recognition of a protein by an imprinted polymer can be divided into three steps. The first step is transporting of the protein molecule from the liquid to the vicinity of the surface. Convective and diffusive motions in liquid are mainly responsible for this process. The second step occurs, when the proteins are closely approaching the surface, which results in their initial attachment. Finally, a protein finalizes the adsorption by increasing its number of binding points with the surface. However, the respective non-covalent interaction can in principle also occur on the non-imprinted surfaces resulting in unspecific binding, while specific binding sites in the imprinted polymer are ideally adapted to their respective template. The last step is desorption. However, in some cases protein adsorption in fact turns out irreversible.

4.1.1 Polymer optimization

Monomer and crosslinker

The initial step of polymer imprinting technique is choosing suitable monomer. As already mentioned, the WGA lectin surface contains both hydrophobic ranges caused by the side chains of glycine as well as cysteine and hydrophilic ranges resulting from amine (-NH₂) and carboxyl (-COOH) groups which form hydrogen bonds with appropriate functional groups of monomers such as another amine (-NH₂) and carboxyl (-COOH) group. Therefore, Acrylamide (AAM) and Methacrylic acid (MAA) were considered, because their functional groups are amine (-NH₂) and carboxyl (-COOH), respectively, and it can be assumed that several functional groups (-OH, -NH₂, -COOH, main-chain amide groups, and others) of WGA can be brought to optimal interaction with the functional groups of AAM and MAA monomer. In order to increase the imprinting efficiency, more hydrophobic monomers, such as Butylmethacrylate (BMA) or Methylmethacrylate (MMA) were added. Generally speaking, two different co-polymer systems were applied in this research: The copolymer system selected consists of Acrylamide (AAM), Methacrylic acid (MAA) and Butylmethacrylate (BMA) or Methylmethacrylate (MMA). When comparing both systems, the Butylmethacrylate copolymer has higher hydrophobicity than the Methylmethacrylate copolymer system resulting which might lead to high responses in the non-imprint.

In order to achieve effective imprinting, optimizing the crosslinker is an important factor, both concerning its amount and its type. First of all, the functional groups of monomers should be uniformly distributed within polymer network. Second, monomer and crosslinker should react similarly during polymerization to avoid the formation of block copolymeric systems polymerization. Therefore, within this work, *N,N'*-(1,2-Dihydroxyethylene) bisacrylamide (DHEBA) was chosen, because its chemical structure is similar to the functional monomers, so the residues of monomer can be expected to be uniformly distributed with this long chain crosslinker. The structures of each monomers and crosslinker as well as the possible radical initiators are shown in Figure 45.

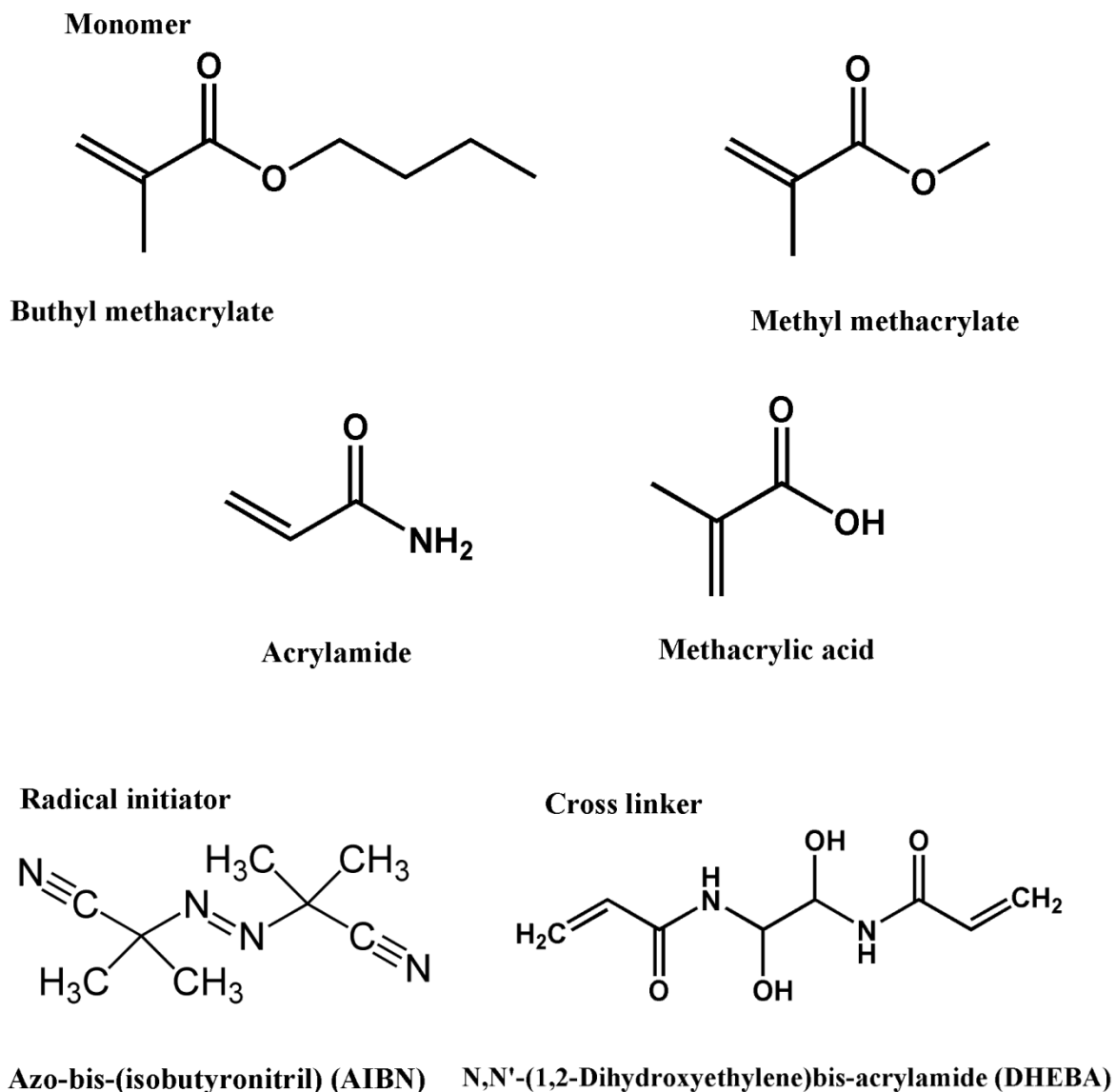


Figure 45 The structures of monomers, cross linker and radical initiator

Solvent

One of the most important points for successful protein imprinting is to promote the formation of optimal non-covalent (hydrogen bond, hydrophobic interaction) adducts in the reaction mixture. Of course, the solvent must sufficiently dissolve all of components,

including monomer, cross-linker and radical initiator. The solubility of each component in different solvent is shown in Table 4.

Table 4 The solubility of all monomer, cross linker and initiator in different solvent

Solvent	AAM	MAA	BMA	MMA	DHEBA	AIBN
Water	+	+	+	+	-	-
DMF	+	+	+	+	+	+
THF	+	+	+	+	-	+
DMSO	+	+	+	+	+	+

+ soluble - not soluble

From this point of view, DMSO turned out to be the most suitable solvent, because it is able to dissolve all reaction components. Moreover, DMSO is a polar, aprotic solvent and does not have the ability to be hydrogen bond donor and interfere with complex formation. Using protic solvents such as alcohols, should be avoided in this case since they can competitively prevent the hydrogen bonding.

4.1.2 STM analysis of WGA stamp and the imprinted surface

According to the first step of surface imprinting such as the biospecies as well as protein molecules is the sample stamp preparation. To verify that the protein was immobilized on the substrate without the recrystallization of buffer, we applied high resolution microscopy. Due to the size of individual protein which is normally smaller than resolution limit of atomic force microscopy, the study in protein immobilization on surface is substantial challenge. To achieve in this task, we need the high resolution microscopy such as

STM to generate the protein stamp image. For this purpose, gold surface was sputtered on the protein stamp sample with 40 nm in thickness lead to the conducting surface.

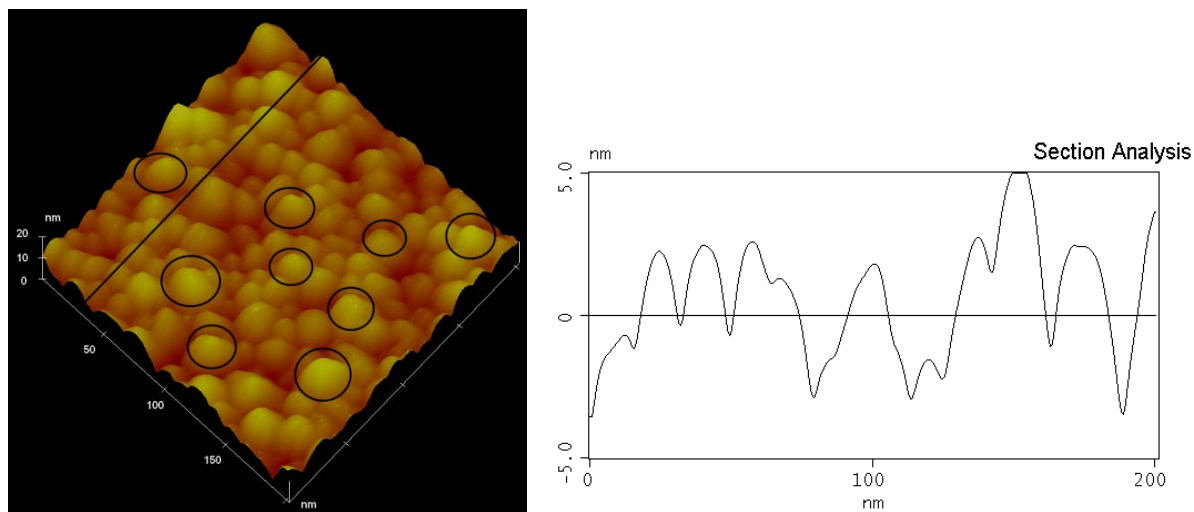


Figure 46 Scanning tunneling microscopy image of WGA stamp with $V_{bias} = 500$ mV and $I_{set\ point} = 50$ pA. **(Right)** WGA stamping for imprinting on co-polymer surface. *Circles* indicate immobilized WGA on glass slide. **(Left)** Section analysis for protein immobilization along the line draw in right image

Obviously, the stamp surface consists of approximately circular structures with an average diameter of 13.3 nm a height of 4.6 nm. The latter can be deduced from the section analysis given in Figure 46. To make this clearer, the images of a few of the individual WGA molecules are marked by circles. After verifying the structure and principal usability of the WGA stamps, the next step is to evaluate them in terms of applicability during the synthetic processes leading to MIP.

Therefore, we also sputtered different polymer surfaces with gold, namely the polymethacrylate MIP and the respective non-imprinted matrix. Figure 47 shows the outcome of this approach, namely the nonimprinted surface in part (a) and the imprinted one

in part (b), respectively. Despite the fact that the images look similar in some parts, STM analysis also reveals distinct differences: the NIP shows a rough surface consisting of granular structures separated by very narrow space between them. The individual average size of those granules is about 30 nm in diameter. In contrast to this, MIP surfaces as depicted in Figure 47b reveal several cavities. In general, their diameters reach from 14 to 28 nm, as can also be seen by the ones marked with circles in the figure. This perfectly fits the modeled size for the proteins. Hence, the cavities are obviously the imprinting result of single WGA or dimers: in first approximation, both WGA and cavity have a size of approximately 20 nm in diameter. Actually, the dimensions of cavity do not exactly fit the theoretical size due to the experimental procedures during stamp preparation: procedures were not optimized to achieve an exact monolayer of template protein on the stamp, which thus contains partial multilayer on it resulting in imprinted sites that are larger than a single protein molecule.

Additional differences between MIP and NIP surfaces reveal themselves when regarding the respective section analyses that can be seen in Figure 47c. In NIP, the maximum vertical deepness of the “cavity” between the globular structures is 4 nm. Additionally, their width is always below 10 nm. Such steep structures are typical for intergranular spaces that are independent of any possible template. For MIP, the picture is completely different: the deepest cavity reaches up to 9 nm with roughly 20-25 nm width. Fortunately for us, this size is matching the one of a WGA dimer as investigated and published by Pei et al.¹³. The different surface morphologies of MIP and NIP as obtained by STM therefore strongly suggest that stamping strategies lead to the desired surface pattern. Furthermore, to the very best of our knowledge, this is one of the first successful approaches to actually visualize protein recognition sites on a polymer surface.

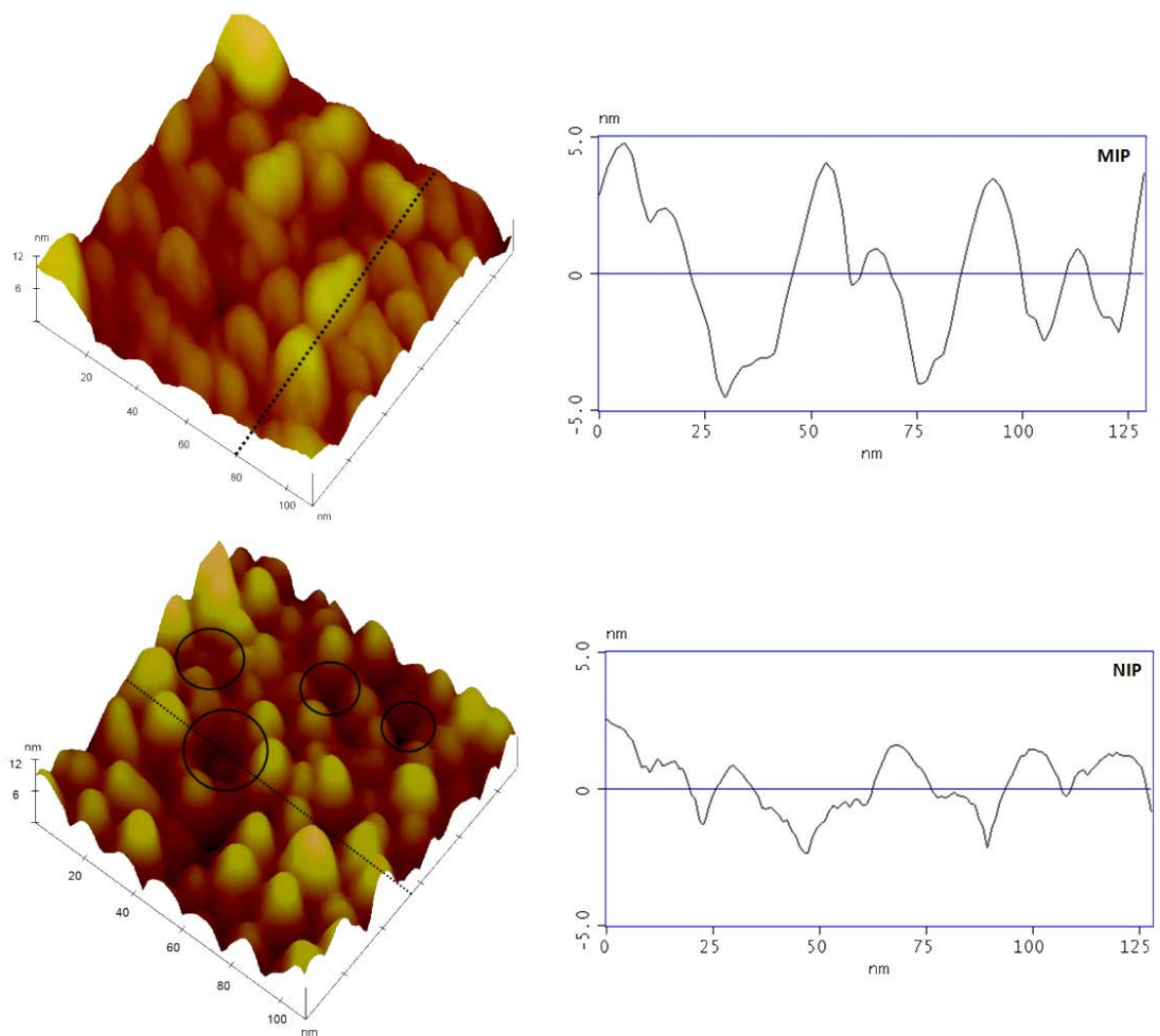


Figure 47 Scanning tunneling microscope (STM) image of **(top)** Nonimprinted polymer and section analysis for NIP along the dashed lines **(bottom)** wheat germ agglutinin (WGA) imprinted on methacrylate copolymer with WGA imprinted cavities (in the circle) and section analysis for WGA molecularly imprinted polymer along the dashed lines in with $V_{\text{bias}}=500 \text{ mV}$ and $I_{\text{set point}}=50 \text{ pA}$.

4.1.3 Sensor characteristic of Butylmethacrylate co-polymer system

Butylmethacrylate-based co-polymers systems were the starting point of the design of MIP sensor for WGA due to the comparably large hydrophobic group. For this purpose, four different ratios of monomers (AAM, MAA, BMA and DHEBA) were tested. The detailed compositions of the respective layer are shown in Table 5.

Table 5 Monomer ratios of butylmethacrylate copolymer system

	AAM		MAA		BMA		DHEBA		AIBN
	Mass (mg)	Mole (mmol)	Mass (mg)	Mole (mmol)	Mass (mg)	Mole (mmol)	Mass (mg)	Mole (mmol)	Mass (mg)
2:2:1	20	0.28	20	0.23	20	0.14	30	0.15	1
2:1:2	10	0.28	10	0.12	40	0.28	30	0.15	1
1:1:2	10	0.14	10	0.12	40	0.28	30	0.15	1
1.5:1.5:1	20	0.28	25	0.29	25	0.18	30	0.15	1

After adding all components, the mixtures were pre-polymerized under UV for 2 hours. Then, the respective frequency changes were recorded by 10 MHz QCM. First, the system was exposed to PBS (10 mM, pH 7.4) until obtaining the stable signal for 20 minutes. After switching the solution to 0.5 mg/ml of WGA in PBS, the respective frequency shifts were recorded in stopped flow. The resulting sensor responses of the four different systems are summarized in Figure 48.

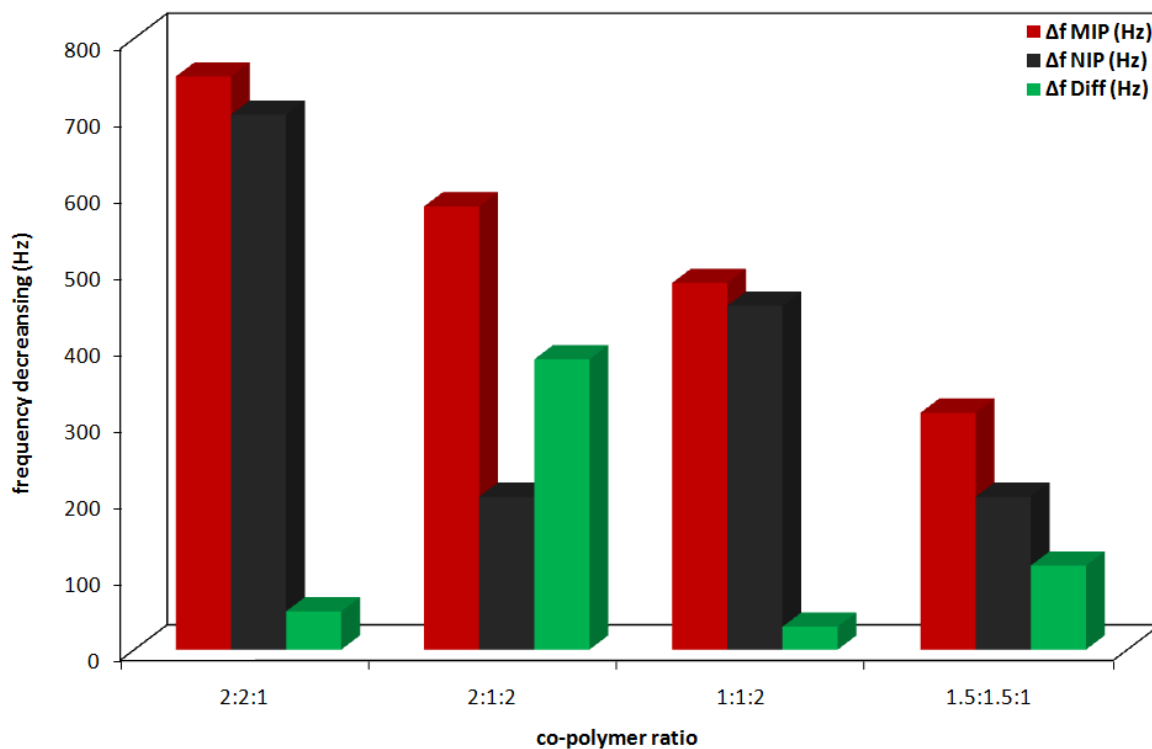


Figure 48 10 MHz QCM responses of MIP, NIP obtained from different copolymer ratios against WGA 0.5 mg/ml, at 25 °C. Green columns show the difference between the respective two MIP and NIP signals

As can be seen, the copolymer with the monomer ratio of 2:2:1 (AAM:MMA:BMA) leads to the highest sensitivity compared to any other copolymer. The reason is that it contains several amide (-NH₂) functional groups from AAM as well as carboxyl groups (-COOH) from MAA, which can lead to hydrogen bonding to WGA lectin. Moreover, this copolymer system also has substantial ability for the hydrophobic interaction between functional group of BMA and WGA lectin. Summarizing, the 2:2:1 copolymer system hence yields high interaction between WGA lectin and copolymer. However, the material in some way is even “too efficient” in interacting, because the respective NIP also give rise to high sensor responses reaching more than 90% of the frequency shift caused by the MIP. Therefore, we decreased both the number of carboxyl and amide groups by using less MMA resulting in a molar ratio of 1.5:1.5:1. In this system, the sensitivity decreased while the selective part of

binding, i.e. the difference in response between NIP and MIP, increased. In contrast to the 2:2:1 copolymer, the structure of this copolymer (1.5:1.5:1) obviously yields lower nonspecific interaction to WGA lectin, so the MIP incorporates the template 2.5 times more favorably, than the non-imprint.

In the next step, we aimed at further enhancing the difference in binding between NIP and MIP by decreasing the interaction between WGA lectin and polymer surface and enhancing the interaction between WGA and functional groups of monomer/crosslinker within the imprinted cavities. It is well known that hydrogen bonding is stronger than hydrophobic interactions, i.e. the interaction enthalpies are more negative. Therefore, we decreased hydrogen bonding part and in return increased hydrophobic interactions to reduce the effects on the NIP material. This reasoning lead to the third and the fourth copolymer system: 1:1:2 and 2:1:2. Obviously, the frequency difference between NIP and MIP occurring because of specific binding at the imprinted electrode in 2:1:2 copolymer are larger than in the case of the 2:2:1 and 1.5:1.5:1 copolymers. Unfortunately, the sensitivity decreased due to reducing the amount of hydrogen bonds.

Compared to the 2:2:1 copolymer, they have lower sensitivity. The 1:1:2 material also loses some of the difference in frequency shift between NIP- and MIP-coated electrode, because the amount of functional groups suitable for hydrogen bonding including amide and carboxyl were reduced to reach half the number in the 2:2:1 copolymer. Together with this, the hydrophobic interaction part was increased, but this interaction is less strong than hydrogen bonding.

Comparing all the three copolymer systems discussed so far, the 1.5:1.5:1 matrix has the lowest sensitivity, but best sensitivity. Therefore, we optimized polymerization time by using the 1.5:1.5:1 copolymer to enhance this parameter, because it turned out that when the polymerization time is long enough, the interaction network can be optimized in a better way and the resulting polymer structures are more stable after complete polymerization. Therefore, the polymerization procedure was adjusted for this reason. After pre-polymerization at 70 °C, the polymer was drop-coated onto both electrodes, respectively. Then, the MIP was generated by pressing the WGA stamp into it followed by polymerization under UV. During this step the polymerization time under UV was varied and resulted in 2

hours, 3 hours and overnight, respectively. The frequency responses of the resulting QCM to 160 $\mu\text{g/ml}$ WGA are shown in Figure 49. Obviously, the sensitivity can be enhanced by increasing the polymerization time.

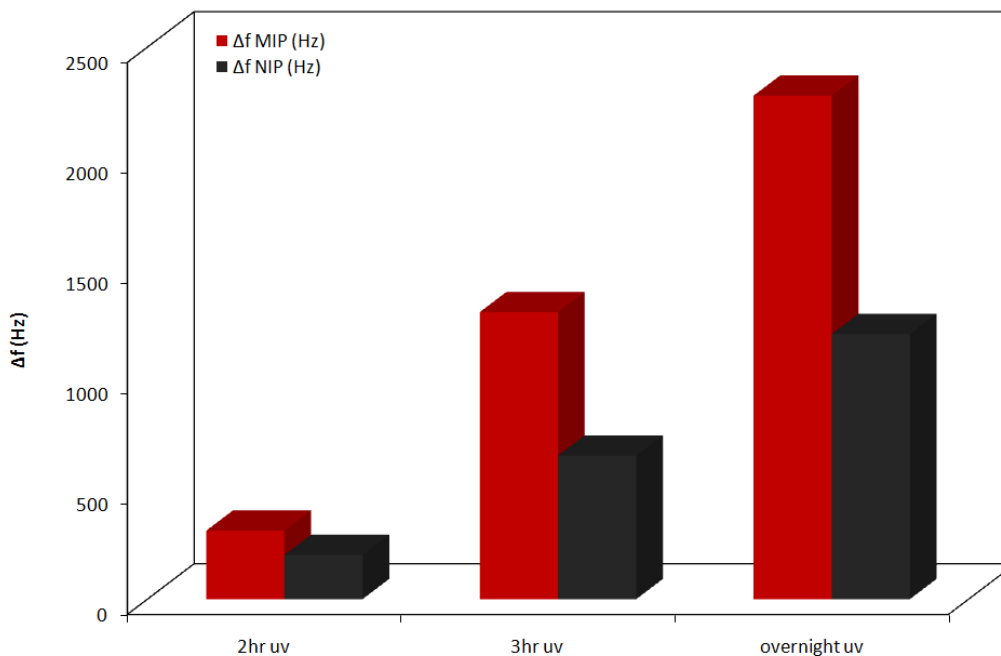


Figure 49 10 MHz QCM responses of MIP and NIP as a function of different UV polymerization times. Analyte: WGA 0.5 mg/ml at 25 °C

As can be seen increasing polymerization time, overnight and 3 hour polymerization enhance the sensor response in 5 times and 3 times as compared to 2 hours polymerization time, respectively. Furthermore, increasing the polymerization time can enhance the binding affinity of MIP as compared to the corresponding non-imprint. When polymerization time is reaches is optimal value, the non-covalent interaction network between protein and the monomers leads to large non-specific signal therefore not increasing the selectivity effect resulting from molecular imprinting.

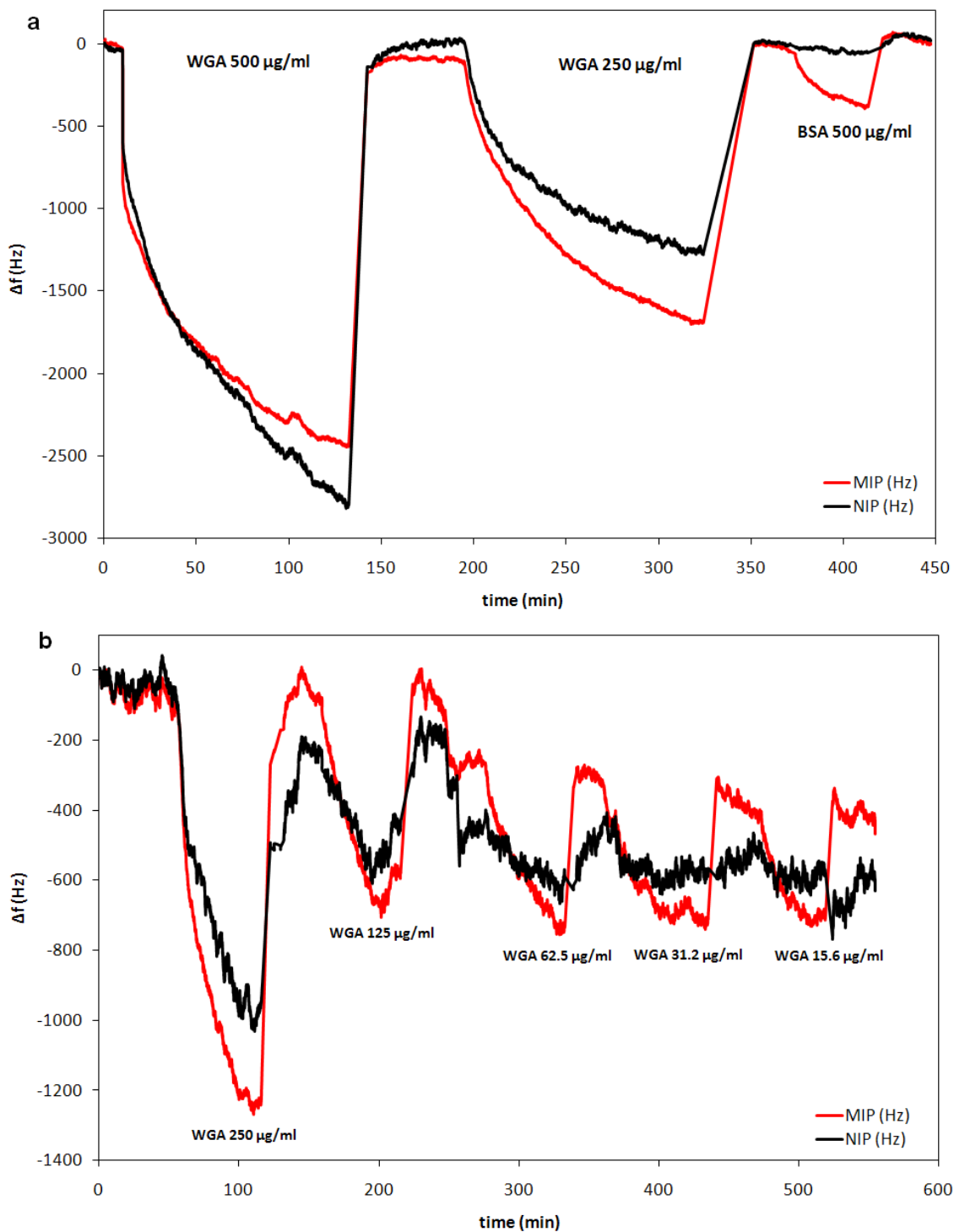


Figure 50 Quartz crystal microbalance (QCM) sensor responses of MIP and NIP towards BSA and different WGA concentrations at 25 °C in the 2:1:2 copolymer ratios with overnight UV polymerization. (a) The sensor response of QCM after one day preparation and (b) is the sensor response of QCM in the different concentration after one month storage

Finally, Figure 48 shows that the 2:1:2 copolymer yields the largest difference in sensor response between NIP and MIP, but it has lower sensitivity than the 2:2:1 copolymer. To enhance this, polymerization was again performed under UV overnight, because as mentioned above this parameter can enhance the sensitivity of MIP. As can be seen in Figure 49, after increasing polymerization time, the sensor response increases to 4.8 times that obtained after 2 hours of polymerization. It has now changed from -580 Hz to -2800 Hz and also depends on WGA concentration. After one month, one can observe only negligible loss in sensitivity, as seen in Figure 50b.

Furthermore, BSA at 0.5 mg/ml was tested with this QCM to confirm selectivity. The frequency changed by -2800 Hz after exposed 0.5 mg/ml WGA lectin, while applying BSA 0.5 mg/ml, the frequency only decreased by 400 Hz. Unfortunately, this copolymer composition yields appreciable sensitivity and selectivity between different analytes but it loses selectivity between NIP and MIP, as can be seen in Figure 50, where the frequency response between NIP and MIP differs only by 350 Hz. In comparison to this, the result in Figure 48 shows a difference of NIP and MIP being much larger than the result in Figure 50. Therefore, this sensor needs to be optimized for achieving good selectivity, sensitivity and imprinting effect (i.e. difference between MIP and NIP). For enhancing the selectivity of MIP, one possibility is changing the functional monomer for reducing or increasing non-covalent interactions. For this reason, the functional monomer is changed from BMA to MMA due to its lower hydrophobicity, which therefore should reduce the non-selective interaction between the polymer system and WGA.

4.1.4 Sensor characteristic of Methylmethacrylate co-polymer system

Butyl methacrylate systems therefore lead to very high non-specific sensor effects rendering the imprinting approach not feasible. Therefore, reducing the hydrophobicity of the copolymer seems a reasonable strategy. Basically, the idea behind it is to not change the monomer ratio in the matrix to avoid the necessity to go through all optimization steps for a second time. Hence, butylmethacrylate was replaced by methylmethacrylate. Therefore, the new polymer system with MMA as monomer was prepared by keeping 2:1:2:1 ratio

including 0.2 mmol (15.2 mg) of AAM, 0.1 mmol (8.6 mg) of MAA, 0.2 mmol (20 mg) of MMA and 0.1 mmol (20 mg) of DHEBA as crosslinker. Then, the polymerization was carried out following the procedure of the BMA copolymer experiment, namely briefly: The mixture was prepolymerized at 70 °C following polymerization under UV for overnight. Afterwards, the respective QCM was installed into the measuring cell for recording sensor responses. The sensor characteristics in Figure 51 shows the response of the quartz towards WGA and BSA ($c = 250 \mu\text{g/ml}$), respectively. However, after injecting 250 $\mu\text{g/ml}$ of WGA, the frequency shift of this copolymer turned out nearly 6 times less than in the case of the butyl methacrylate copolymer in the same ratio, probably due to the lower hydrophobicity of methymethacrylate as compared to buthylmethacrylate.

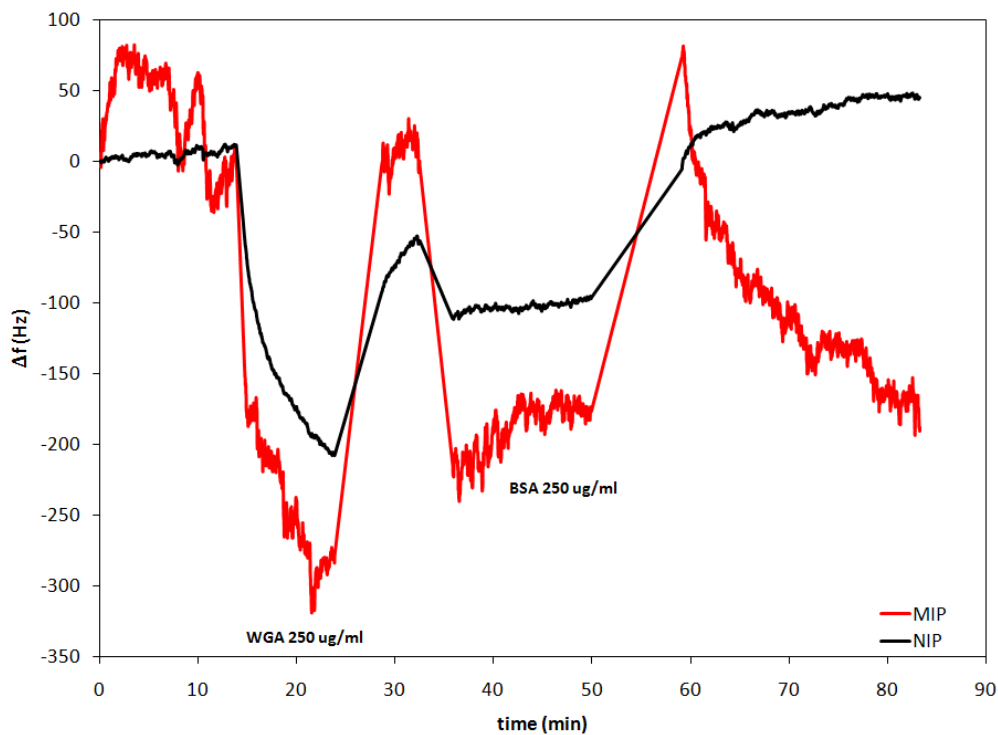


Figure 51 Quartz crystal microbalance (QCM) sensor responses of MIP and NIP towards BSA and WGA (250 $\mu\text{g/ml}$) at 25 °C with AAM/MAA/MMA/DHEBA (2:1:2:1) copolymer

Selectivity measurements revealed that the methymethacrylate copolymer leads to less different results between BSA and WGA, respectively, as can be seen in Figure 51: after the QCM has been exposed to 250 $\mu\text{g/ml}$ of BSA, the frequency of MIP decreased to 200 Hz that is only 100 Hz less than frequency response of WGA 250 $\mu\text{g/ml}$. Furthermore, specific binding at the imprinted cavities leads to 100 Hz more frequency shift on MIP than on the NIP. Therefore, this copolymer system is potentially interesting for the purpose, but it needs to be further optimized by reducing the hydrophobicity. As could be seen, this strategy increases the amount of selective interaction. Therefore, the monomer mixture was kept at the same ratio except for decreasing to MMA 0.1 mmol. The new copolymer ratio therefore was 2:1:1:1 of AAM: MAA: MMA: DHEBA. Its QCM results after exposing it to 250 $\mu\text{g/ml}$ of BSA and WGA, respectively, are shown in Figure 52.

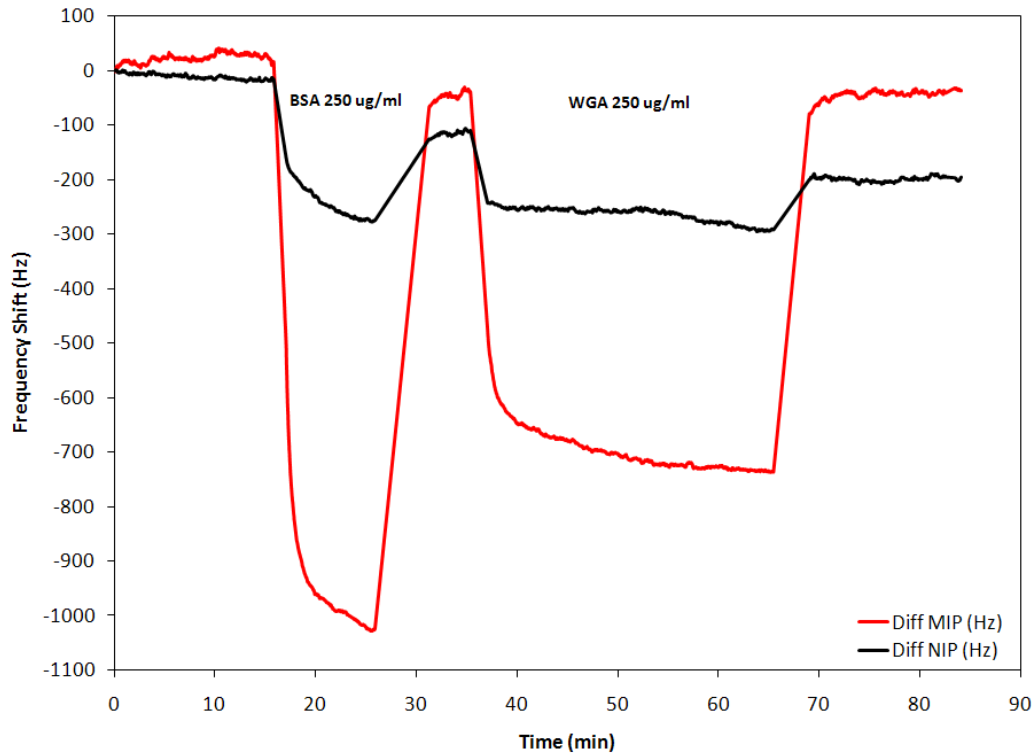


Figure 52 Quartz crystal microbalance (QCM) sensor responses of MIP and NIP towards BSA and different WGA concentrations at 25 °C with AAM/MAA/MMA/DHEBA (2:1:1:1) copolymer

After short equilibration (roughly 15 minutes), the dual electrode QCM was exposed to 250 $\mu\text{g/ml}$ of BSA. Immediately, the frequency of the MIP-coated channel decreased by 1050 Hz while the NIP yielded only -280 Hz. After washing and ensuring full reversibility of the signal, 250 $\mu\text{g/ml}$ of WGA was injected into measuring cell. One can observe that frequency of MIP has decreased by 750 Hz, whereas the NIP electrode changed only by -200 Hz. This indicates more appreciable imprinting effect as such. However, the sensor responses also show that selectivity needs further attention: The imprinted cavities do not interact with WGA, but also to a larger extent with BSA. The reason for this may be traced back to the level of cross-linker: As the ratio of total monomer and crosslinker is 4:1 the resulting polymer structures are soft and flexible. When BSA whose dimensions are very similar to WGA, interacts with the imprinted cavities, the polymer seem to adjust its structure to being more suitable to BSA, also because the functional groups around cavities show strong interaction to BSA. To overcome this problem, the use of crosslinker agent, including the type of crosslinker and monomer/crosslinker ratio, has to be optimized in order to preserve the binding properties of the protein. The system should be able to “freeze” an image of the altered tertiary structure introducing additional non-covalent bonds between functionalities which are present on the protein surface (and sometimes between distinct protein molecules). For this purpose, first the crosslinker agent was changed to N,N'-methylene bisacrylamide (MBAM) (see Figure 53) to replace DHEBA. The difference between two compounds is determined by the hydroxy groups between the two amide groups. Furthermore, the chain length of MBAM is smaller than the one of DHEBA thus leading to less flexibility of the copolymer structure.

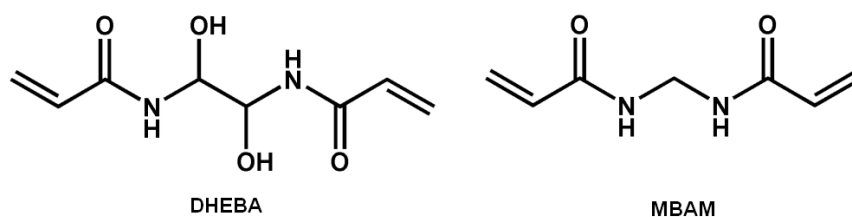


Figure 53 Structure of crosslinker: DHEBA and MBAM

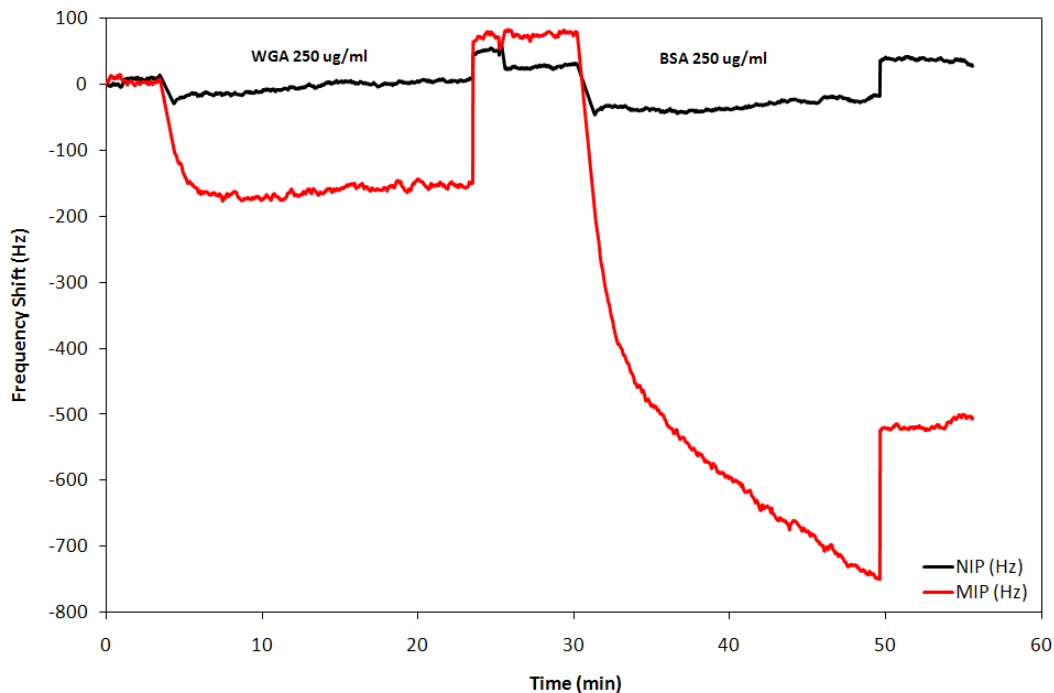


Figure 54 Quartz crystal microbalance (QCM) sensor responses of MIP and NIP towards BSA and different WGA concentrations at 25 °C with AAM/MAA/MMA/MBAM (2:1:1:1) copolymer

The result of applying MBAM as the crosslinker is shown in Figure 54. Selectivity did not improve, because BSA leads to larger frequency responses than WGA thus proving the initial assumption wrong. Moreover, sensitivity has also decreased. Therefore, the next optimization step is keeping DHEBA as the crosslinker and then increasing the amount of crosslinker within the polymeric matrix.

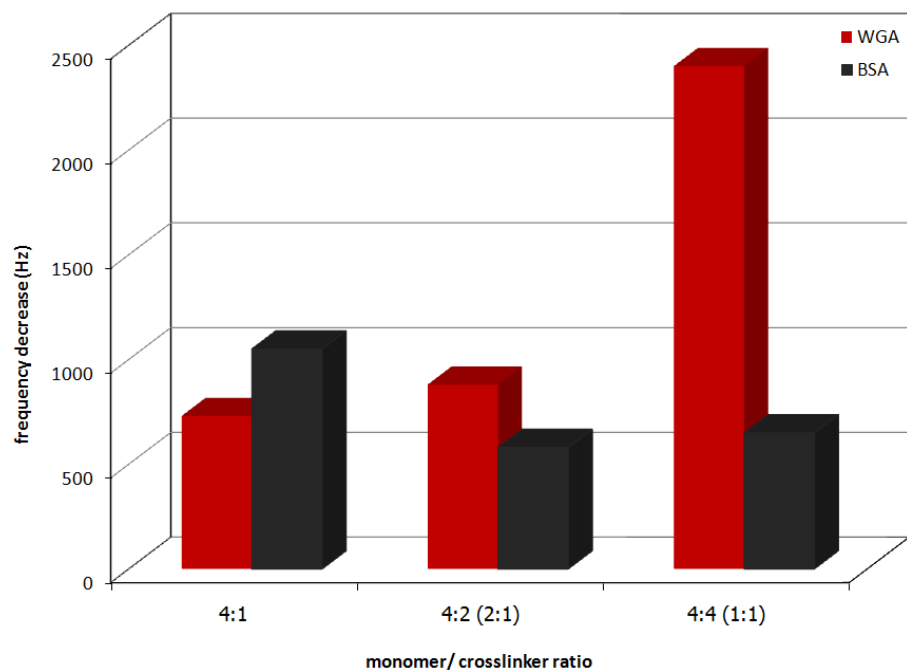


Figure 55 Comparison of the QCM sensor responses of MIP when changing the total monomer-to-crosslinker. Frequency decreases were recorded after injecting 250 $\mu\text{g/ml}$ of WGA and BSA protein at 25 $^{\circ}\text{C}$, respectively.

Therefore, the ratio of total monomer to crosslinker is changed from 4:1 to 4:2 (2:1) and 4:4 (1:1). Due to the increasing amount of crosslinker, the resulting structure should be less flexible and harder which should lead to better selectivity. Figure 55 summarizes the outcomes of this effort: Obviously, increasing the amount of crosslinker did not only enhance selectivity, but also the sensitivity of the MIP. The frequency shifts obtained are increased by 1.2 times and 3 times after increasing the amount of crosslinker 2 and 4 times, respectively, leading to much more appreciable sensor properties. Furthermore, the selectivity is improved following the increase of crosslinker ratio: BSA binding is substantially reduced as compared to WGA leading to ultimate selectivity factors of more than four. Therefore, all results indicate that AAM:MAA:MMA:DHEEBA in 2:1:1:4 is the most suitable copolymer within this monomer system for recognizing WGA lectin.

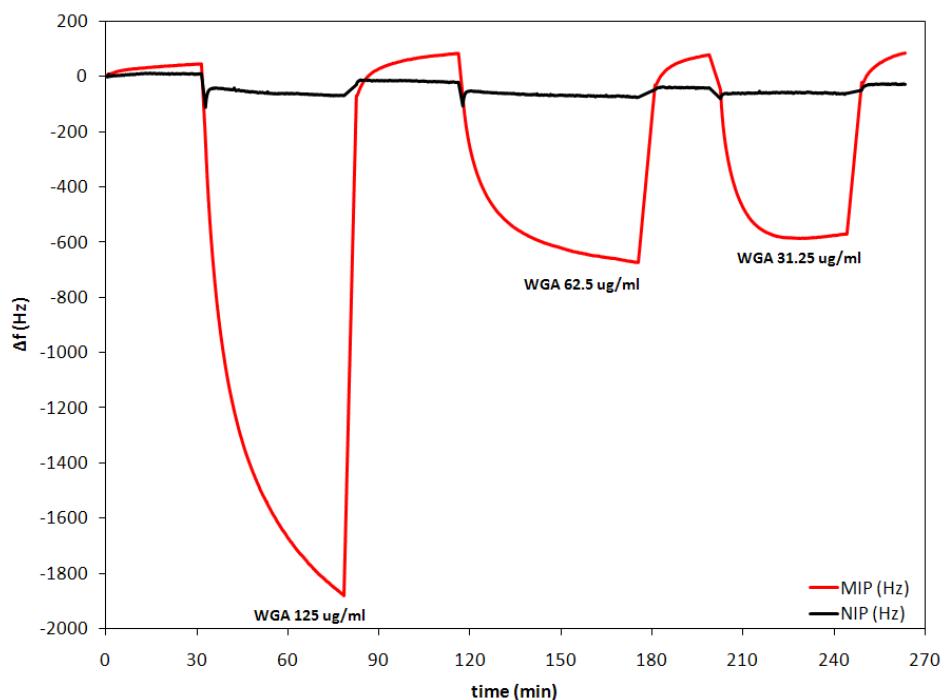


Figure 56 10 MHz Quartz crystal microbalance (QCM) sensor responses of MIP and NIP towards different WGA concentrations at 25 °C with AAM/MAA/MMA/MBAM (2:1:1:4) copolymer

Having thus obtained optimal copolymer conditions, the sensor characteristics of the resulting methacrylate system have to be assessed. The frequency response towards WGA in three different concentrations is shown in Figure 56. After exposing the QCM to 125 $\mu\text{g/ml}$ of WGA, the frequency on the MIP-coated electrode immediately decreases by 1900 Hz. On the NIP, however, only 50 Hz could be observed. Moreover, the MIP electrode frequency response also depends on WGA concentration, while the NIP leads to the same shift of -50 Hz for all WGA concentrations. This verifies that the imprinted cavities on MIP are indeed specific to WGA. Furthermore, the signals on both channels can be reverted by washing with sodium dodecyl sulfate/acetic acid (SDS/AcOH) leading to the dynamic response behavior of the QCM sensors. Also, low noise level has been observed on both electrodes (in a range of 10 Hz) in solvent and protein solution, which can be referred to the rather smooth surface.

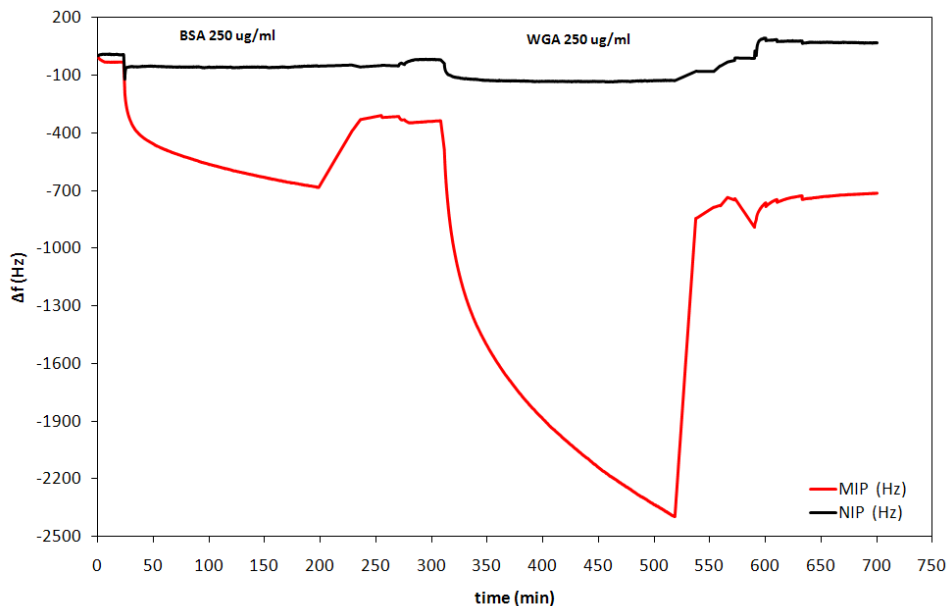


Figure 57 10 MHz Quartz crystal microbalance (QCM) sensor responses of MIP and NIP towards 250 $\mu\text{g/ml}$ of BSA and WGA at 25 $^{\circ}\text{C}$ with AAM/MAA/MMA/MBAM (2:1:1:4) copolymer

Moreover, the selectivity of the MIP was confirmed as shown in Figure 57: After stable frequency is reached, 250 $\mu\text{g/ml}$ of BSA was injected, assessed and followed by WGA in similar concentration. The frequency response is roughly -700 Hz for BSA and -2400 Hz for WGA, which nearly 4 times larger, while the NIP changed only -50 Hz towards both BSA and WGA. Therefore, these results are a strong indicator of successful WGA imprinting, because the frequency decrease on MIP and NIP electrode refer to the mass uptake into the surface and the MIP is more responsive to WGA than BSA.

4.2 Non-Sauerbrey behavior

During reproducibility experiments with the optimized polymer AAM/MAA/MMA/DHEBA (2:1:1:4) in the vast majority of cases the QCM results obtained look like the one depicted in Figure 58. Obviously, in this case the MIP also yields high, concentration-dependent frequency responses to WGA. Moreover, BSA leads to substantially lower responses on the template layer, as shown in Figure 59

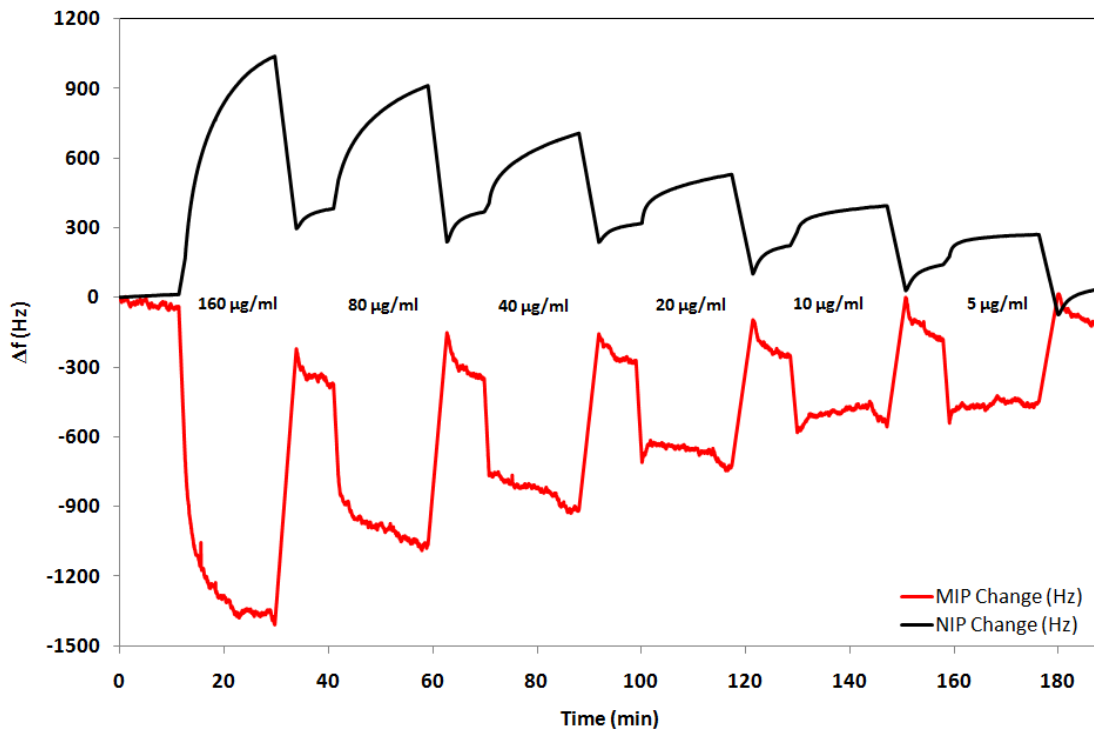


Figure 58 Reproducibility of 10 MHz Quartz crystal microbalance (QCM) sensor responses of MIP and NIP towards different WGA concentrations at 25 °C with AAM/MAA/MMA/MBAM (2:1:1:4) copolymer

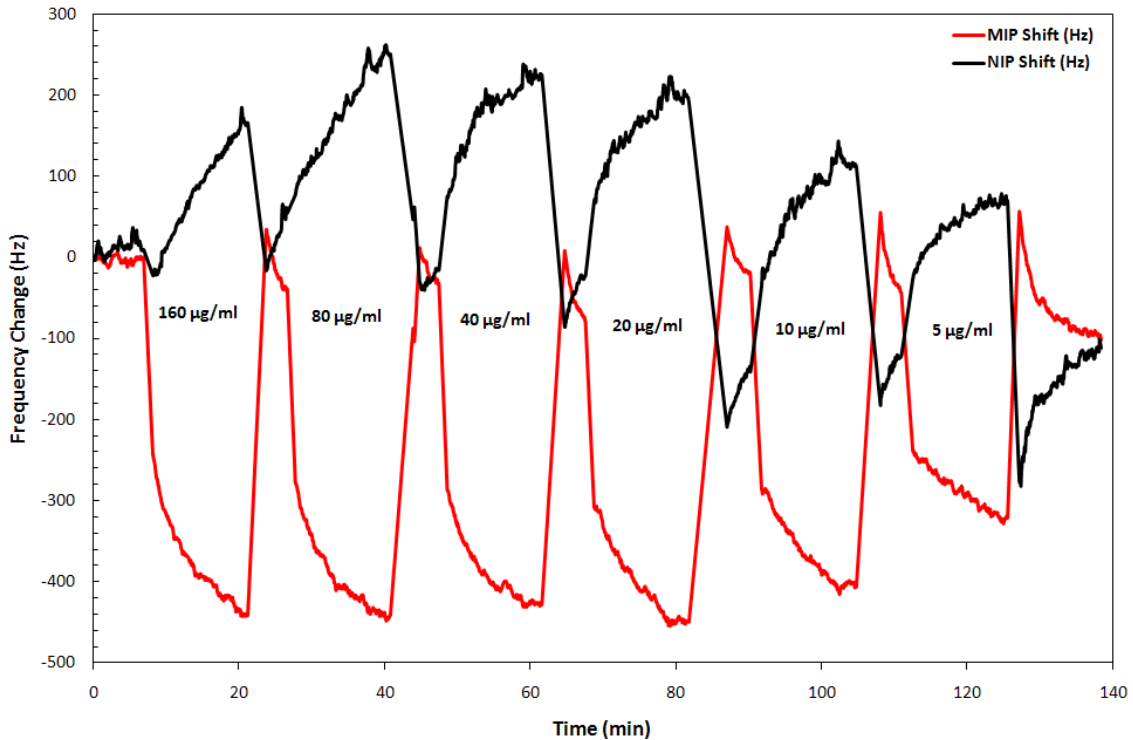


Figure 59 10 MHz Quartz crystal microbalance (QCM) sensor responses of MIP and NIP towards different BSA concentrations at 25 °C with AAM/MAA/MMA/MBAM (2:1:1:4) copolymer

However, the NIP-coated channel in both cases shows positive frequency shifts and thus does not follow the Sauerbrey behavior that a mass increase on the electrode of a QCM leads to decreasing frequency. The Sauerbrey theory explains the behavior of piezoelectric material when additional mass on the piezoelectric surface leads to a frequency shift as sketched in Figure 60. When this coating forms an ideally rigid surface, the shearing wave will propagate through it from the piezoelectric material and leading to increased wavelength and therefore decreased frequency.

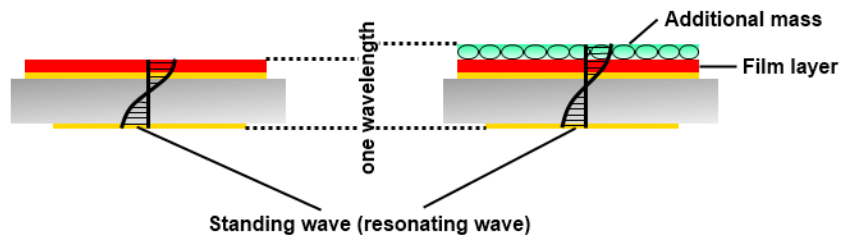


Figure 60 Effect of resonator thickness increase on the oscillation cavity.

Obviously, the positive change in NIP electrode indicates that the assumptions underlying the Sauerbrey behavior is not valid in this case, because network analyzer measurements revealed that no layer material is lost during the measurements. Obviously, there is only weak interaction between biomolecule and NIP polymer surface. Therefore, no ideally rigid layer is formed on the respective QCM electrode, which leads to the observation of positive frequency changes. Similar effects can also be found in other biological systems, such as yeasts and viruses^{58, 59}. A possible quantitative explanation of this effect has been given by Lucklum et al.,⁶⁰ who investigated the effect of viscosity on the piezoelectric material. The slip of free bioparticles on the surface can thus indeed lead to increasing frequencies of QCM. The NIP material shows a very flat and smooth surface (at least in the dimension of the proteins. WGA molecules adsorbed on this surface remain mobile and act almost like “balls”. When the QCM start to oscillate, they will start moving on the surface by rolling forward and backward leading to the observed effects.

Such phenomena are not only found for WGA as the analyte, but also for BSA on the same QCM as show in Figure 59 giving the frequency responses of MIP and NIP in six different concentration, respectively. Again the MIP yield the expected negative sign in frequency change, while the NIP changes to higher frequencies. However, the frequency responses of both layers are smaller towards BSA than towards WGA due to their different size, geometry and surface chemistry. Moreover, the frequency responses of BSA are only have as large as the ones caused by WGA due to the unspecific interaction to polymer surface, even though there are similar in the size. The frequency responses of MIP electrode depend on BSA concentration and reach saturation at the high concentrations. Even though BSA is slightly larger than WGA it can interact with the cavities sufficiently to prevent

rolling. Therefore, they move together with QCM leading to the observed negative frequency change at MIP.

In summary, WGA lectin is tightly bound in MIP cavities resulting in the larger decrease in frequency as compared to BSA. This follows the Sauerbrey theory. BSA sensor characteristic reveals lower sensitivity and saturation at lower values. However, this is not the case for the NIP, on which protein molecules remain mobile and thus give rise to non-Sauerbrey frequency shifts. Furthermore, the frequency of both electrodes immediately responds to the analytes and also depends on WGA lectin concentration thus establishing a method for quantitative sensing.

4.3 Brunauer-Emmett-Teller (*BET*) analysis

The kinetic adsorption of biomolecules on receptor surfaces can in principle be explained by three different isotherms including the Langmuir, Freundlich or BET isotherm. For small biomolecules, such proteins or viruses, the Freundlich isotherm is often used to describe the interaction with MIP⁶¹ in liquid phase. In case the Freundlich isotherm is not valid, because multilayer adsorption of the respective species occurs, the BET isotherm for liquid phase⁶² would be applied. Usually, the BET model is used to describe the multilayer adsorption of gases on porous materials⁶³. Depending on the differences in energy defined by the Boltzmann exponential factor $\exp(-\Delta E/RT)$, the interaction energy ΔE , the thermal energy RT , and the exchange rates between sites, the BET equation can be modified to be also applicable to adsorption phenomena in liquid phase. However, when doing so for proteins, one has to substitute partial pressure of gas, p by protein concentration in solution, c . Attention has to be paid when replacing the saturation vapor pressure of gas, p_0 with the corresponding term in liquid phase. In the classical BET isotherm, p_0 denotes the surface saturation partial pressure in gas phase. For protein adsorption we have replaced it by the maximum possible monolayer protein concentration on the surface, c_0 . Linearization leads to the following term:

$$\frac{c}{n(c_0-c)} = \frac{1}{n_m b} + \frac{b-1}{n_m b} \left(\frac{c}{c_0} \right) \quad (11)$$

The number of adsorbed protein molecules in the sensitive layer (n) can be derived by the frequency shift of the sensor. Their sensitivity of QCM can be calculated from the Sauerbrey equation (12). Filling in all the material constants results in a sensitivity of 4.61 Hz/ng.

$$\Delta f = -\frac{2f_0^2}{A\sqrt{\rho_q\mu_q}} \Delta m \quad (12)$$

The parameter n_m describes the number of privileged site in the layer. The parameter b is given as

$$b = \exp\left(\frac{\Delta E}{RT}\right) \quad (13)$$

where energy ΔE is the difference of interaction energies between favorable and less-favorable binding sites.

4.3.1 Interaction Isotherm – Binding properties

The full sensor characteristic of WGA and BSA in the different concentration is shown in Figure 61. Evidently, WGA shows increasing frequency response without saturation or convergence at the high concentrations. This behavior can ideally be described by the BET isotherm taking into account multilayer adsorption. Table 6 summarizes the amount of layers adsorbed on the MIP at the different WGA solution concentrations:

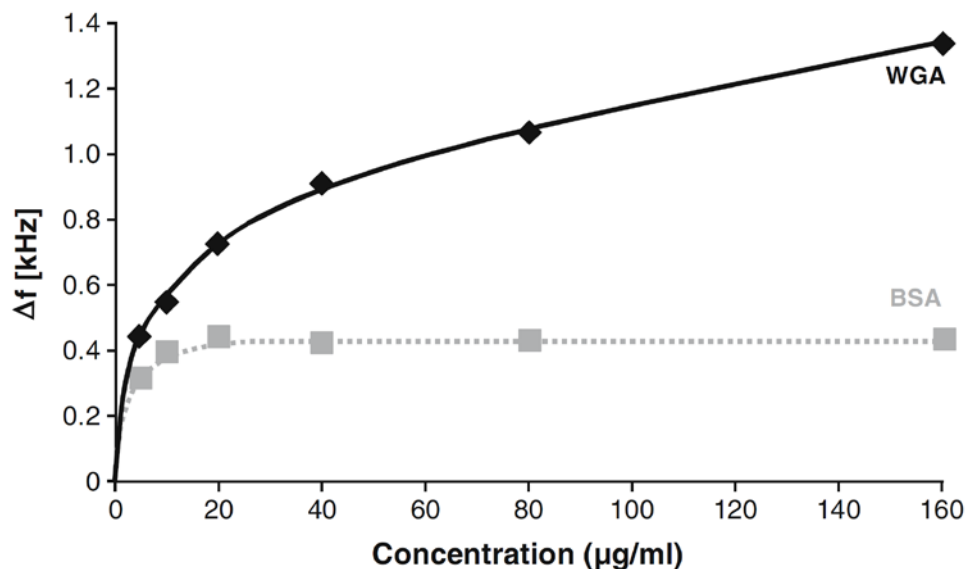


Figure 61 WGA-MIP: 10-MHz QCM sensor characteristics of WGA and BSA at 25 °C

Table 6 Correlation between WGA lectin concentration and number of adsorbed WGA layers on a 10-MHz quartz crystal microbalance

WGA concentration (μg/ml)	No. of layers
160	25
80	20
40	17
20	13
10	10
5	8
1	4

Obviously, already at the lowest concentration 1 μg/ml of WGA - multilayer adsorption occurs. This further indicates the strong interaction between the analyte and the imprinted cavities. However, the amount of protein actually adsorbed tightly on the QCM is astonishing. Obviously, the occupied binding sites on the imprinted surface function as

crystallization seeds for the protein. Similar effects have already been observed in earlier studies on protein MIP⁶⁴.

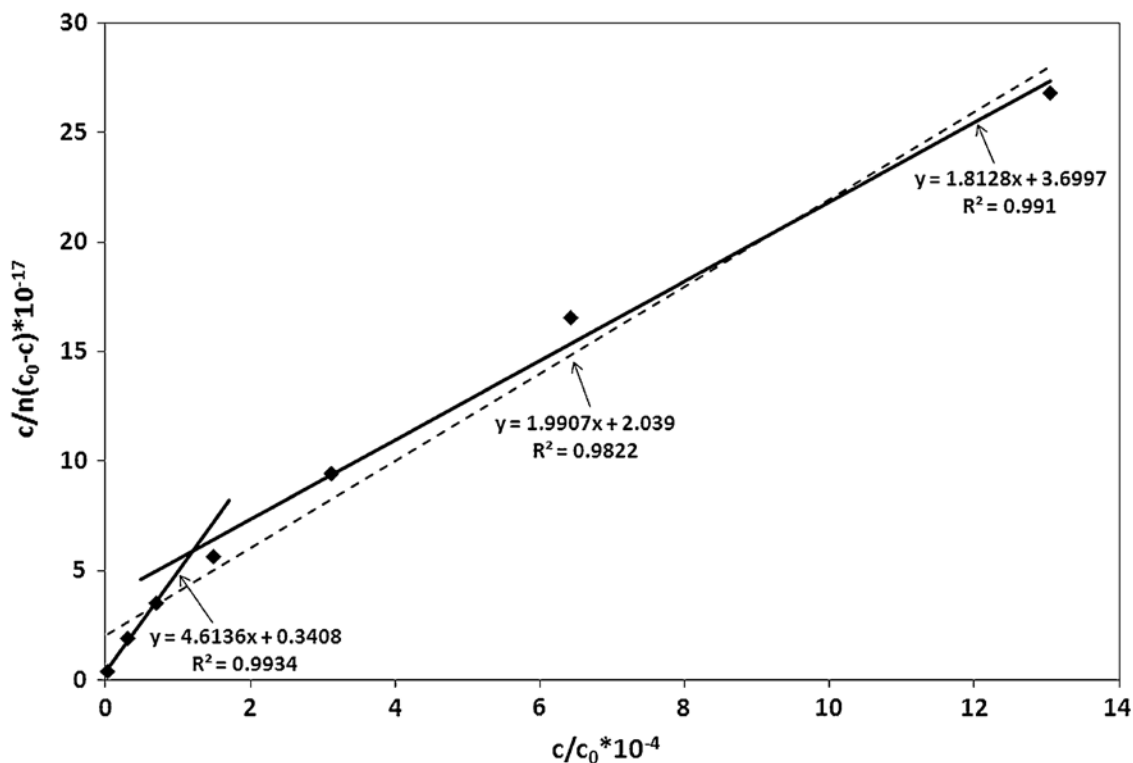


Figure 62 Linearized Brunauer–Emmett–Teller adsorption isotherm of WGA lectin according to equation (11). The dashed line represents the overall adsorption behavior of WGA lectin with $R^2=0.98$, whereas the solid lines represent two adsorption behaviors at high and low concentration with $R^2=0.99$

Figure 62 shows the linearized BET isotherm derived from the QCM sensor characteristic in Figure 61 and equation (11). As already mentioned, this allows calculating n_m and b from the intercept and slope of the linear. The results of this calculation are shown in Table 7.

Table 7 Calculated value for each parameter from Figure 60 and Equation (11) and (13)

Parameter	BET single range	BET Two ranges	
		Low Concentration	High Concentration
n_m	5.02×10^{12}	2.17×10^{12}	5.51×10^{12}
b	7744.60	135376.59	4900.86
ΔE (kJ/mol)	22.19	29.28	21.05
R^2	0.98	0.99	0.99

First, the BET calculation is applied over the full concentration range yielding a linear with $R^2 = 0.98$. The number of favorable binding site can be calculated as 5×10^{12} . Furthermore, the energy difference between favorable and unfavorable binding sites in the MIP layer was evaluated from parameter b and the Boltzmann exponential factor in equation as 22.19 kJ/mol. Moreover, the number of protein molecules bound on the surface is 4.86×10^{12} at the high concentration (160 $\mu\text{g/ml}$, -1341 Hz) which corresponds to roughly 97% of the available favorable binding sites, and it is 7.83×10^{11} for the low concentration (1 $\mu\text{g/ml}$, -216 Hz), which corresponds to 16% of the available favorable binding sites. In contrast this, during BSA binding adsorption reaches saturation indicating favorable selectivity of the MIP.

However, the linear BET isotherm in Figure 62 does not exactly match all data, because they deviate systematically from the modeled curve. This leads to a second approximation: there seems to be two different concentration ranges that need separate consideration. Therefore, BET analysis is applied independently on the two ranges, which is also depicted in Figure 62 as solid lines. In the low concentration range (1 $\mu\text{g/ml}$ to 10 $\mu\text{g/ml}$), n_m can be calculated as 2.17×10^{12} with a $\Delta E=29.3$ kJ/mol. For high concentration (20 $\mu\text{g/ml}$ to 160 $\mu\text{g/ml}$), n_m and ΔE were evaluated as 5.51×10^{12} and 21.05 kJ/mol, respectively. In both cases, the correlation coefficient is 0.99, which is better than in the single linear model. For the low concentration range, the energy difference between favorable and unfavorable binding sites corresponds to roughly three hydrogen bonds per protein molecule, which seems reasonable in this case. Even though already at low concentration multilayers are adsorbed, the WGA-MIP interaction is still energetically favored over the WGA-WGA interaction leading to the adsorption of further layers of protein

during “crystallization” on the surface. In the low concentration range at 20 $\mu\text{g/ml}$, 92% of the favorable binding sites are already occupied, whereas this value is 88% for the high concentration range (160 $\mu\text{g/ml}$). One has to keep in mind, however, that the sites are different in these two cases: until a solution concentration of 20 $\mu\text{g/ml}$, there are obviously still unoccupied highly affine binding sites on the MIP. When exceeding this concentration, adsorption is governed by WGA-WGA interactions.

Chapter 5

Comparison of sensors: Receptor Analogue vs. MIP

Real time biosensors can be used in different ways to recognize and obtain information regarding biomolecular interaction. For the recognition and detection of WGA there are basically two techniques as described in the previous chapters. One is immobilizing a receptor or a receptor analogue on the surface (GlcNAc in our case) and another one is molecular imprinting. In principle each technique has different advantages and drawbacks depending on purpose investigation. In terms of the use as a sensor recognition layer, both sensitivity and selectivity have to be evaluated. Figure 63 summarizes the sensor responses of the two receptor systems towards six different concentrations of WGA. Furthermore, Table 8 directly compares the amount of protein molecules adsorbed on the two sensor layers at these concentrations:

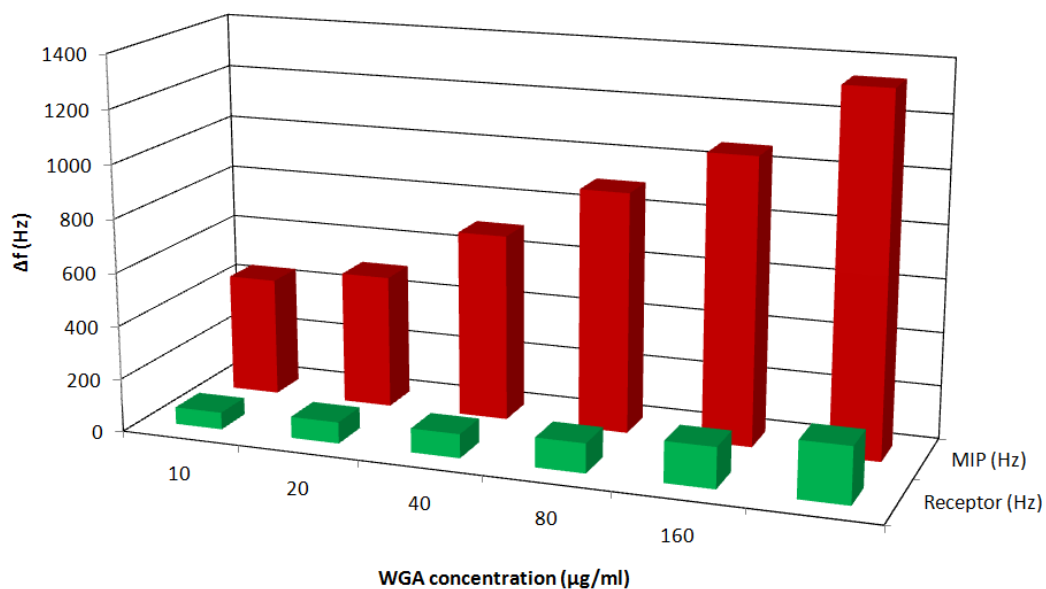


Figure 63 Comparison of sensitivity of both sensors

Table 8 Number of WGA molecule adsorbed on sensor layers

WGA concentration ($\mu\text{g/ml}$)	GlcNAc immobilization molecule ($\times 10^{11}$)	MIP molecule ($\times 10^{11}$)
160	7.69	48.64
80	5.62	38.81
40	4.06	33.08
20	3.19	26.48
10	2.76	19.95
5	2.36	16.18

Obviously, the MIP technique is much more sensitive than the immobilized glycosides, namely by almost an order of magnitude slightly depending on concentration. This is mainly due to the fact that the latter binds only a monolayer of analyte. For the purpose of sensing low amounts of protein, therefore, the MIP is more suitable than the immobilized receptor analogue.

When considering selectivity towards BSA, we exposed a QCM to 160 $\mu\text{g/ml}$ of WGA and BSA, respectively. The resulting sensor responses are summarized in Figure 64 by normalizing them to the sensor response of WGA.

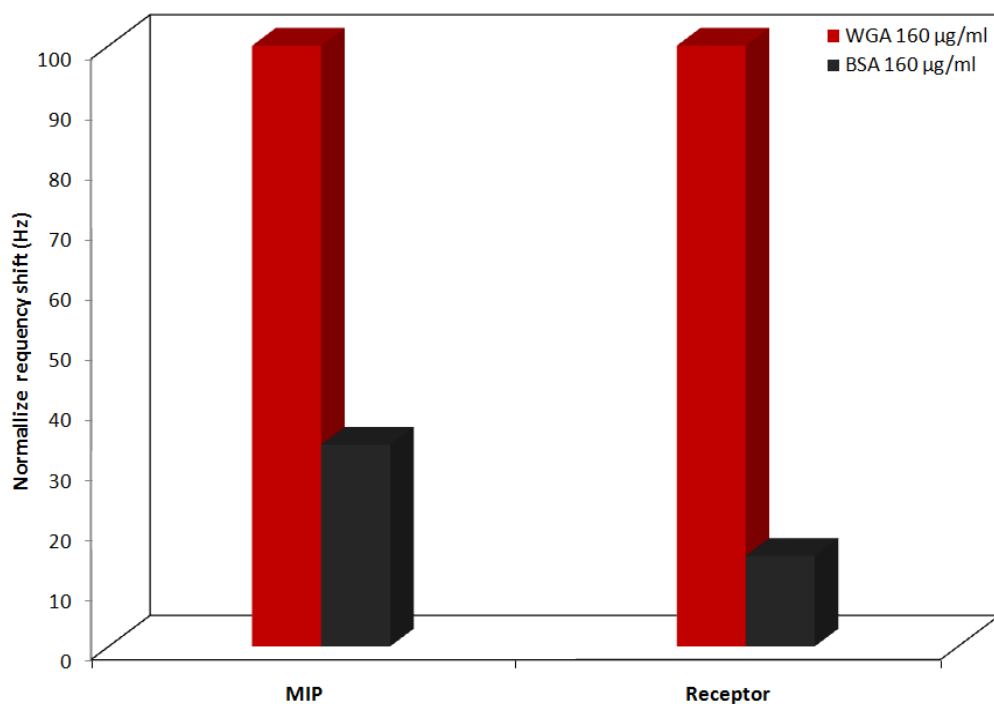


Figure 64 Comparison of selectivity of both sensors with 160 µg/ml of WGA and BSA, respectively

Obviously, the immobilized receptor analogue yields higher selectivity than MIP: its normalized frequency shift toward BSA is only about half of that for the MIP. Considering the ratio of sensor responses between BSA and WGA for each technique, the ratio of WGA/BSA of the MIP is roughly 3, while the immobilized receptors reach about 6. The reason for this difference is that WGA itself has highly specific affinity towards the GlcNAc chain (affinity constant in the order of magnitude of $10^2 M^{-1}$). Furthermore, the binding interaction of WGA to GlcNAc can be further strengthened when increasing the number of GlcNAc molecules bound to one another in the receptor via 1-4 glycosidic bonds (1-4 linkage form). Therefore, within this work we used the 1-4 linkage of the GlcNAc to nitrobenzene for mimicking the natural receptor. Moreover, we conserved the polarity of the molecule by choosing cysteine as the linker between Gold surface and GlcNAc. This selectivity is also reproduced in the adsorption energies obtained from the respective binding

isotherms: for GlcNAc $\Delta G = -34.82 \text{ kJ/mol}$, while the MIP results in $\Delta G = -22.18 \text{ kJ/mol}$. Assumed that the interaction energies for BSA are similar in both cases, this explains the selective difference.

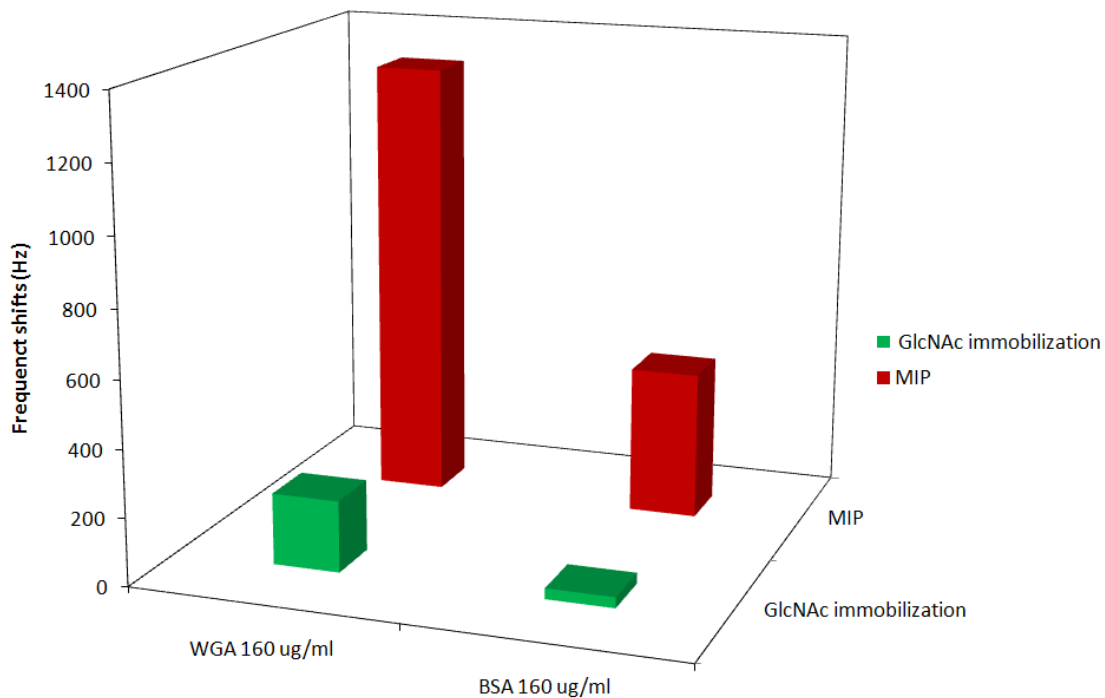


Figure 65 Comparison of selectivity and sensitivity of both sensors with 160 µg/ml of WGA and BSA, respectively

Finally, Figure 65 summarizes the data of both sensitivity and selectivity: it again clearly shows that the glycosidic receptor yield very appreciable selectivity but the MIP has higher sensitivity by a factor of ~ 7 . This is astonishing especially given the fact that the selective binding sites in the MIP are based on an interaction network pre-formed during synthesis between the target protein and commercially available “standard” monomers. Therefore, this work clearly shows that rational materials design allows synthesizing receptor materials, whose selectivity is already quite close to those derived from nature. This inherently opens the way for biosensing with artificial recognition materials.

Conclusion

The recognition of WGA lectin was investigated in two different techniques namely molecularly imprinted polymer (MIP) and receptor immobilization on Quartz crystal microbalance (QCM). Both methods recognize WGA in terms of quantitative and qualitative even though the receptor immobilization has efficiency in selectivity over the MIP but it yields lower in sensitivity than MIP. They exhibit the difference binding mechanism – the MIP itself works as the “recrystallization seed” on the polymer surface whereas the receptor immobilization has the multivalent interaction on its receptor.

Outlook

As lectin is a glycoprotein that recognizes the proteins on cell surfaces, it can be used as the model and developed to the sensor and also used as the visual screening medicine and mutation for future pathogenic detection such as the influenza virus. The advantages of both techniques are real time detection, small amount of sample, stability at room temperature and the neutral pH.

Abstract

Wheat germ agglutinin (WGA) is a plant lectin that plays a crucial role in biotechnology and biosensors as it interacts with viruses, cells during infection events and also with oligosaccharides that are normally found on cell surfaces of several organisms. Therefore, it is an interesting analyte for mass sensitive sensing in terms of recognition and interaction phenomena. Within this work, WGA was selectively detected by two different techniques including immobilized carbohydrates and molecularly imprinted polymers (MIP) used as recognition elements on quartz crystal microbalance (QCM). Scanning tunneling microscopy (STM) was used to study the surfaces generated by those techniques. As STM requires a conductive surface, gold was sputtered onto the polymer for generating the STM image. Thus cavities having the dimension of WGA dimer could be observed in the resulting molecularly imprinted polymers (MIP). In the case of immobilized receptor analogues, *N*-acetyl-*D*-glucosamine (GlcNAc) modified with *p*-nitrophenol-cysteine was immobilized on gold for construction of the sensitive layer. Due to the size of WGA molecules, a self-assembled monolayer of GlcNAc is unsuitable for binding as enough space is needed between binding sites to achieve optimal results. Therefore, cysteine molecules were used as spacers between each GlcNAc. Sensor characteristics reveal that the frequency decreased only by -30 Hz if pure GlcNAc is immobilized, which changed to roundly -210 Hz for the mixed surface layer at 160 $\mu\text{g/ml}$ of WGA which in factor of 7. Furthermore, the maximum adsorption layer at the high concentration of WGA is nearly a monolayer (0.98 layers). Therefore, the binding constant was calculated with the Langmuir model. In parallel, WGA was used as the template for molecular imprinting in methacrylate co-polymer system. The sensor characteristics were recorded from 160 $\mu\text{g/ml}$ to 1 $\mu\text{g/ml}$ of WGA. In contrast to this, the adsorption behavior of WGA on the MIP surface occurred in multilayers starting from low concentrations (1 $\mu\text{g/ml}$). The studies on the WGA–MIP adsorption behavior suggest that the MIP itself works as a “crystallizing nucleus” for the protein, even though the nonimprinted material disfavors WGA adsorption. This can be seen by the fact that up to 25 molecular layers of protein are deposited on the MIP in the observed concentration range,

whereas the NIP coated electrodes yield positive frequency shifts indicating anti-Sauerbrey behavior. In terms of adsorption investigation, the BET isotherm was applied to MIP for evaluating the binding properties of WGA due to this multilayer adsorption. Even though the interaction of WGA on glycoside surface is the multivalent interaction but the adsorption layer is occurred only monolayer adsorption leads to applying of Langmuir adsorption model. In comparison, the MIP method shows a substantially higher sensitivity (-1320 Hz for 160 $\mu\text{g/ml}$) than the immobilized receptor analogue (-210 Hz for 160 $\mu\text{g/ml}$). In terms of selectivity towards bovine serum albumin (BSA), the MIP has lower selectivity which reaches a factor of ~ 3 than the artificial receptor yields ~ 7 . Therefore, this investigation indicated that the carbohydrate is better than the MIP in term of selectivity whereas MIP yields higher than artificial receptor for sensitivity.

Zusammenfassung

Bei Wheat germ agglutinin (WGA) handelt es sich um ein Pflanzenlektin, das eine grundlegende Rolle in der Biotechnologie und der Biosensorik spielt, weil es mit Viren und Zellen im Zuge von Infektionsvorgängen ebenso reagiert, wie mit Oligosacchariden, die auf den Zelloberflächen verschiedener Organismen vorhanden sind. Daher ist WGA auch interessanter Analyt für massensensitive Messungen, die Einblicke in die Erkennung und die ihr zugrundeliegenden Wechselwirkungen gestatten. Im Zuge dieser Arbeit wurden zwei verschiedene Rezeptorstrategien zur Sensorik von WGA mittels Quarzmikrowaage (quartz crystal microbalance – QCM) entwickelt, nämlich die Immobilisierung glykosidischer Rezeptoranaloga sowie molekular geprägte Polymer (molecularly imprinted polymers – MIP). Die entsprechenden Oberflächen wurden auch mittels Rastertunnelmikroskopie charakterisiert. Da diese Technik leitende Oberflächen benötigt, wurden auf die MIP Goldschichten durch Sputtering aufgebracht. Dadurch war es möglich tatsächlich Kavitäten in der Größe von WGA-Dimeren auf der Oberfläche zu visualisieren. Als Rezeptoranalogen wurde mit p-Nitrophenol und dann Cystein modifiziertes N-Acetyl-D-Glucosamin verwendet und über die SH-Gruppe des Cysteins auf Goldoberflächen immobilisiert. Aufgrund der Größe der Analytmoleküle erwies sich die Beschichtung mit einer kompletten Monolage des Rezeptors nicht als zielführend, da die Bindung dann sterisch behindert wurde. Deswegen mußten Cysteinmoleküle co-immobilisiert werden, um genügenden Abstand zwischen den Glykosiden sicherzustellen: auf der Monolage konnte führte eine Lösung mit 160µg/ml WGA auf der QCM nur zu einer Frequenzantwort von -30Hz, wogegen im Fall der Co-Immobilisierung -210 Hz, also das Siebenfache, erreicht werden konnten. Diese – für die vorliegende Studie maximale – Lösungskonzentration führt zu einer fast kompletten Monolage von WGA (0,98 Monolagen) auf der Sensoroberfläche. Daher lassen sich die Bindungskonstanten mittels eines Langmuir-Modells berechnen. Dazu wurde die Sensorcharakteristik in einem Konzentrationsbereich von 1 µg/ml bis 160 µg/ml aufgenommen. Im Gegensatz dazu adsorbieren MIP bereits bei niedrigen Lösungskonzentrationen (1 µg/ml) bereits Multilayer von WGA, womit ein modifiziertes

BET-Modell für die Charakterisierung der Adsorptionsotherme herangezogen wurde. Das Adsorptionsverhalten legt den Schluß nahe, daß das MIP als „Kristallisationskeim“ für das Protein fungiert, obwohl das nichtgeprägte Material die Adsorption nicht begünstigt. Dies ist insbesondere auch daran zu bemerken, daß bis zu 25 Molekullagen auf dem MIP adsorbieren, wogegen die jeweiligen ungeprägten Referenzelektroden positive Frequenzantworten und damit Anti-Sauerbrey-Verhalten zeigen. Beim glykosidischen Rezeptoranalogen wird dagegen trotz maximal einer Monolage durch die Sensorschicht geboten, obwohl ein WGA-Molekül mehrere Bindungsstellen hat. Damit läßt sich dessen Verhalten durch eine Langmuir-Isotherme beschreiben.

Im Vergleich der beiden Methoden lassen sich auf den MIP wesentlich höhere Sensoreffekte erzielen: beispielsweise bei 160 µg/ml WGA sind es -1320 Hz im Vergleich zu -210 Hz für den Rezeptor. Die Selektivität gegenüber Bovinem Serumalbumin (BSA) ist dagegen mit einem Selektivitätsfaktor von drei im Fall des MIP niedriger, als für das Glykosid, das sieben erreicht. Daher ist bei diesem also die Selektivität besser, die Sensitivität dagegen geringer, als beim MIP.

References

1. Sumner, J.B. The globulins of the jack bean, *Canavalia ensiformis*. *Journal of Biological Chemistry* **37**, 137-142 (1919).
2. Hardman, K.D. & Ainsworth, C.F. Structure of concanavalin A at 2.4-Å resolution. *Biochemistry* **11**, 4910-4919 (1972).
3. Lis, H. & Sharon, N. Lectins: Carbohydrate-Specific Proteins That Mediate Cellular Recognition. *Chem Rev* **98**, 637-674 (1998).
4. Bezkorovainy, A., Springer, G.F. & Desai, P.R. Physicochemical properties of the eel anti-human blood-group H(O) antibody. *Biochemistry* **10**, 3761-3764 (1971).
5. Burger, M.M. A difference in the architecture of the surface membrane of normal and virally transformed cells. *Proc Natl Acad Sci U S A* **62**, 994-1001 (1969).
6. Burger, M.M. & Goldberg, A.R. Identification of a tumor-specific determinant on neoplastic cell surfaces. *Proc Natl Acad Sci U S A* **57**, 359-366 (1967).
7. Ozanne, B. & Sambrook, J. Binding of radioactively labelled concanavalin A and wheat germ agglutinin to normal and virus-transformed cells. *Nat New Biol* **232**, 156-160 (1971).
8. Nagata, Y. & Burger, M.M. Wheat germ agglutinin. Isolation and crystallization. *J Biol Chem* **247**, 2248-2250 (1972).
9. Sharon, N., Lis, H. & SpringerLink (Online service) (Springer Science+Business Media B.V., Dordrecht; 2007).
10. Privat, J.P., Delmotte, F., Mialonier, G., Bouchard, P. & Monsigny, M. Fluorescence studies of saccharide binding to wheat-germ agglutinin (lectin). *Eur J Biochem* **47**, 5-14 (1974).

11. Bains, G., Lee, R.T., Lee, Y.C. & Freire, E. Microcalorimetric Study of Wheat-Germ-Agglutinin Binding to N-Acetylglucosamine and Its Oligomers. *Biochemistry* **31**, 12624-12628 (1992).
12. Schwefel, D. et al. Structural basis of multivalent binding to wheat germ agglutinin. *J Am Chem Soc* **132**, 8704-8719 (2010).
13. Pei, Z., Anderson, H., Aastrup, T. & Ramstrom, O. Study of real-time lectin-carbohydrate interactions on the surface of a quartz crystal microbalance. *Biosens Bioelectron* **21**, 60-66 (2005).
14. Huang, G.L., Yang, H., Mei, X.Y., Liu, M.X. & Ma, Y.T. Fluorophore-assisted carbohydrate electrophoresis as detection method for carbohydrate-protein interactions. *Appl Biochem Biotechnol* **136**, 17-22 (2007).
15. Beccati, D. et al. SPR studies of carbohydrate-protein interactions: signal enhancement of low-molecular-mass analytes by organoplatinum(II)-labeling. *Chembiochem* **6**, 1196-1203 (2005).
16. Foley, K.J., Forzani, E., Tao, N. & Joshi, L. Label-free realtime detection of sugars on lectin-modified high-resolution differential (HRD) surface plasmon resonance (SPR) sensors. *Glycobiology* **16**, 1156-1156 (2006).
17. Wilczewski, M. et al. Promotion of sugar-lectin recognition through the multiple sugar presentation offered by regioselectively addressable functionalized templates (RAFT): a QCM-D and SPR study. *Org Biomol Chem* **6**, 1114-1122 (2008).
18. Star, A. et al. Nanoelectronic Detection of Lectin-Carbohydrate Interactions Using Carbon Nanotubes. *Nano Lett* **11**, 170-175 (2011).
19. Sugawara, K., Kamiya, N., Hirabayashi, G. & Kuramitz, H. Voltammetric evaluation for the binding of wheat germ agglutinin to glucosamine-modified magnetic microbead. *Talanta* **72**, 1123-1128 (2007).
20. Sugawara, K. et al. Voltammetric detection of lectin using sugar labeled with electroactive substance. *Anal Sci* **17**, 21-25 (2001).

21. Bossi, A., Bonini, F., Turner, A.P.F. & Piletsky, S.A. Molecularly imprinted polymers for the recognition of proteins: The state of the art. *Biosens Bioelectron* **22**, 1131-1137 (2007).
22. Cooper, M.A., Uludag, Y., Piletsky, S.A. & Turner, A.P.F. Piezoelectric sensors based on molecular imprinted polymers for detection of low molecular mass analytes. *Febs J* **274**, 5471-5480 (2007).
23. Ratner, B.D., Shi, H.Q., Tsai, W.B., Garrison, M.D. & Ferrari, S. Template-imprinted nanostructured surfaces for protein recognition. *Nature* **398**, 593-597 (1999).
24. Mosbach, K. Molecular Imprinting. *Trends Biochem Sci* **19**, 9-14 (1994).
25. Dickert, F.L., Hayden, O., Lieberzeit, P.A. & Palfinger, C. Sensor materials - Detecting molecules, mixtures and microorganisms. *Mater Res Soc Symp P* **723**, 25-34 (2002).
26. Dickert, F.L. & Lieberzeit, P.A. Rapid bioanalysis with chemical sensors: novel strategies for devices and artificial recognition membranes. *Analytical and Bioanalytical Chemistry* **391**, 1629-1639 (2008).
27. Dickert, F.L. et al. Quality assessment with molecularly imprinted microsensors - degradation processes in automotive oils. *P Soc Photo-Opt Ins* **3857**, 14-22 (1999).
28. Ertl, P. et al. Detection of viruses with molecularly imprinted polymers integrated on a microfluidic biochip using contact-less dielectric microsensors. *Lab Chip* **9**, 3549-3556 (2009).
29. Komiyama, M. Molecular imprinting: from fundamentals to applications. (John Wiley, Weinheim; 2003).
30. Wulff, G. & Knorr, K. Stoichiometric noncovalent interaction in molecular imprinting. *Bioseparation* **10**, 257-276 (2001).
31. Marty, J.D. & Mauzac, M. Molecular imprinting: State of the art and perspectives. *Adv Polym Sci* **172**, 1-35 (2005).

32. Curie, P.C.a.J. Développement, par pression, de l'électricité polaire dans les cristaux hémihédres à faces inclinées. *Comptes Rendus* **91**, 294-295 (1880).
33. Hankel, W.G. Über die aktinound piezoelektrischen eigenschaften des bergkrystalles und ihre beziehung zu den thermoelektrischen. *Abh. Sächs.* **12**, 457 (1881).
34. Kalantar-zadeh, K. & Fry, B. Nanotechnology-enabled sensors. (Springer, New York ; London; 2008).
35. Janata, J.r. Principles of chemical sensors. (Plenum Press, New York; 1989).
36. Hayashi, M., Xu, X.Y. & Tan, Q.T. Versatile and mild synthesis of di- and trisaccharidic 2-enopyranosyl cyanides by cyanation of per-O-acetylglycals with trimethylsilyl cyanide catalyzed by palladium(II) acetate. *Synthesis-Stuttgart*, 770-776 (2008).
37. Boysen, M.M.K., Grugel, H. & Minuth, T. Novel Olefin-Phosphorus Hybrid and Diene Ligands Derived from Carbohydrates. *Synthesis-Stuttgart*, 3248-3258 (2010).
38. Polt, R., Mitchell, S.A., Pratt, M.R. & Hruby, V.J. Solid-phase synthesis of O-linked glycopeptide analogues of enkephalin. *Journal of Organic Chemistry* **66**, 2327-2342 (2001).
39. R. U. Lemieux, R.M.R. The azidonitration of tri-O-acetyl-D-galactal. *Can J Chemistry* **57**, 1244 (1979).
40. Chih-Wei Chang, S.-S.C., Chin-Sheng Chao and Kwok-Kong T. Mong, A mild and general method for preparation of α -glycosyl chlorides. *Tetrahedron Letters* **50**, 4536-4540 (2009).
41. Singh S, P.J., Samuel CJ, Critchley P, Crout DH. Glycosidase-catalysed oligosaccharide synthesis: preparation of N-acetylchitooligosaccharides using the beta-N-acetylhexosaminidase of *Aspergillus oryzae*. *Carbohydrare Research*, 279-305 (1995).

42. Pavel KRIST, M.K., István F. PELYVÁS, Pavla SIMERSKÁ and Vladimír KŘEN
Synthesis of 4-nitrophenyl-2-acetamido-2-deoxy- β -D-mannopyranoside and 4-nitrophenyl-2-acetamido-2-deoxy- α -D-mannopyranoside. *Collection of Czechoslovak Chemical Communications* **68**, 801-811 (2003).
43. Podder, S.K., Surolia, A. & Bachhawa, B.K. Specificity of Carbohydrate-Lectin Recognition - Interaction of a Lectin from Ricinus-Communis Beans with Simple Saccharides and Concanavalin A. *European Journal of Biochemistry* **44**, 151-160 (1974).
44. Matsuura, K., Hayashi, K. & Kobayashi, K. On-off switching of gene expression regulated with carbohydrate-lectin interaction. *Biomacromolecules* **6**, 2533-2540 (2005).
45. Kakehi, K., Oda, Y., Kinoshita, M. & Nakayama, K. Evaluation of fluorescence polarization method for binding study in carbohydrate-lectin interaction. *Biol Pharm Bull* **21**, 1215-1217 (1998).
46. Podder, S.K., Surolia, A. & Bachhawat, B.K. Dynamics of Carbohydrate-Lectin Interaction - Interaction Para-Nitrophenyl-Beta-D-Galactose with a Lectin from Ricinus-Communis. *FEBS Lett* **85**, 313-316 (1978).
47. Ray, S. & Chatterjee, B.P. Carbohydrate-Lectin Interactions .1. Purification of Ant-Egg Glycoprotein and Its Interaction with Jacalin. *Carbohydr Res* **191**, 305-314 (1989).
48. Kobayashi, K., Matsuura, K. & Hayashi, K. Artificial regulation of transcription applying carbohydrate-lectin interaction. *Chem Commun*, 1140-1141 (2002).
49. Wrodnigg, T.M. & Stutz, A.E. The Heyns rearrangement revisited: An exceptionally simple two-step chemical synthesis of D-lactosamine from lactulose. *Angewandte Chemie-International Edition* **38**, 827-828 (1999).
50. Withers, S.G. & Vocadlo, D.J. Detailed comparative analysis of the catalytic mechanisms of beta-N-acetylglucosaminidases from families 3 and 20 of glycoside hydrolases. *Biochemistry* **44**, 12809-12818 (2005).

51. Roy, R. & Tropper, F.D. Carbohydrate Protein Interactions - Syntheses of Agglutination Inhibitors of Wheat-Germ-Agglutinin by Phase-Transfer Catalysis. *Can J Chem* **69**, 817-821 (1991).
52. Dekany, G., Bornaghi, L., Papageorgiou, J. & Taylor, S. A novel amino protecting group: DTPM. *Tetrahedron Letters* **42**, 3129-3132 (2001).
53. Zhang, G.S., Chen, J., Min, A.M. & Zhang, L.H. Synthesis of 5'-O-(2-azido-2-deoxy-alpha-D-glycosyl)nucleosides and their antitumor activities. *Helv Chim Acta* **86**, 2073-2081 (2003).
54. Zervosen, A. & Elling, L. A novel three-enzyme reaction cycle for the synthesis of N-acetylglucosamine with in situ regeneration of uridine 5'-diphosphate glucose and uridine 5'-diphosphate galactose. *J Am Chem Soc* **118**, 1836-1840 (1996).
55. R. U. Lemieux, J.-I.H. The mechanism of the anomerization of the tetra-O-acetyl-D-glucopyranosyl chlorides. *Can J Chemistry* **43**, 2162-2173 (1965).
56. Che, A.F., Huang, X.J. & Xu, Z.K. Protein adsorption on a glycosylated polyacrylonitrile surface: monitoring with QCM and SPR. *Macromol Biosci* **10**, 955-962 (2010).
57. Mori, T., Toyoda, M., Ohtsuka, T. & Okahata, Y. Kinetic analyses for bindings of concanavalin A to dispersed and condensed mannose surfaces on a quartz crystal microbalance. *Anal Biochem* **395**, 211-216 (2009).
58. Lieberzeit, P.A. et al. From nanopatterning to functionality - surface and bulk imprinting for analytical purposes. *Superlattice Microst* **36**, 133-142 (2004).
59. Dickert, F. et al. Borderline applications of QCM-devices: synthetic antibodies for analytes in both nm- and mu m-dimensions. *Sensor Actuat B-Chem* **95**, 20-24 (2003).
60. Lucklum, R., Behling, C. & Hauptmann, P. Role of mass accumulation and viscoelastic film properties for the response of acoustic-wave based chemical sensors. *Anal Chem* **71**, 2488-2496 (1999).

61. Shimizu, K.D. et al. Characterization of the imprint effect and the influence of imprinting conditions on affinity, capacity, and heterogeneity in molecularly imprinted polymers using the Freundlich isotherm-affinity distribution analysis. *Anal Chem* **76**, 1123-1133 (2004).
62. Mohammadzadeh, J.S.S., Ebadi, A. & Khudiev, A. What is the correct form of BET isotherm for modeling liquid phase adsorption? *Adsorption* **15**, 65-73 (2009).
63. Dickert, F.L., Haunschild, A., Kuschow, V., Reif, M. & Stathopoulos, H. Mass-sensitive detection of solvent vapors. Mechanistic studies on host guest sensor principles by FT-IR spectroscopy and BET adsorption analysis. *Anal Chem* **68**, 1058-1061 (1996).
64. Dickert, F.L. et al. Nano- and micro-structuring of sensor materials - from molecule to cell detection. *Synthetic Met* **138**, 65-69 (2003).

CURRICULUM VITAE

Ms. Thipvaree Wangchareansak

Department of Analytical Chemistry and Food Chemistry, University of Vienna, Vienna,
1090, Austria

E-mail: a0902527@unet.univie.ac.at

PERSONAL DATA

- Born on 21st January 1984 in Bangkok, Thailand
- Nationality: Thai

EDUCATION

- University of Vienna, Vienna, Austria, 2009-present

Ph.D. Research in Analytical Chemistry, Area of Specialization: Molecular Imprinting
Polymer of Proteins and Viruses on Quartz crystal microbalance

- Kasetsart University, Bangkok, Thailand, 2007-present

Ph.D. in Physical Chemistry, 2007, Area of Specialization: Computational Chemistry, DNA
Cloning and protein expression, Biosensors and electrochemistry

- Burapha University, Chonburi, Thailand, 2002-2006

B.Sc. in Physics, Theory and Computational Physics

AWARDS and SCHOLARSHIP

- Postgraduate Research Award, 2007-present

Five-year PhD scholarship from The Royal Golden Jubilee Ph.D Program, ASEA UNINET, *OeAD* - Österreichischer Akademischer Austauschdienst

- Undergraduate Research Award, 2002-2006

Teacher Professional Development Project (TPDP) from The Institute for the Promotion of Teaching Science and Technology (IPST)

RESEARCH EXPERIENCE

- Practical work in Computational Chemistry and Bioinformatics at Department of Physical Chemistry, Kasetsart University (Research adviser: Assist. Prof. Chak Sangma)

- Practical work in the sensor laboratory on quartz crystal microbalance at Department of Analytical Chemistry, University of Vienna (Research adviser: Ao. Univ.-Prof. Peter Lieberzeit)

- Training in carbohydrate synthesis laboratory at Department of Pharmaceutical Technology and Biopharmaceutics, University of Vienna (Research adviser: Prof. Frank M Unger).

- Practical work in protein engineering laboratory at Department of Biochemistry, Kasetsart University (Research adviser: Assist. Prof. *Kiattawee* Choowongkamon)

- Training work in computational physics in topic of Numerical Technique for solving Integral Equation of Wave Function Passing through Multiple Scattering by MATLAB program (Research adviser: Dr. Nupan Kheaomaingam)

PRESENTATIONS

- **Oral Presentation:** Artificial Receptors for Membrane Glycoproteins – Comparing Systems Derived from Nature with Imprinted Polymers at 5th International Conference on Surfaces, Coatings and Nanostructure Material (NANOSMAT-5), Reims, France on 19-21 October 2010
- **Oral Presentation:** Host Type Selectivity Prediction for Bird flu Virus at 13th international Annual Symposium on Computational Science and Engineering (ANSCSE), Kasetsart University, Bangkok, Thailand on March 25-27, 2009
- **Oral Presentation:** Numerical Technique for solving Integral Equation of Wave Function Passing through Multiple Scattering at Congress on The Institute for the Promotion of Teaching Science and Technology 2005, *Impact* Exhibition & Convention Center, Thailand

SKILLS

Instrument

NMR, SEM/TEM, FTIR, Photoluminescence, UV-Vis spectroscopy, Scanning Tunnelling Microscope (STM), Atomic Force Microscope (AFM)

Technical experiments

Molecular Imprinting Polymer (MIP) and Quartz crystal Microbalance (QCM), DNA cloning and Protein expression, Computational Chemistry: Quantum calculation and Molecular dynamics simulations (MD), Programming: MATLAB, C program, FORTRAN, Chemical and enzyme synthesis of oligosaccharides and surface modification